Australian Government
Department of Defence
Defence Science and
Technology Organisation

Giselle: A Mutually Orthogonal Triple Twin-loop Ground-symmetrical Broadband Receiving Antenna for the HF Band

W. Martinsen

Command, Control, Communications and Intelligence Division
Defence Science and Technology Organisation

DSTO-TR-2321

ABSTRACT

This report describes development of a tri-axial mutually orthogonal broadband twin-loop receiving antenna for the HF band. The three twin-loops have been arranged so that they exhibit the same distributed parameters between themselves and ground. The upper frequency limit of the antenna is discussed and a method for extending the low frequency cut-off is presented. The antenna noise factor is calculated from measured data.

Published by

Command, Control, Communications and Intelligence Division
DSTO Defence Science and Technology Organisation
PO Box 1500
Edinburgh South Australia 5111 Australia

Telephone: (08) 8259 5555
Fax: (08) 8259 6567

AR-014-584
July 2009

APPROVED FOR PUBLIC RELEASE

Giselle: A Mutually Orthogonal Triple Twin-loop Ground-symmetrical Broadband Receiving Antenna for the HF Band

Executive Summary

Traditional mutually orthogonal tri-axial loop antennas have distributed parameters to the ground that are not consistent between the three loops. This non-symmetrical characteristic adds complexity to the analysis of signals received from each of the loops. Also, the distributed inductance (L) and capacitance (C) of each loop form a resonant circuit limiting the loop's usefulness for broadband work.

The tri-axial twin-loop antenna design presented in this report has the same distributed parameters to ground on all three loops (ground-symmetrical) easing the analysis burden on the received data. The final version of the antenna presented can cover the complete HF band and is ideal for studying the polarisation of received signals with the view of mitigating HF polarisation fading.

The inherent noise produced by the Giselle antenna is less than the expected man-made noise for a quiet rural site; therefore the Giselle antenna can also be used as a compact tri-axial polarisation diversity surveillance antenna for the whole of the HF band. It is capable of discriminating between locally transmitted ground wave signals and those transmitted at some distance and received via sky-wave by monitoring for any signs of rotation in the received signal's polarisation.

Authors

W. Martinsen
Command,Control,Communications Intelligence Div

Wayne Martinsen was indentured as an apprentice communications technician in 1972 with Transport Communications Pty. Ltd. (Buranda, Qld.). He attended Yeronga Technical College (Brisbane, Qld.) where he received honours in the majority of his subjects. In 1975 his apprenticeship indentures were transferred to The Radio Centre (Archerfield Aerodrome, Qld.) where he was employed as an Air Maintenance Engineer, Category Radio. He was involved in all aspects of repair and maintenance of avionics systems associated with the light aircraft industry. Upon completing his training as an apprentice he sat for and passed various Dept. of Transport Licensed Air Maintenance Engineer (L.A.M.E.) exams. In 1977 he joined the R.A.A.F. and after graduating from their School of Radio, where he received training in military systems, he worked on a wide variety of airborne communications, navigation and anti-submarine warfare systems. In 1987 he was discharged from the R.A.A.F. and applied for a position with D.S.T.O. at Edinburgh, South Australia. He was offered and accepted the position of Technical Officer (Engineering). Here he was tasked with the design and development of R.F. circuits required for tropospheric and ionospheric research.

Contents

1. Introduction

Long range propagation in the HF band relies on the reflection of radio waves from ionised layers in the Earth's ionosphere. The presence of the earth's magnetic field in the ionosphere results in the wave splitting into two characteristic modes (the ordinary and extraordinary) with different polarisations. These waves travel different paths; moreover in general the amplitudes of the ordinary and extraordinary waves are different due to differential D-region absorption, giving rise to a resultant wave that is elliptically polarised [20, pg. 235].

With a singly polarised receiving antenna, the output signal is proportional to the projection of the polarisation state of the receiving antenna. Polarisation or Faraday fading results from temporal changes in the polarisation of the incident wave brought about by the time variations of the phase differences between the characteristic modes. We note in passing that Faraday fading is not the only mechanism which causes the received signal to fluctuate. In particular, the ionosphere usually possesses several distinct layers, each of which may provide a path connecting the transmitter to the receiver. As the layers vary in time, so signals propagating via the corresponding paths will interfere, resulting in fading at the receive antenna. Of course the presence of the magnetic field splits each of these layer-defined paths into its characteristic modes.

The degradation of an HF skywave communication channel caused by fading can be reduced by diversity reception. Spatial diversity of the receive antennas is normally employed to mitigate interference fading while polarisation diversity is used to counter the effects of the Faraday fading.

To counter polarisation fading, it is necessary at the very least to avoid situations where the incident signal polarisation is close to being orthogonal to the polarisation state of the receiving antenna. One way to do this is to employ two or more orthogonally-oriented but singly polarised receive antennas, and select the output from the antenna which, at any instant, is yielding the strongest signal because its polarisation state is closest to being aligned with that of the incident wave. This approach can be implemented with simple conventional antennas.

A superior approach is to measure the electric or magnetic field vector of the incident wave. This maximises the output signal whilst affording new possibilities for retrieving information encoded in the polarisation state, including direction-of-arrival and the mode of propagation. In order to make this kind of measurement, the antenna must be able to sample the electromagnetic field without appreciable distortion or bias; deficiencies which to greater or lesser extent are present in existing polarimetric antennas.

Traditional mutually orthogonal tri-axial loop antennas (i.e. NS and EW loop plus a waist loop) used for polarisation diversity have distributed parameters with respect to ground that are not consistent between the three loops. This asymmetrical characteristic adds complexity to the analysis of the received signals and reduces sensitivity. Further, the distributed inductance (L) and capacitance (C) of each loop form a resonant circuit limiting the loop's usefulness for broadband work. The benefits of a polarimetric array prompted the decision to

seek a solution to the ground symmetry problem and the resonance caused by its distributed parameters.

This paper describes the development of a co-located tri-axial ground-symmetrical broadband receiving twin-loop antenna array for polarisation measurements in the HF band. In order to understand the design of the broadband twin-loop receiving antenna which is used in the Giselle design, it is first necessary to have a working knowledge of basic loop theory. This includes:

- how a single turn receiving loop antenna works,
- how various configurations of multi-turn receiving loop antennas work and their limitations,
- peak and dip in a broadband receiving loop's frequency response caused by non-uniform currents flowing throughout the length of the loop's conductor creating standing waves,
- degradation of the loop's classic figure of eight pattern by imbalances in the loop with respect to the ground (vertical antenna effect),
- degradation of the loop's classic figure of eight pattern through the *E* field causing a current to flow in the connecting co-ax cable's outer braid used between the loop and its receiver, and finally,
- construction techniques employed to counter degradation of the loop's null caused by the vertical antenna effect and the co-ax feed line.

Readers who are not familiar with some of the above dot points may wish to first read *Appendix A* on basic loop theory.

1.1 Initial Parameters for the Design of the Loop, Bandpass Filter and RF Amplifier

Small broadband loop antennas are insensitive by their nature and are usually made acceptable over a narrow band by bringing them to resonance at the wanted frequency thus multiplying the induced voltage by the circuit Q. It is intended that the loop antenna design under consideration be non-resonant and cover as much of the HF band as possible.

Traditional loop antennas have distributed L and C that form a resonant circuit and this is seen as a localised peak in the loop's response. The distributed L and C can be transformed into a transmission line thus negating the peaking effect of resonance.

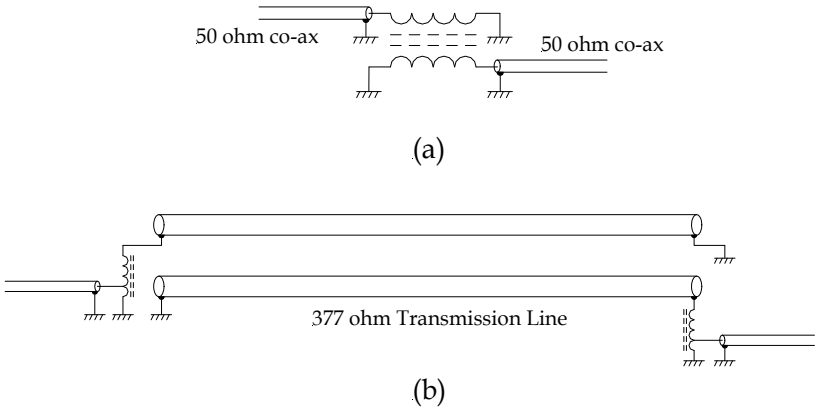

Figure 1: Progression from a twisted pair toroidal type transmission line transformer to an open parallel wire transmission line

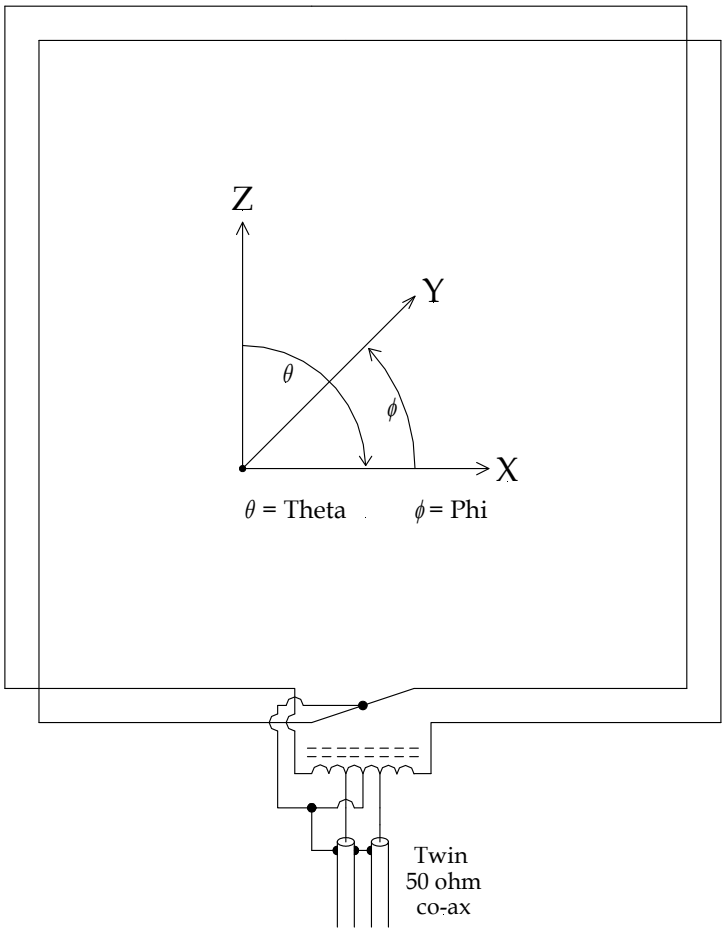

Figure 2: Prototype twin-loop antenna based on an open parallel wire transmission line

Figure 1(a) shows a typical broadband 1:1 transmission line transformer wound on a powdered iron toroid using a twisted pair of fine insulated wire with a Z_o (characteristic impedance) the same as the co-ax cable. In Figure 1(b) the powdered iron material constraining the lines of magnetic flux has been removed. The twisted pair has been replaced with two lengths of 6.35 mm diameter aluminium tubes spaced to give a Z_o of 377 Ω, the same as free space. RF autotransformers were used to match this transmission line to the 50 Ω co-ax. The parallel tubes were bent at right angles in four places forming two parallel square loops. The two autotransformers were combined into one balanced transformer, see Figure 2.

The 377 Ω impedance for the parallel wire transmission line from which the loop antenna was made was chosen purely as a starting point. This value will be modified as the design of the loop is developed and a better understanding of its characteristics are realised. Balanced shielded feed lines, twin 50 Ω co-ax between the loop and the amplifier box and twin 75 Ω co-ax between the output of the amplifier and the remote receiver, will be used to manage unwanted induced currents in the co-ax's outer braid.

A 2-30 MHz balanced filter was designed by modifying an unbalanced 50 Ω filter into a balanced 100 Ω. The highpass side of the filter is needed to attenuate the strong AM radio stations, especially for large loops. This highpass filter also performs another function. The field intensity distribution of a cloud to ground lightning strike peaks at approximately 9 KHz with a f^{-1} frequency dependence from 100 KHz to 2 MHz, f^{-2} between 2 MHz and 10 MHz, and f^{-5} above 10 MHz [23]; (f^{-1} = 6 dB/oct; f^{-2} = 12 dB/oct;… f^{-5} = 30 dB/oct.). From this it can be seen that the majority of energy radiated from a ground strike lies below 2 MHz. It is a simple matter to isolate this energy from the input of the RF amplifier by installing a 2 MHz highpass filter between the loop antenna and the amplifier's input. This filter should have a low out-of-passband impedance effectively placing a short circuit across the antenna thus preventing the generation of large induced voltages that have the potential to cause permanent damage to the amplifier's active devices. The lowpass side of the filter attenuates VHF television and FM broadcast stations. Both the highpass and lowpass filters are needed to prevent these strong stations from generating nonlinear distortion products within the band of interest. These two filters have been combined into one complex 100 ohm balanced filter.

The long run of twin co-axial cable between the loop antenna and the receiver will have insertion losses in the order of a few dB depending upon the cable's length and characteristics. An RF amplifier is therefore needed to prevent the cable losses from increasing the antenna's noise figure and hence degrading the loop's sensitivity. The RF amplifier was based on a push-pull design using a matched pair of BFG235 bipolar transistors. The push-pull configuration inherently suppresses the amplifier's internally generated even order distortion products. A resistive feedback amplifier was chosen because it is easier to mass-produce and has quite acceptable specifications for its intended application. The gain of the transistors has been kept as high as possible to minimise the degrading effects the feedback network has on the transistor's noise figure. Feedback, especially resistive feedback, degrades the transistors inherent noise figure. The lower the designed gain, the greater is the required feedback and the greater the increase in the device's noise figure. The 22 dB of gain was a compromise between the devices inherent gain/bandwidth product and the feedback's ability to maintain

the 22 dB of gain across the required bandwidth. The transistors inherent distributed C has the effect of decreasing the devices input impedance (the Miller effect in amplifiers) as the frequency is raised. Inductors have been placed in series with the transistor's emitter resistors to help stabilise the push-pull amplifier's input impedance to a balanced 100 Ω resistive. The down side of these inductors is a reduction in gain of about 1 dB at the high end of the band. An amplifier having a non-varying resistive input impedance across the band of interest was considered more important than a constant gain. The constant resistive input impedance minimises any capacitance seen at the amplifier's input from being reflected across the loop's terminations creating unwanted resonances with the loop's distributed inductance. The transistors dissipate 1.3 watts of heat each so measures have been taken to transfer this heat into the metal of the amplifier box. This heat then dissipates via convection currents in the outside air.

Standard three terminal voltage regulators are notoriously noisy, their dynamic output impedances for the noise generator being typically less than an ohm. It is very difficult to attenuate noise emanating from such a low dynamic impedance. This noise usually manifests as an increase in amplifier noise figure as the frequency is lowered from approximately 10 MHz. A special low noise voltage regulator was designed to prevent the degradation of the amplifier's noise figure at the lower frequencies.

2. The Loop Design

Figure 3 is the NEC-2 simulated response of a single turn 1 m/side square loop antenna with a 377 Ω termination; notice the large depth of null at 90 degrees in (B). This is a loop antenna's ideal response and is the benchmark that will be used. A major problem with receive loop antennas whose physical dimensions are small when compared with their operating wavelength is their lack of sensitivity. The left hand side of the graph shows the loop's circulating current in amps for a plane wave of 1 V/m. Multiplying this current by the loop's terminating impedance gives the loop's output voltage. Adding extra turns in an effort to improve the loop's sensitivity usually results in the degradation of the depth of null and a wandering of the nulls spatial location with frequency.

NEC-2 was used to simulate a two-turn box loop of 1m per side, 74 mm between the two turns and with 6.35 mm diameter conductors. Figure 4(A) is a visual representation of the loop antenna. The dot at the bottom of the loop shows the location of the 377 Ω resistive load. Figure 4(B) is the NEC-2 simulation of the receive pattern response of this box style loop. If a vertical section is taken at the phi (90) position, then the bottom trace is the response at 2 MHz with 2 MHz increments on each successive trace up to 30 MHz at the top. Notice the poor depth of nulls becoming worse as the frequency is raised. Also notice the gradual shift in the nulls location with increasing frequency. The peak in the response of 0.00064 A can be seen at a frequency of approximately 16 MHz.

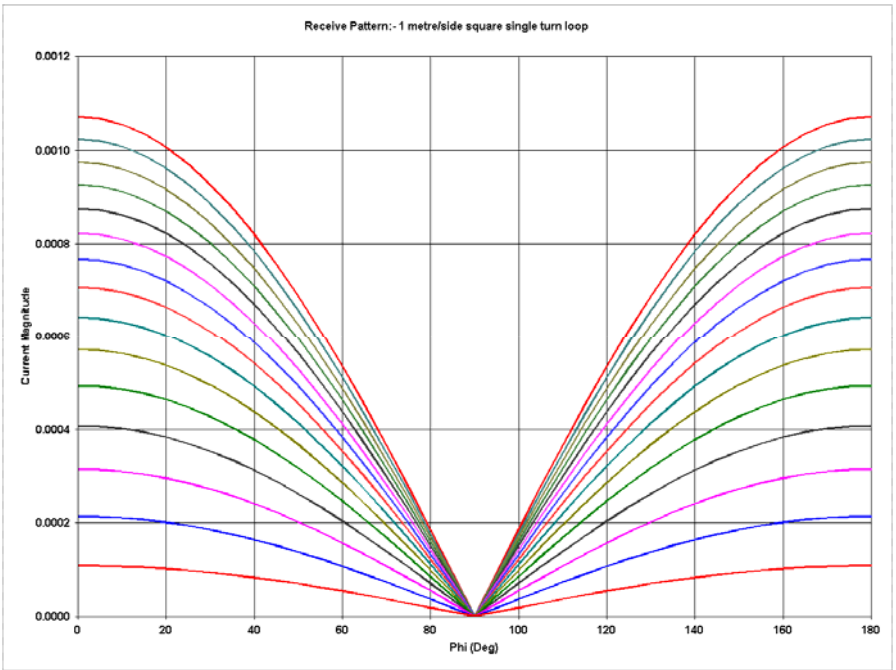

(A) Linear scale

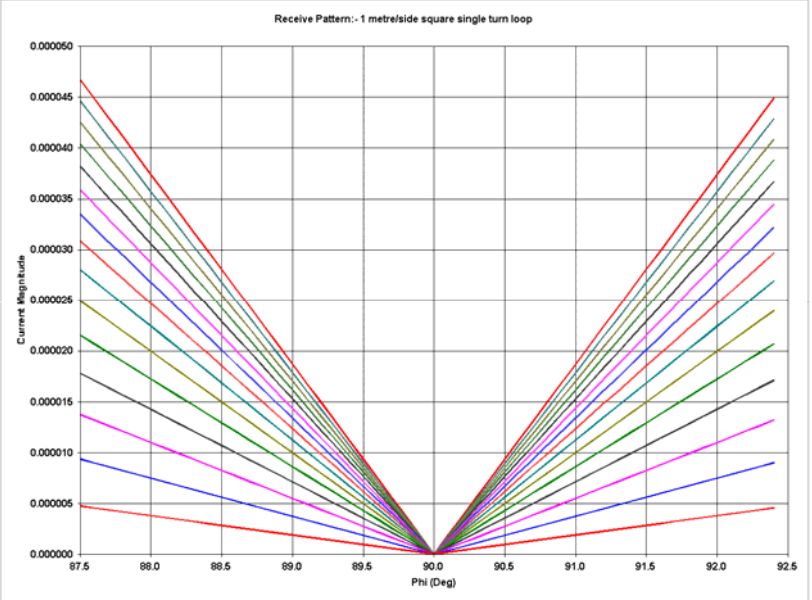

(B) The null at 90 degrees in more detail

Figure 3: NEC-2 receive pattern response of a one metre per side single turn square loop, 2 MHz at the bottom in 2 MHz increments to 30 MHz at the top

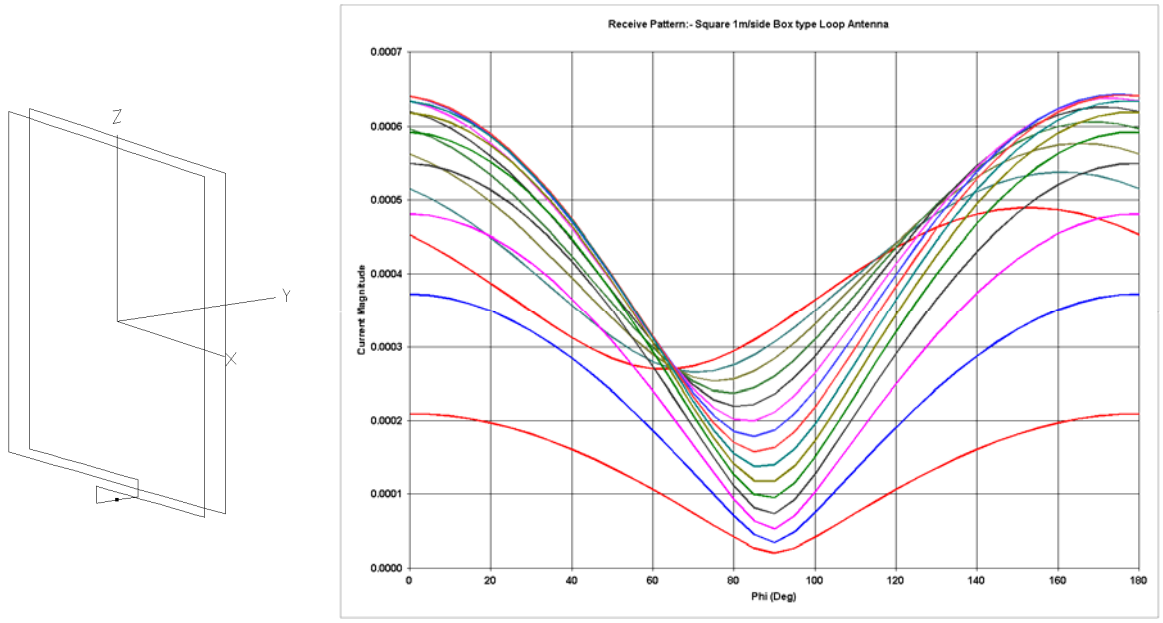

(A) (B)

Figure 4: (A) wire model of 1m/side two-turn loop box style antenna and (B) NEC-2 receive pattern response

2.1 The Cross Connected Twin-Loop Antenna

A crossover connection was added to the loop antenna, Figure 5(A). This crossover connection seen at the top of the loops displaces each of the two loops equally in the Y plane. Close examination will show the voltages induced into the two loops from a plane wave travelling in the Y direction are connected via the crossover network such that they are series opposing and hence cancel at the loop's output terminals. This was modelled on a 1 m/side twin loop using NEC-2 to see if the deep null could be restored in the two-turn loop. As can be see in Figure 5(B), the depth of null has been restored. There is also a peak in the response at approximately 14 MHz. This needs to be addressed but first the antenna design so far needs to be proven.

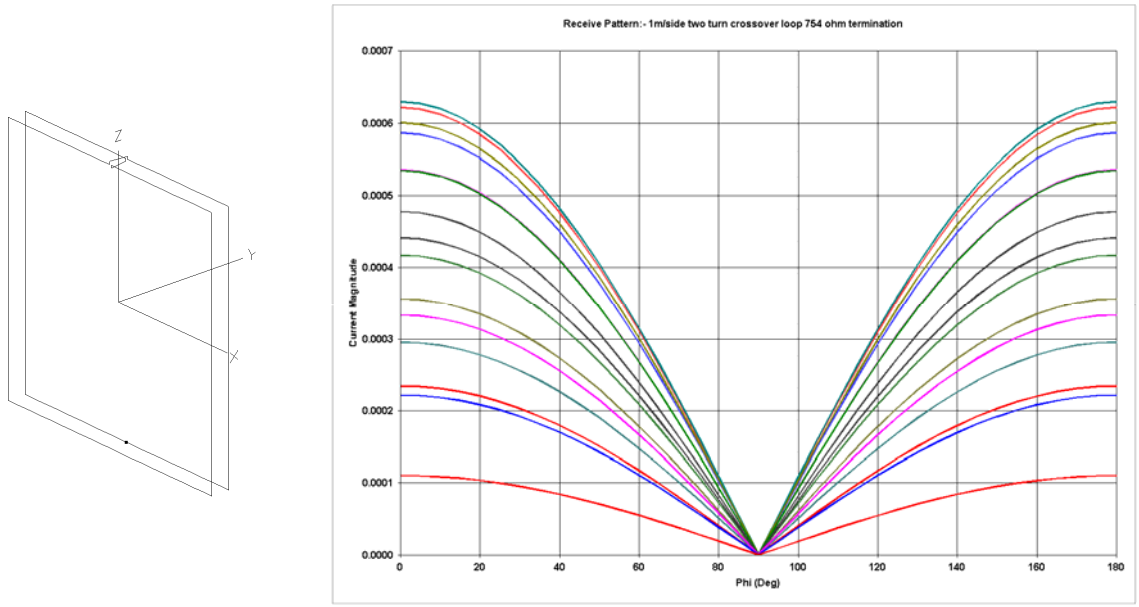

(A) (B)

Figure 5: (A) wire model of the two turn cross connected loop antenna and (B) NEC-2 receive pattern response with 754 Ω termination. The peak in the response (dark green trace) is at 14 MHz.

A 1.15 m/side loop antenna (1m long aluminium tubes plus 75 mm length of wire at each end connecting the tubes together) was built to test the twin-loop design using 6.35 mm diameter aluminium tubes with a spacing of 74 mm between turns. The crossover at the top of the loop was made using a length of 300 Ω TV ribbon which was given a 180 degree twist. The flat dielectric of the 300 Ω parallel wire transmission line ensures a constant distance between the wires throughout the twist maintaining symmetry. Also, the very thin wire of the ribbon relative to the diameter of the aluminium tubes ensure its induced voltages from a passing plane wave has minimal effect on the overall loop performance. RF autotransformers were used to step up the impedance of each half of the twin 50 Ω co-ax to 377 Ω. The total impedance presented to the loop terminals was 754 Ω. A length of twin RG316 50 Ω co-ax connects the balanced output of the loop matching transformer to a 100 Ω balanced 2-30 MHz filter used to band limit the loop's response. The band-limited signal was then feed to the balanced 100 Ω input of a low noise high intercept push-pull +22 dB gain amplifier. The balanced 150 Ω output form the amplifier feeds a long run of twin 75 Ω co-ax connecting the output of the loop antenna amplifier to the receiver.

The balanced co-axial feeds are part of the strategy to combat the distortion of the loop's classic figure-of-eight pattern. This is covered in detail in *Appendix A*. The balanced 150 Ω from the twin 75 Ω co-ax is converted to 50 Ω unbalanced at the receiver to feed its unbalanced R.F. input. The twin co-ax is also used to supply the push-pull amplifier with its D.C. power. Minimum nulls of –30 dB for ground wave signals at random frequencies across the HF band were measured with this 1.15 metre/side square loop antenna.

The antenna was externally excited from an elevated 5 m vertical monopole connected to the output of a signal generator and the field strength at the loop's location monitored with a R&S (Rohde & Schwarz) HE010 active *E* field probe. This field trial of the antenna showed a sharp resonance at approximately 14.5 MHz as can be seen in Figure 6 where the output signal showed substantial phase and gain changes. Local AM radio stations can also be seen as peaks at approximately 1.5 MHz.

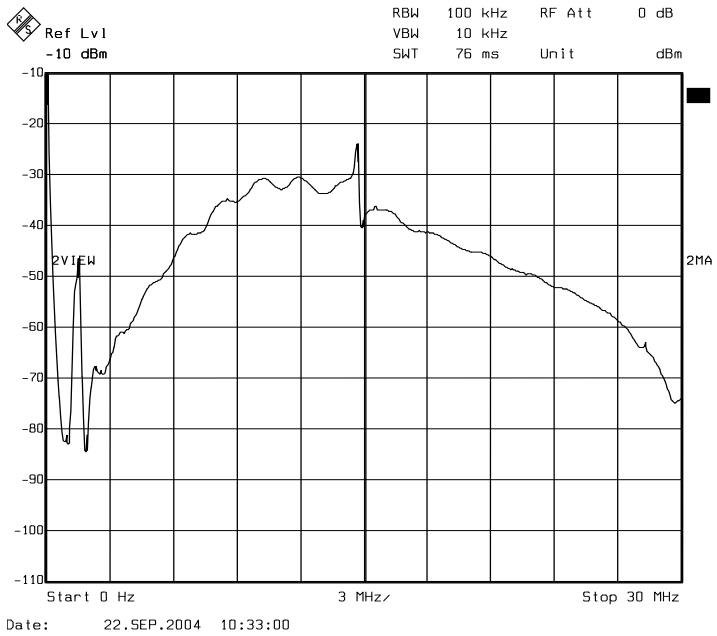

Figure 6: 1.15 m/side cross connected twin-loop antenna frequency response. Notice the resonance and gain change at approximately 14.5 MHz.

2.2 Analysing the Results of the Initial Field Trial on the Cross-Connected Twin-Loop using a Single Termination

Equation (1), (from *Appendix A* equation (A.7)) was used to generate the magenta graph seen in Figure 7. It should be noted that the exact magnitude of the induced voltage is dependant upon the loop terminating impedance and this has not been considered. Equation (1) was therefore used to predict the shape of the frequency response, that is, the approximate frequency of the broad peak and the subsequent first dip. These indicate the useful operating frequency range for a given loop.

$$V_{O/C} = \left| 2ENh \sin\left(180\frac{sf}{300}\right) \cos\left(90\frac{(2h+2s)Nf}{vn300}\right) \cos\phi \right| \tag{1}$$

where: $V_{O/C}$ = relative instantaneous loop open circuit output voltage (volts)
E = instantaneous magnitude of oscillating E field (volts/m)
h = height of rectangular loop (m)
s = width of rectangular loop (m)
N = number of turns in loop
n = number of evenly spaced terminating resistors
f = frequency of oscillating E field (MHz)
ϕ = angle between the loop plane and direction of travel of oscillating E field.
v = 0.925 = velocity factor for the 1.15 m/side square loop which brings the calculated frequency of the first null into agreement with NEC-2 and observed results.

Note: All sin and cos terms are in degrees and not radians as is usually expected.

As can be seen there is relative agreement between the magenta plot of Figure 7 (shape of the loop response versus frequency predicted by equation (1)) and the measured results of the loop antenna in Figure 6.

Having a single 754 Ω termination for the two turns was seen to be the cause of the dip at 29.5 MHz and the resonance just below 15 MHz. These two frequencies are related and best explained using transmission line theory. But first, the transmission line needs to be distorted into a form more easily recognised by the RF practitioner.

Figure 8(A) is representative of the current loop in which the two turns have been unfolded and formed into one large circular turn. In (B) the termination and its diagonally opposite point have been pulled apart until finally in (C) the single turn loop forms a parallel wire transmission line with the termination at one end and a short circuit at the other. The standing wave pattern can now be more easily understood.

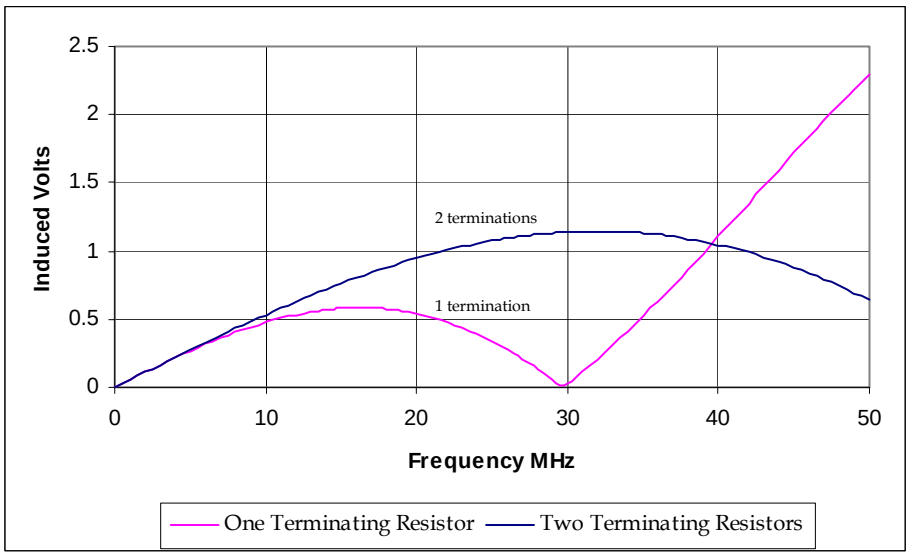

Figure 7: The calculated frequency response, equation (1), of the 1.15 m/side square loop with only one terminating resistor for the two loops and two terminating resistors each placed between the finish of one loop and the start of the other

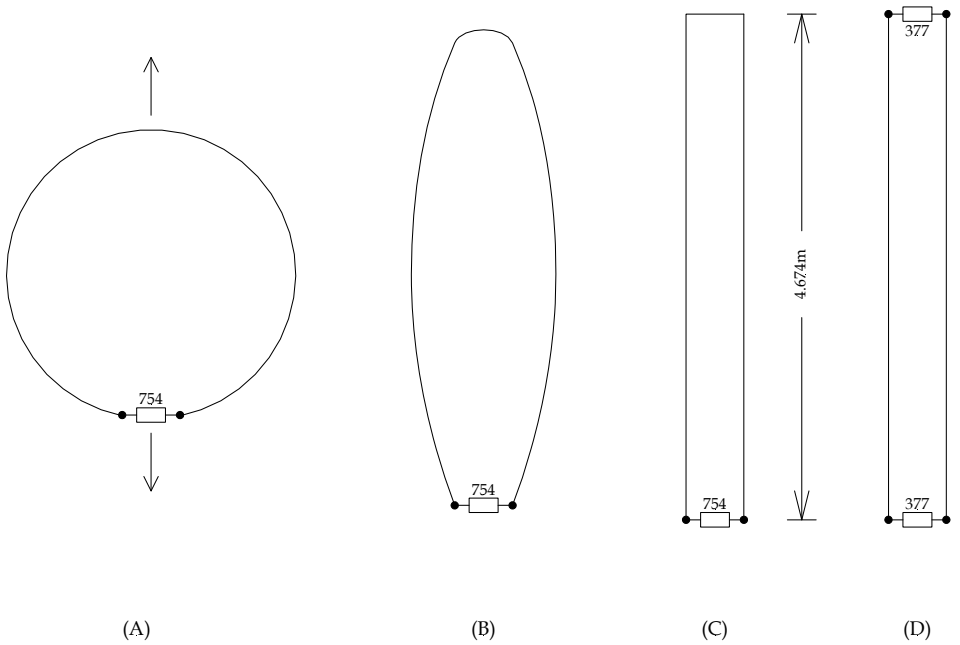

Figure 8: A single turn loop stretched apart at the termination and its diagonally opposing point until it forms a parallel wire transmission line

A shorted 0.25 λ transmission line will appear as a parallel resonant circuit across the resistively termination end. The total length of conductor in the two-turn loop is 9.348 m (8 rods and hook-up wire of 1.15 m long plus two lengths of wire 0.074 m long in the 300 Ω ribbon) therefore from the analogy of Figure 8, the length of the transmission line will be 9.348/2 = 4.674 m. Using equation (2) with n=4 the frequency at which this length of line appears 0.25 λ long is 14.84 MHz.

$$f_{MHz} = v\frac{300}{nl} \tag{2}$$

where: f_{MHz} = approximate resonant frequency caused by a standing wave pattern (MHz)
v = 0.925 = velocity factor as used in equation (1)
l = total length of equivalent parallel wire transmission line (m)
n = 2 for the dip in the response caused by a short circuit placed at the far end of a line length of 0.5 λ, or = 4 for the resonance seen at the peak in the response for a short circuit placed at the far end of a line length of 0.25 λ

This is the frequency where the short circuited 0.25 λ transmission line appears as a parallel resonant circuit across the termination end. A short circuit placed at the far end of a 0.5 λ transmission line appears as a short circuit at the termination end. Again using equation (2) this time n=2 the frequency at which this happens is 29.68 MHz or twice the frequency where the shorted line appears parallel resonant. The line now appears as a series resonant circuit across the termination causing the observed dip in the response.

These in band resonances can be suppressed by removing the short at the far end of the line and replacing it with a resistive termination, Figure 8(D). The twin-loop now mimics a

transmission line with a termination at both ends. The differential inductance and capacitance of the two turn loop were measured as L_{diff} = 6.16 uH and C_{dist} = 35 pF. The loop matching circuit was reconfigured so that the balanced output of each loop was connected to its own unbalanced 50 Ω co-axial line, see Figure 9. Careful attention was paid to transformer phasing to ensure the signals from the twin-loop's two terminations appear differentially between the two co-axial centre conductors.

Equation (1) was used to approximate the shape of the loop's response to an externally applied *E* field when the loop is terminated with two evenly displaced resistive loads. The length *l* of conductor will now be that which exists between terminations i.e. 1.15 x 4 + 0.074 = 4.674 m. The total open circuit output voltage from the two loops will therefore be the summation of the voltages from each termination or 2 *V*. This is seen as the dark blue plot in Figure 7. As can be seen the dip in the 0.5 λ response has been shifted to 59.36 MHz or twice the previous dip frequency. The increase in antenna gain at the upper frequency end of the HF band is self-evident.

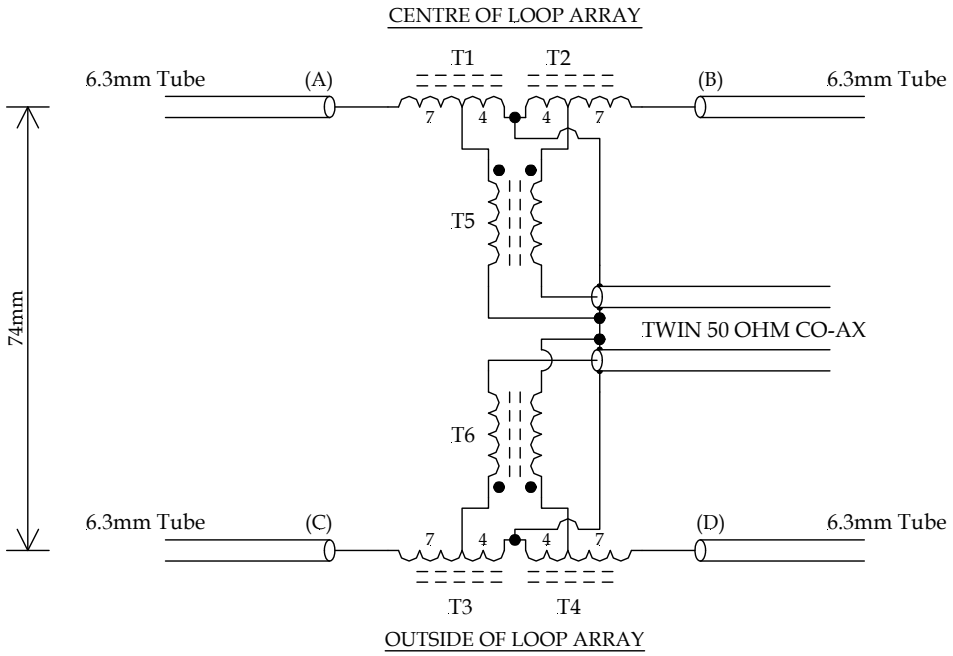

Figure 9: Schematic of the loop matching network

2.3 Field Tests on the Dual Terminated Twin-Loop Prototype Design

Figure 10 is the field response of the HE010 *E* field probe used to measure the strength of the *E* field at the location of the loop being tested. A 2 MHz highpass filter was needed on the HE010 probe's output to suppress the AM stations preventing them from overloading the test instrument. Figure 11 shows the twin-loop antenna's response carried out under the same conditions as that of Figure 6. Note the improvement in the response in the upper part of the

HF band. The loop's depth of null was not affected by the change in the way the loop was terminated. This design can now be used as the basis of a tri-axial ground-symmetrical loop for the HF band.

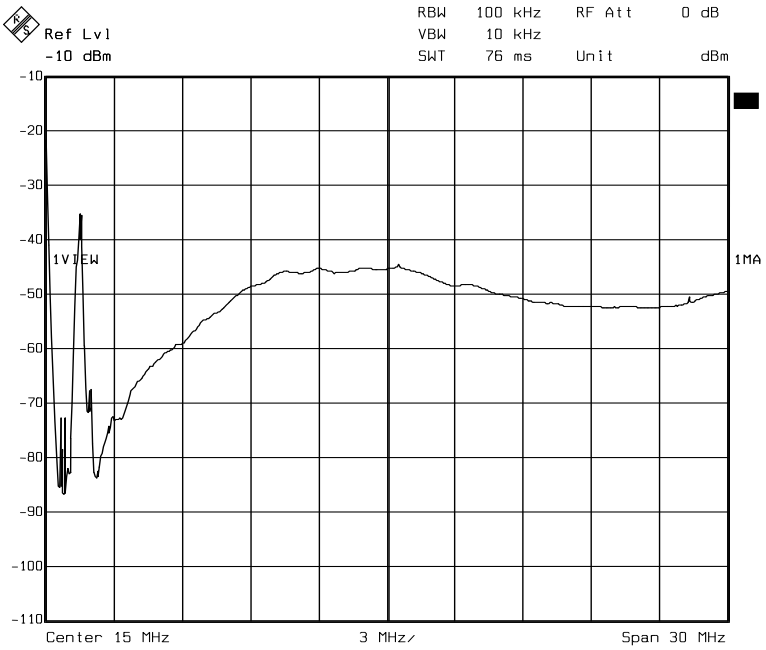

Figure 10: Frequency response of the externally excited HE010 E field probe at the same location as the twin-loop

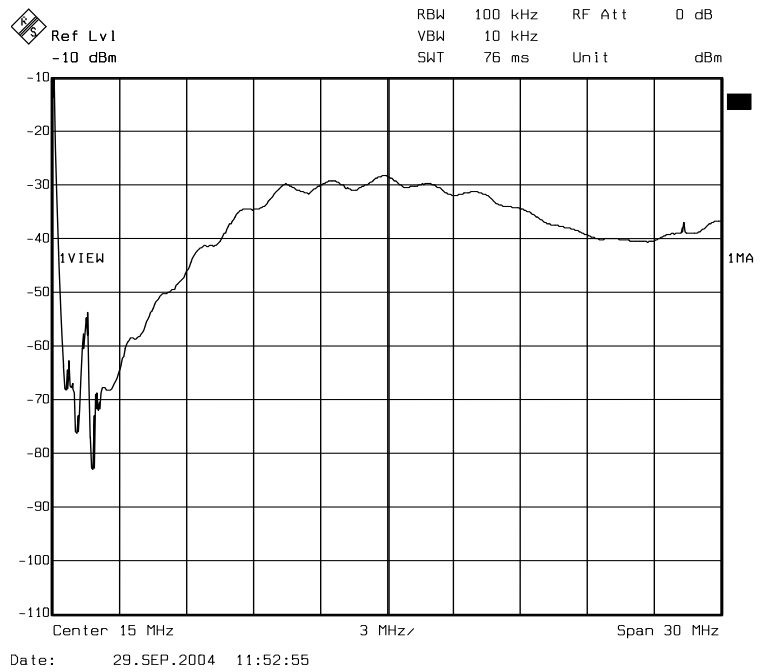

Figure 11: Frequency response of the externally excited 1.15 m/side cross connected twin-loop antenna with two independent loads between the turns of the loop

3. The Giselle Antenna

The name Giselle is an extension of the acronym GSL short for **G**round-**S**ymmetrical **L**oop.

A 1.15 m/side tri-axial loop antenna, Figure 12, based on a regular octahedron was chosen because the three loops thus configured have the same distributed parameters between each other and between the three orthogonal loops and ground. The loop's crossover points are at the four corners of the three loops. 1 mm PTFE insulated wire was used to connect the 6.35 mm diameter aluminium tubes at the corners of each of the loops to keep capacitive coupling between the orthogonal loops at the crossovers to a minimum preserving the loops' depth of nulls. The loops feed points are at the middle of each arm of the three sides of the three loops used to form an equilateral triangle. This triangle forms the base of the octahedron and is parallel to the ground and elevated above it by one metre via a length of 160 mm diameter PVC water pipe. Minimum nulls of –30 dB have been measured for ground wave signals across the HF band.

The antenna noise figure (f_{dB}) (see *Appendix B* for its derivation) was calculated using the following equation:

$$f_{dB} = 10\log_{10}\left(\frac{R_L D\lambda^2}{480\pi^2 h_e^2} \bullet \frac{n_o}{G\,k\,T_o B}\right) \tag{3}$$

and from a knowledge of;

- the *E* field strength obtained from the HE010 *E* field probe antenna, Figure 10, and the manufactures published antenna factor of 17 dB for the antenna,
- the response of one of the three loops in the Giselle antenna to the *E* field paying particular attention to the loops orientation to the transmit antenna, Figure 11. (A correction factor of 1.2208 was applied to the voltage magnitude derived from Figure 11 to compensate for the 35 degree difference between the plane of the Giselle loop and the vertical transmit monopole antenna), and,
- the Giselle antenna system (loop plus +22 dB gain loop amplifier) intrinsic output noise level obtained from a measurement made by installing the antenna in a screened room to exclude any external fields.

Table 1 lists the results of equation (3).

Table 1: Calculated noise figure versus frequency for the 1.15 m/side square loop used in the Giselle antenna

Frequency MHz	Loop and Amplifier Noise Figure dB
2	45.04
3	36.05
4	35.05
5	30.52
6	26.88
7	22.7
8	19.63
9	16.1
10	16.87
11	16.21
12	17.28
13	13.09
14	13.04
15	8.92
16	11.05
17	10.12
18	8.6
19	8.85
20	8.23
21	8.99
22	8.7
23	10.18
24	11.6
25	12.18
26	10.84
27	8.8
28	9.02
29	6.89
30	9.85

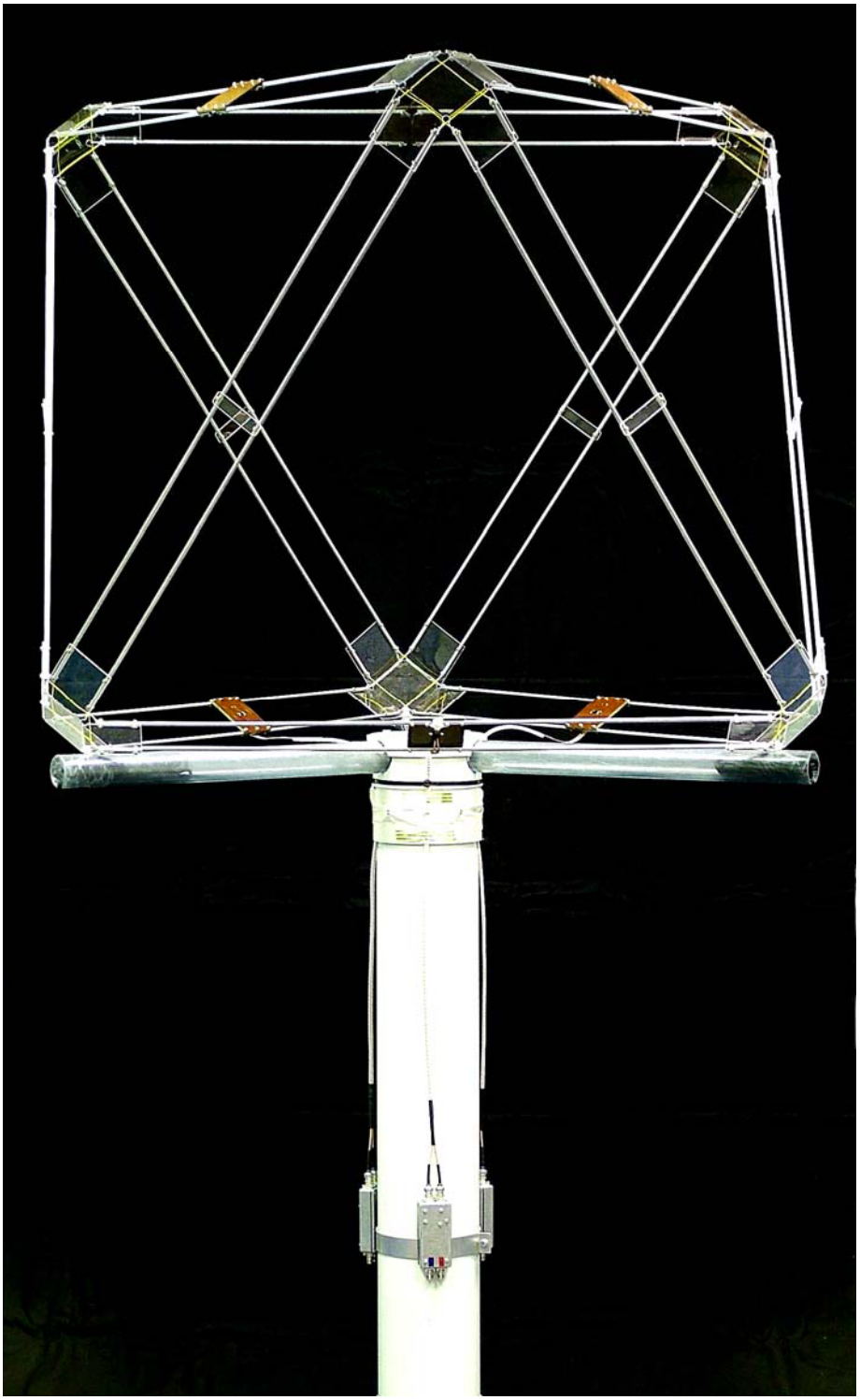

Figure 12: The fully assembled MKI Giselle antenna

3.1 Determining the Best Shape for the Loop

Armed with the knowledge gained through the construction of the MKI Giselle antenna, steps can now be taken to improve the design. First, the MKI antenna was based on a square. This was done for convenience and is not the ideal shape to maximise the gain of a loop using a given length of conductor. Equation (A.2) in *Appendix A* shows that the loop sensitivity is proportional to its area. Equation (4) (derived from information contained in [12, ch. 4] was used to carry out a quick analysis on the interior area of circumscribed regular polygons of a fixed 1 m perimeter. It shows that the closer the polygon resembles a circle, the greater is the enclosed area. Table 2 lists the results of equation (4) using an Excel spreadsheet for 1 m perimeter regular polygons where n= 3 to 10 with the final entry of a 1 m perimeter circle.

$$A = \frac{l^2}{4n\tan\left(\frac{180}{n}\right)} \tag{4}$$

where: A = area of polygon
n = number of sides of regular polygon
l = length of perimeter of regular polygon
Note: angles are in degrees

Table 2: Interior area of various regular circumscribed polygons with a perimeter of 1 metre

Number of sides	Area (m^2)
3	0.048113
4	0.062500
5	0.068819
6	0.072169
7	0.074161
8	0.075444
9	0.076319
10	0.076942
Circle	0.079577

The eight sided polygon has a special interest as it has pairs of parallel sides at right angles to other pairs. This would make it easier to construct orthogonal loops. Using the data from Table 2, the expected increase in gain (dB) from changing the shape of the loop form a square to an octagon using the same length of conductor is:

$$20\log\left(\frac{0.075444}{0.0625}\right) = 1.63_{dB} \tag{5}$$

The difference in gain (dB) between an octagon and the ideal shape of a circle is:

$$20\log\left(\frac{0.075444}{0.079577}\right) = -0.46_{dB} \tag{6}$$

With the octagonal shape being only 0.46 dB less sensitive than the ideal shape of a circle, the octagonal loop will be adopted.

3.2 Increasing the Loop's Differential Inductance

Measurements carried out on the dual terminated square twin-loop receive antennas with sides ranging from 0.5 m/side to 1.15 m/side have indicated that it is the differential inductive reactance relative to the value of the termination resistors that dictates the low frequency cut-off in the loop's response. The straight two-turn solenoid wound inductance, which is generally much higher in value, appears to be made ineffective through the use of two equally spaced terminations. *Appendix C* discusses the difference between these two inductances.

The lower –3 dB cut-off frequency of the twin-loops in the Giselle antenna can be approximated by calculating the frequency where the loop's distributed differential inductive reactance equals one of the loop's terminating resistances. The twin-loop is viewed more as a parallel wire transmission line with a termination at each end than as a two-turn solenoidal coil with two evenly placed terminations. This will become clearer as the twin-loops characteristics are eventually examined.

$$f_{-3dB} = \frac{R}{2\pi L_{dist}} \tag{7}$$

where: L_{dist} = loop's measured differential inductance (H)
R = loop's terminating resistance (Ω)

The MKI antenna had a measured differential inductance of 6.16 uH. With a termination resistance at both ends of the transmission line of 377 Ω, the lower –3 dB cut-off frequency using equation (7) was 9.7 MHz. It is envisaged that the final design of the loop will cover the whole of the HF band. The low frequency response will therefore need to be extended either:

- by lowering the loop's terminating resistance which would also in turn lower the loop's sensitivity or,
- by increasing the loop's differential inductance.

Loop antennas are insensitive by their nature, decreasing the terminating resistance will not be considered.

The differential inductance L_{diff} of a pair of parallel conductors can be calculated by [11, pg. 363]:

$$L_{diff} = 0.004 l \left(\ln \frac{D}{r} + \frac{1}{4} - \frac{D}{l} \right) \tag{8}$$

where: L_{diff} = differential-mode inductance of parallel conductors (μH)
l = length of parallel conductors (cm)
D = distance between centres of parallel conductors (cm)
r = radius of parallel conductors (cm)

This inductance is the lumped element equivalent seen in shunt with the two terminations. From equation (8), the three variables that can be manipulated to increase the L_{diff} are,

- distance between the conductors (D),
- the length of the parallel conductors (l), and
- the radius of the conductors (r).

The twin-loop's differential inductance can be increased by increasing the area of the loop or, to look at it another way, by adding more length (l) to the parallel wires. This in turn would also increase the loop's sensitivity. Increasing the spacing (D) between the two loops would also increase the differential inductance appearing between the two turns of the loop. Increasing the spacing increases the volume of space in which the loop occupied. This too would increase the loop's sensitivity.

With the octagonal shape being adopted, the logical distance between the two parallel octagonal loops is the length of one of the sides of the octagon. Constructing three mutually orthogonal loops using these guidelines soon reveals the natural symmetry of the Small Rhombicuboctahedron, Figure 13. The total length of 0.66 m for one of the sides of the octagonal loop, which is also the distance (D) between the parallel loops, was dictated by the width of the double doors used to gain entry/exit to the RF Laboratory where the antenna is to be constructed and initially tested. 5 mm radius (r) aluminium tubes were chosen as a compromise between keeping the distributed capacitance between orthogonal loops to manageable levels thus preserving the loop's depth of null, and the small increase in loop sensitivity that can be achieved through using large diameter conductors. The crossover network at the top of the loop was made from a 180 degree twist on a 0.66 m length of commercial 300 Ω TV ribbon. Measurements made on the L_{diff} (1034 nH) and distributed C (11.5 pF) of the 0.66 m length of ribbon revealed a characteristic impedance of approximately 300 Ω.

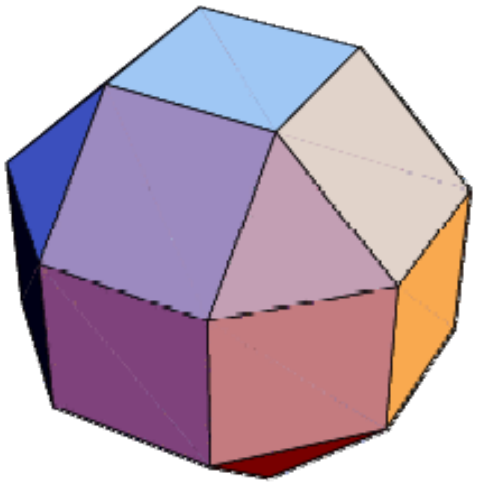

Figure 13: The Small Rhombicuboctahedron

The calculated differential inductance, equation (8), for such a loop where l=0.66 x 8=5.28 m is 10.58 uH, add to this is the measured L_{diff} of a 0.66 cm long 300 Ω ribbon of 1.034 uH gives an expected total differential inductance of 11.6 uH. Putting this expected value into equation (7) gives a lower cut-off frequency of 5.16 MHz. Low frequency compensation will be added to lower the cut-off frequency even further. This will be covered later. The Rhombicuboctahedron was constructed using aluminium tubes 0.637 m long with a diameter of 10 mm. 1 mm diameter PTFE insulated hook up wire was used at the crossover points of the orthogonal loops to keep unwanted capacitive coupling to a minimum. The total length of one side of the polygon, aluminium tube and hook-up wire at its ends, is 0.66 m/side. The total differential inductance of one of the twin-loop antennas in the array was measured to be 12.3 uH. The open circuit capacitance was also measured and found to be 47 pF. The other two orthogonal loops returned very simular results.

3.3 Choosing the Value of Termination Resistors

Simulating one of the twin-loops of the 0.66 m/sided Rhombicuboctahedron using NEC-2 revealed maximum power was dissipated in the termination resistors from a plane wave at 3 MHz when the total value of the resistors was 231.8 Ω. Also, it was found that maximum power was dissipated in the resistors at 30 MHz when the resistors totalled 2318 Ω. These reflect the values of the differential inductive reactance of the twin-loop at these frequencies. Several other frequencies were chosen at random to confirm that this was true across the band. The ideal value of termination resistors was found to be frequency dependent reflecting the value of the loop's differential inductive reactance. A fixed value compromise is the geometric mean of the two values at the extremities of the band of operation or $\sqrt{231.8 \times 2318} = 733$ Ω. This resistor is equally divided between the two terminations giving a value of 366 Ω each. This is very close to the 377 to 50 Ω matching network that has already been designed and used in the MKI antenna. The same matching network will therefore be used in the MKII design.

3.4 Parasitic Damping Resistors

Initial in-lab tests revealed a resonance at approximately 12.6 MHz, see Figure 14. In the top trace, the axis of the test loop (see *Appendix E* for details) is held at the geometric centre and in the same plane as the twin-loop. In the bottom trace, the test loop was rotated 90 degrees to measure the twin-loop's depth of null with frequency. The resonance at 12.6 MHz in the top trace looks very similar to the resonance created by the shorted 0.25 λ transmission line seen in Figure 6. No lengths of conductors in the loop that could be viewed in this way were long enough. Some other mechanism was responsible.

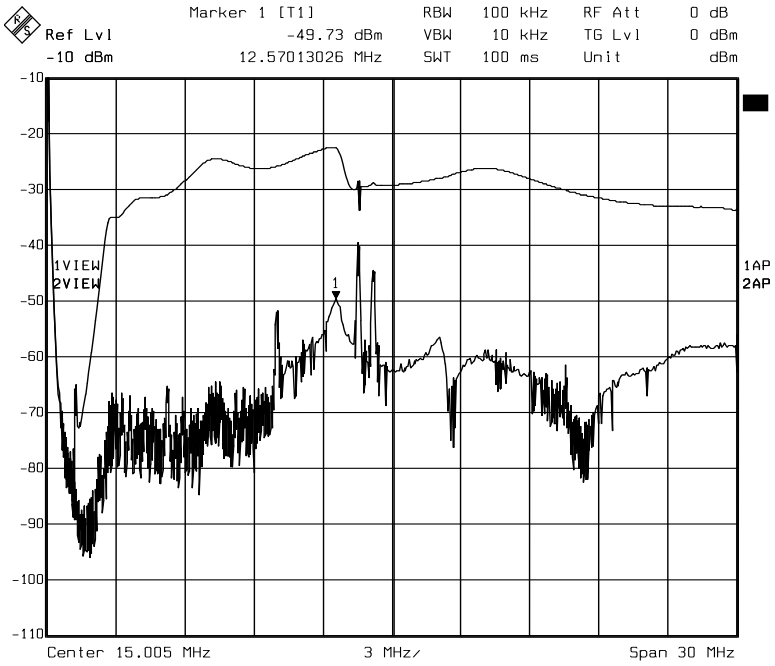

Figure 14: In lab test frequency response of the MK II tri-axial loop antenna. Note the resonance at approximately 12.6 MHz.

A length of transmission line with either one or both ends open or short-circuited is a resonant structure. A search of the geometry of the MKII loops revealed three identical unterminated (at either end) transmission lines capable of causing the resonance. Figure 16 is a simplified schematic of the tri-axial loop antenna. Again, as was done in Figure 8, the loops have been presented in a way that makes the transmission lines readily identifiable. The three terminations of the three loops that are closest to the ground have been held fixed in their position. The terminations at the other ends have been lifted vertically with a half twist on each dragging their respective conductors until a vertical structure of three terminated parallel wire transmission lines 5.94 m high is formed. This vertical structure is then cut vertically between a pair of parallel transmission lines and rolled out flat as seen in Figure 16. At first glance it would appear that all the parallel conductors have terminations at their ends. This is not so. There are three pairs of parallel lines that do not have any terminations at all. These are:

1. conductor pair B,B′ and C,C′
2. conductor pair D,D′ and E,E′
3. conductor pair F,F′ and A,A′.

Remember in 3 the structure was cut vertically and rolled out flat. This pair is the same distance apart as the other two pairs.

Equation (9) was used to generate the plot seen in Figure 15. Notice the very dampened version of the response in Figure 15 is seen in the top trace in Figure 14.

$$A = \tan\left(\frac{2\pi f l}{v300}\right) \tag{9}$$

where: f = frequency (MHz)
l = length of transmission line (m)
v = velocity factor of wave in transmission line

Equation (10) was used to calculate the expected frequency where the length of the line appears resonant, assuming a value of v=1 gives the resonant frequency as 12.6 MHz.

$$f_{MHz} = v\frac{300}{4l} \tag{10}$$

where: f_{MHz} = approximate resonant frequency (MHz)
v = 1 = velocity factor
l = 5.94 = total length of conductor between terminations which includes the length of the 300 Ω ribbon (m)

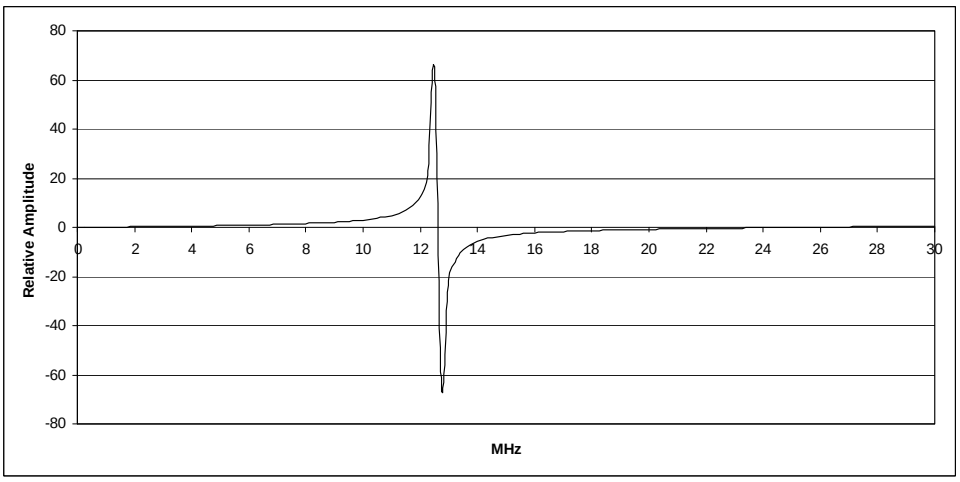

Figure 15: Plot generated by equation (9) showing the expected response of the resonance

Termination resistors cannot be placed at both ends of these lines. Such a solution would indeed tame the resonance at the cost of each line sharing its circulating current flow between all loops, thus reducing the loop sensitivity. Also, the sharing of current would distort the loop's figure of eight pattern. Only a single resistor can be used. Resistors of various values were tried at different points around the loop. A value approximately equal to the total value of termination resistors (750 Ω) was used in the twin-loop and found to give the best all round results. Figure 17 shows the placement of the resistors that gave the best improvement in the suppression of resonance while improving the depth of null.

Figure 18 shows both the improvement in the depth of null and the unwanted resonance. Notice the depth of null exceeds 30 dB for the majority of the HF band. The two discrete frequencies in Figure 18 (between 12 MHz and 15 MHz) are signals radiated by various pieces of equipment in the RF Lab to which the antenna is responding to. The other two orthogonal

loops must have the outputs of their amplifiers correctly terminated when doing depth of null measurements to maintain the balance in coupling between all three twin-loops.

3.5 Low Frequency Compensation

The low frequency cut-off point of the loop can be lowered through adding appropriate series capacitors giving the circuit the characteristics of a highpass filter. Converting the circuit into a highpass filter also aids in the suppression of the strong signals in the AM band. Figure 19(A) is a simplified schematic of the distributed inductance of a parallel wire transmission line in which 'k' is the coefficient of inductive coupling between the two parallel wires that gives rise to the differential inductance.

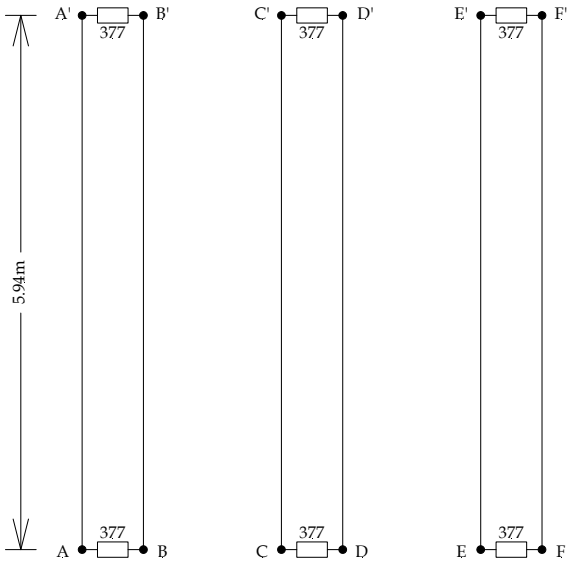

Figure 16: The unfolded, stretched and very much simplified schematic of the tri-axial loop antenna

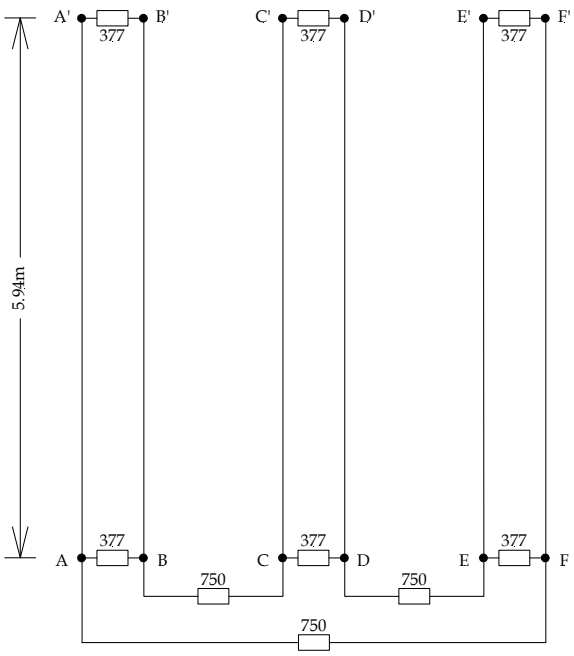

Figure 17: The unfolded simplified schematic of the tri-axial loop antenna showing the position of the parasitic suppression resistors

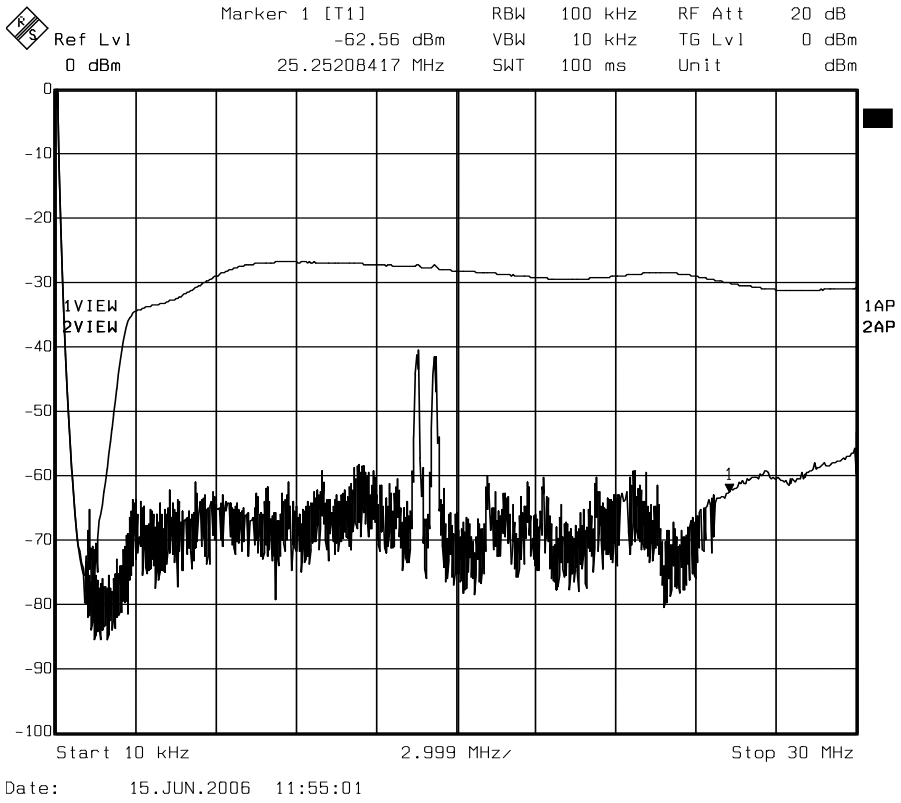

Figure 18: Response with the 750 Ω parasitic suppression resistors fitted. Notice the suppression of the parasitic at 12.6 MHz and the improvement of the null up until the upper end of the band. Loop bandpass filter and push-pull amplifier fitted.

In (B) the distributed inductance has been replaced with its low frequency equivalent lumped inductance. Equation (11) was used to calculate the value of series capacitor as seen in Figure 19(C).

$$C = \frac{L_{diff}}{R^2} \tag{11}$$

Figure 19(C) to (E) shows the progression form a single port to a two port un-balanced and finally to a two port balanced network.

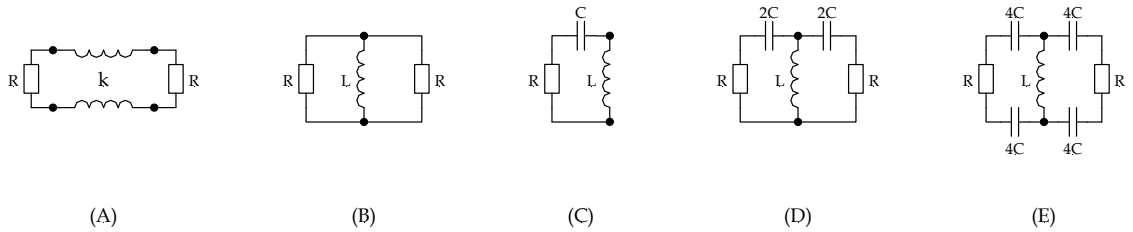

Figure 19: (A) distributed inductance of a parallel wire transmission line. Note the coefficient of coupling k between the two inductors, (B) lumped inductance equivalent, (C) capacitance required for a single port network, (D) capacitance required for an unbalanced two port circuit, (E) capacitance required for a balanced two port circuit

Equation (12) was used to calculate the value of the four compensation capacitors required in the two port balanced circuit.

$$C_{LFcomp} = \frac{4 L_{diff}}{R^2} \tag{12}$$

where: C_{LFcomp} = value of each of the four low frequency compensation capacitors required in the balanced two port network (F)
L_{diff} = low frequency differential inductance (H)
R = filter termination resistance (ohms)

Substituting 12.3 uH for L_{diff} and 377 Ω for R in equation (12) gives a value of 346 pF for the four low frequency compensation capacitors. The nearest preferred value of 330 pF will be used.

Equation (7) has already been used to show the low frequency cut-off point of the uncompensated loop is expected to be 5.4 MHz. The improvement in low frequency cut-off point with compensation can be calculated from filter theory [16, pg. 325] or [4 section 7, pg. 37] using equation (13). Figure 19(E) is a balanced highpass filter where L = 12.3 uH and 4C = 330 pF. Converting the value of 4C in (E), the balanced network, to the value of C as in Figure 19(C) gives 82.5 pF. Using this value of capacitance with the 12.3 uH inductance returns a compensated low frequency cut-off of approximately 2.5 MHz.

$$f = \frac{1}{4\pi\sqrt{LC}} \tag{13}$$

Figure 20 shows the improvement in the low frequency response when tested with the test loop in the RF Lab. Notice the general improvement in the response below approximately 9 MHz. Also notice the improvement in the steepness of the skirt below 3 MHz in the bottom pair of traces. There is also interaction between the highpass filter created by the insertion of the low frequency compensation capacitors and the 2 to 30 MHz balanced filter installed at the input to the balanced amplifier. This interaction is seen as a slight increase in ripple at the low frequency end of the passband.

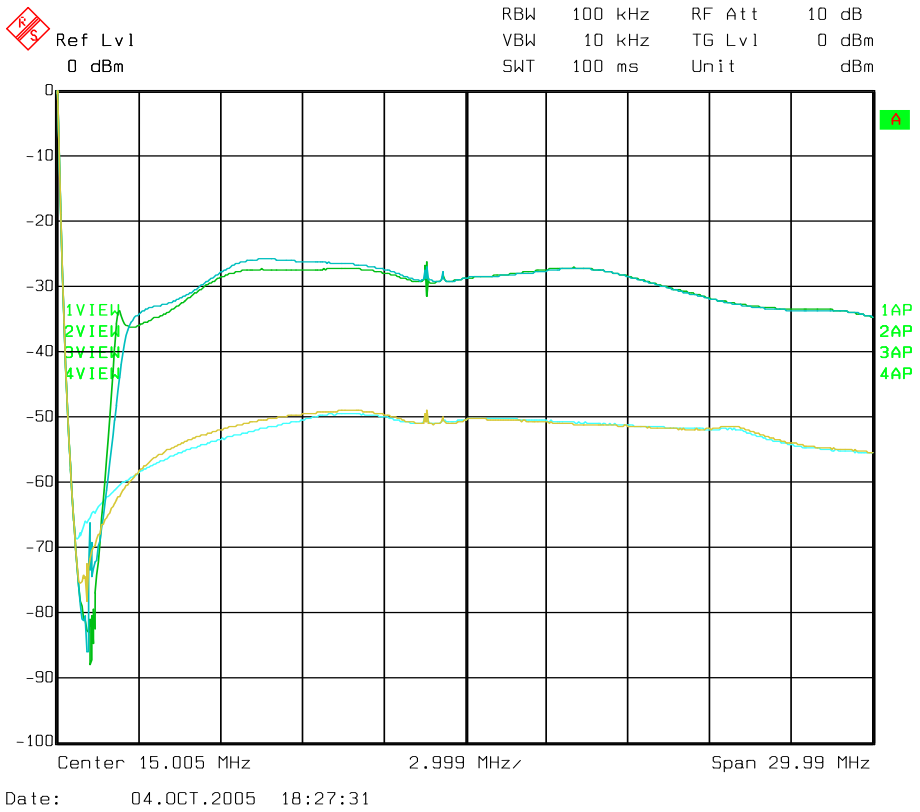

Figure 20: Top pair of traces - Green: amplifier and filter. No low frequency compensation. Blue: amplifier, filter and low frequency compensation applied. Bottom pair of traces - Cyan: no amplifier, filter and no low frequency compensation. Yellow: no amplifier or filter. Low frequency compensation applied.

3.6 Degradation of the Depth-of-Null Through Standing Waves

The voltage source in the Giselle loop is non-uniformly distributed throughout the length of conductor used to sense the travelling plane wave. This induced non-uniform distribution creates standing waves resulting in a fundamental upper frequency limit for a given length of conductor in the loop. Tests carried out on the depth-of-null with frequency revealed that when the total length of conductor between terminations in the twin-loop exceeded 0.5 λ of the plane wave's free space wavelength it degraded the depth-of-null in the loop to less than 30 dB.

Equation (14) was used to generate the plot of Figure 21. The zero crossing at approximately 25 MHz marks the frequency where line length between terminations is 0.5 λ of the wavelength of the plane wave in free space. The 180 degree change in phase above approximately 25 MHz is responsible for the degradation in the depth of null.

$$A = \sin\left(\frac{2\pi f l}{v150n}\right) \tag{14}$$

where: A = relative amplitude
f = frequency (MHz)
l = total length of conductor used in the twin-loop including both lengths of wire in the 300 Ω transmission line (m)
n = number of terminations in the loop
v = velocity factor of induced currents in antenna wire

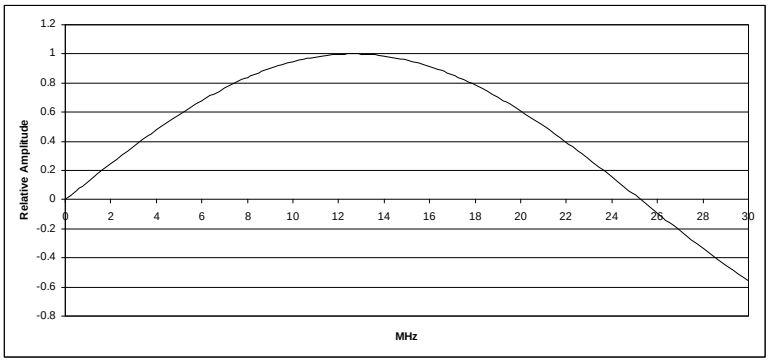

Figure 21: Plot generated using equation (14) of amplitude versus frequency in the twin-loop when excited by a plane wave in free space

Equation (15) is used to find the frequency beyond which the depth of null orthogonal to the plane of the loop and on the loop axis will start to degrade.

$$f_{\max} = \frac{v150n}{l} \tag{15}$$

where: f_{max} = maximum usable frequency before degradation of the null (MHz)
l = total length of conductor used in the twin-loop including both lengths of wire in the 300 ohm transmission line (m)
n = number of terminations in the loop
v = velocity factor of induced currents in antenna wire

For the current loop l = 16 x 0.66 m plus 2 x 0.66 m in the 300 Ω line = 11.88 m, n = 2 and v = 1 which returns a maximum upper frequency of 25.25 MHz. At frequencies above this, the test loop had to be slightly rotated away from the 90 degrees between the plane of the test loop and the plane of the twin-loop to achieve the deepest null. This can be seen in Figure 18 as an increase in magnitude of the bottom trace at frequencies higher than the marker at 25.25 MHz.

3.7 Field Test Measurements

To validate the design, the antenna was installed in the field and its response compared with that predicted from in situ measurements of field strength. Figure 22 shows the measured output of the HE010 *E* field probe at the location of the MKII antenna from which the strength of the *E* field was calculated. Figure 23 is the output of the MKII antenna and Figure 24 is the internally generated noise of the MKII antenna and amplifier as measured in a screened room.

The data from these plots were inserted into equation (3) to calculate the antenna's noise figure as tabulated in Table 3.

The ITU report [18] gives the following equation for calculating the expected man-made noise levels for a quiet rural European receive site for the HF band.

$$F_{am} = 53.6 - 28.6 \log f \tag{16}$$

where F_{am} = median value of man-made noise power in the 0.3 to 250 MHz frequency range for a short vertical lossless grounded monopole antenna (dB)

f = frequency (MHz)

These expected values are also tabulated in Table 3 for comparison. Note that the MK II Giselle antenna's intrinsic noise level is lower than the expected man-made noise for a quiet rural site. Also note the 10dB improvement in noise figure at 3 MHz from the MK I design as seen in Table 1. We note that noise levels in rural Australia have been reported to be as much as 10 to 15 dB lower than the values of equation (16). Adopting any of these as a reference, the internal-to-external noise ratio would be correspondingly decreased, but as the ITU report is regularly cited in reports and texts, it would seem the reference to which comparisons should be made.

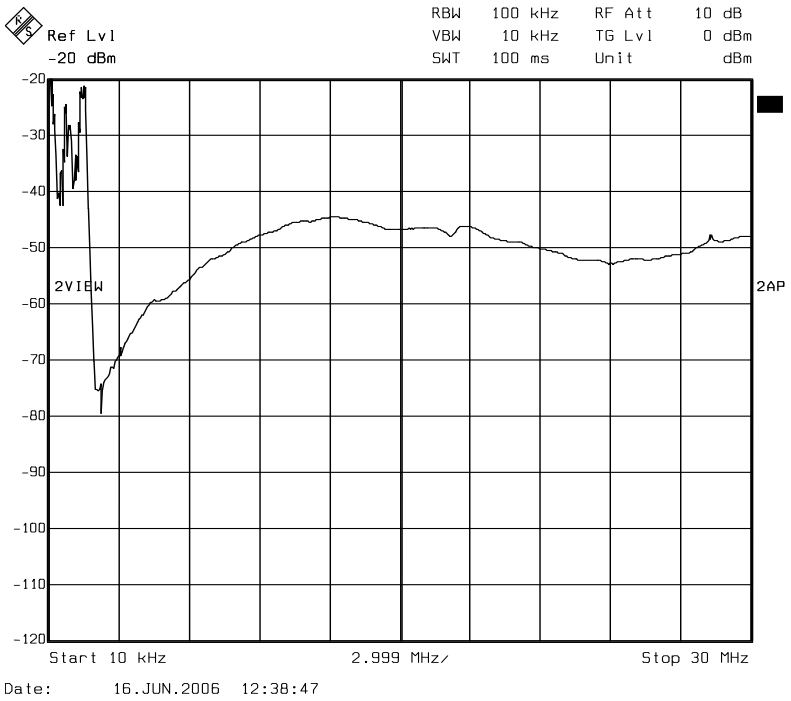

Figure 22: Measured output of the R&S HE010 E field probe at the test location

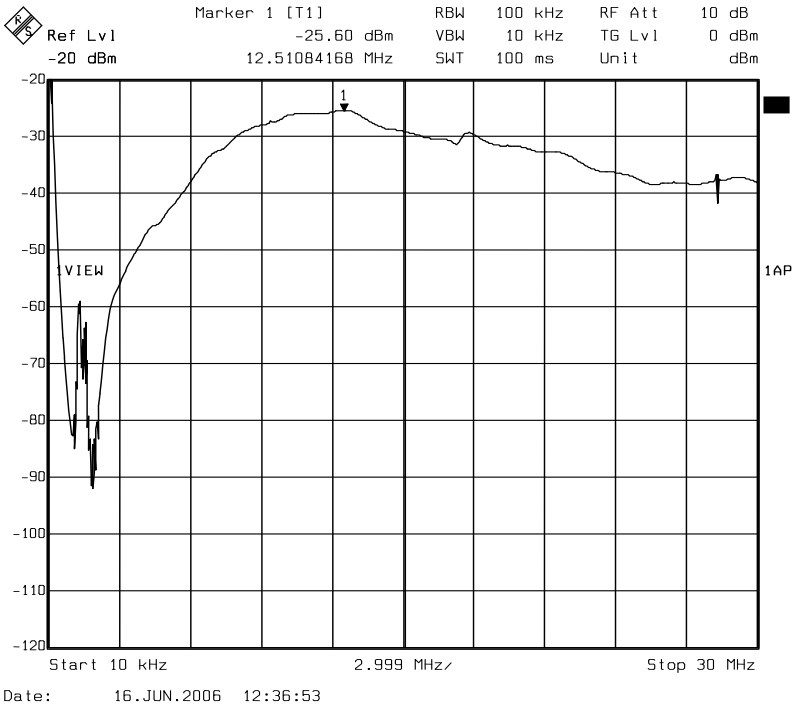

Figure 23: Measured output of the MKII under the same conditions as the R&S HE010 probe

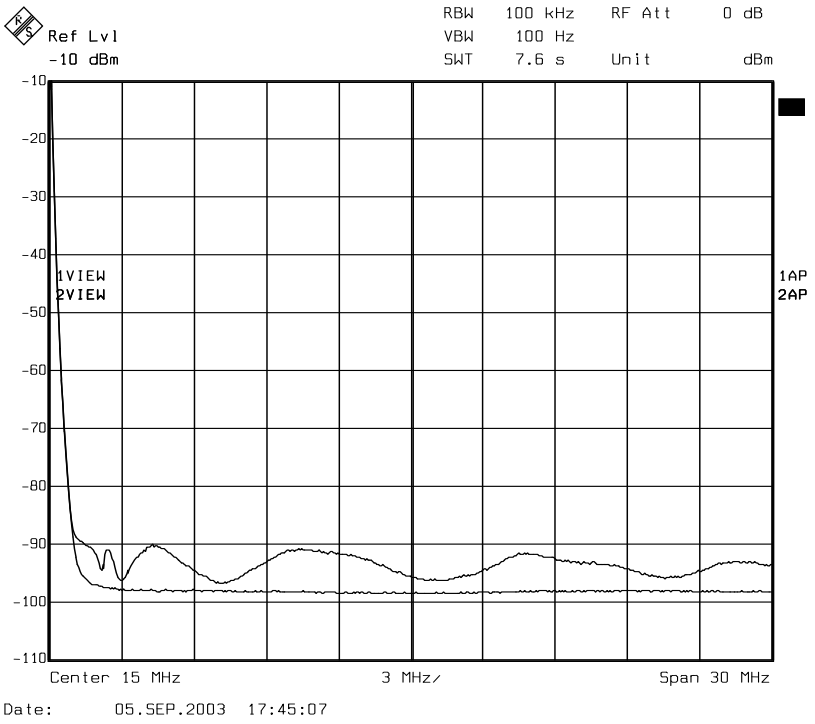

Figure 24: Top trace - measured internally generated noise at the amplifier output of the MKII antenna when installed in a screened room. Bottom trace - noise floor of the spectrum analyser.

Table 3: Calculated noise figure for the Small Rhombicuboctahedron loop antenna with amplifier and the expected median value of measured man made noise in a quiet rural receive site [18]

Frequency MHz	loop and amplifier noise figure dB	Expected median value of man-made noise dB
1		
2	46.6	44.99
3	26.34	39.95
4	21.8	36.38
5	16.83	33.61
6	14.64	31.34
7	12.87	29.43
8	10.66	27.77
9	9.47	26.31
10	8.71	25.0
11	7.8	23.82
12	7.35	22.74
13	5.72	21.74
14	5.28	20.82
15	4.46	19.96
16	5.38	19.16
17	4.08	18.41
18	3.89	17.7
19	4.23	17.03
20	3.63	16.39
21	3.48	15.78
22	3.45	15.21
23	4.59	14.65
24	4.4	14.13
25	6.41	13.62
26	6.03	13.13
27	6.57	12.66
28	7.56	12.21
29	6.49	11.77
30	6.79	11.35

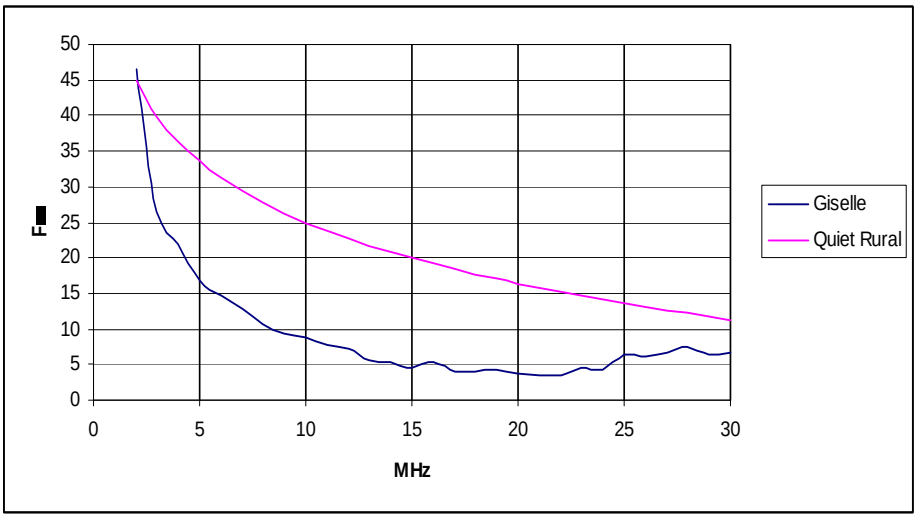

Figure 25: The data in Table 3 presented as a graph

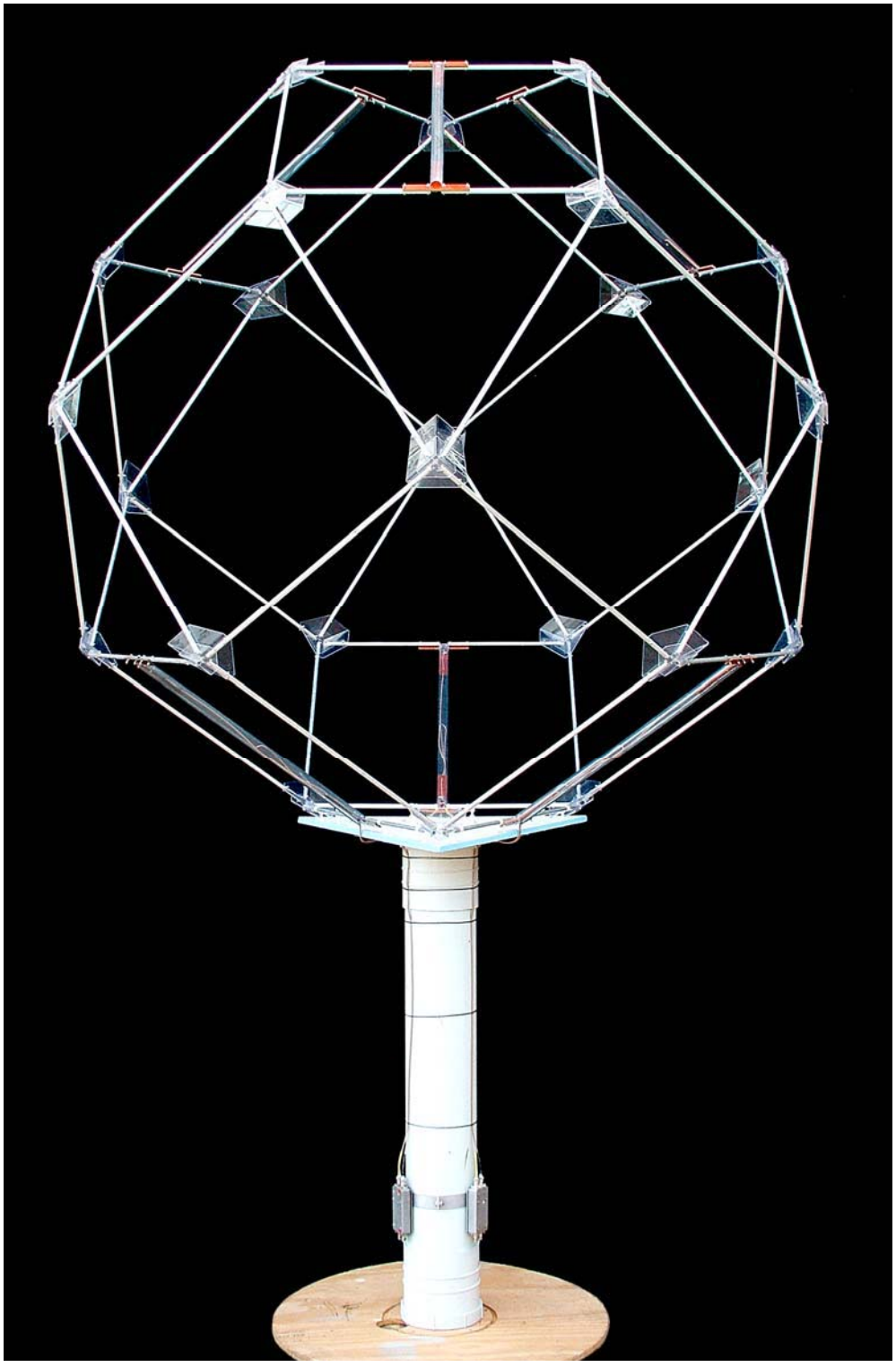

Figure 26: The assembled Small Rhombicuboctahedron tri-axial twin-loop antenna

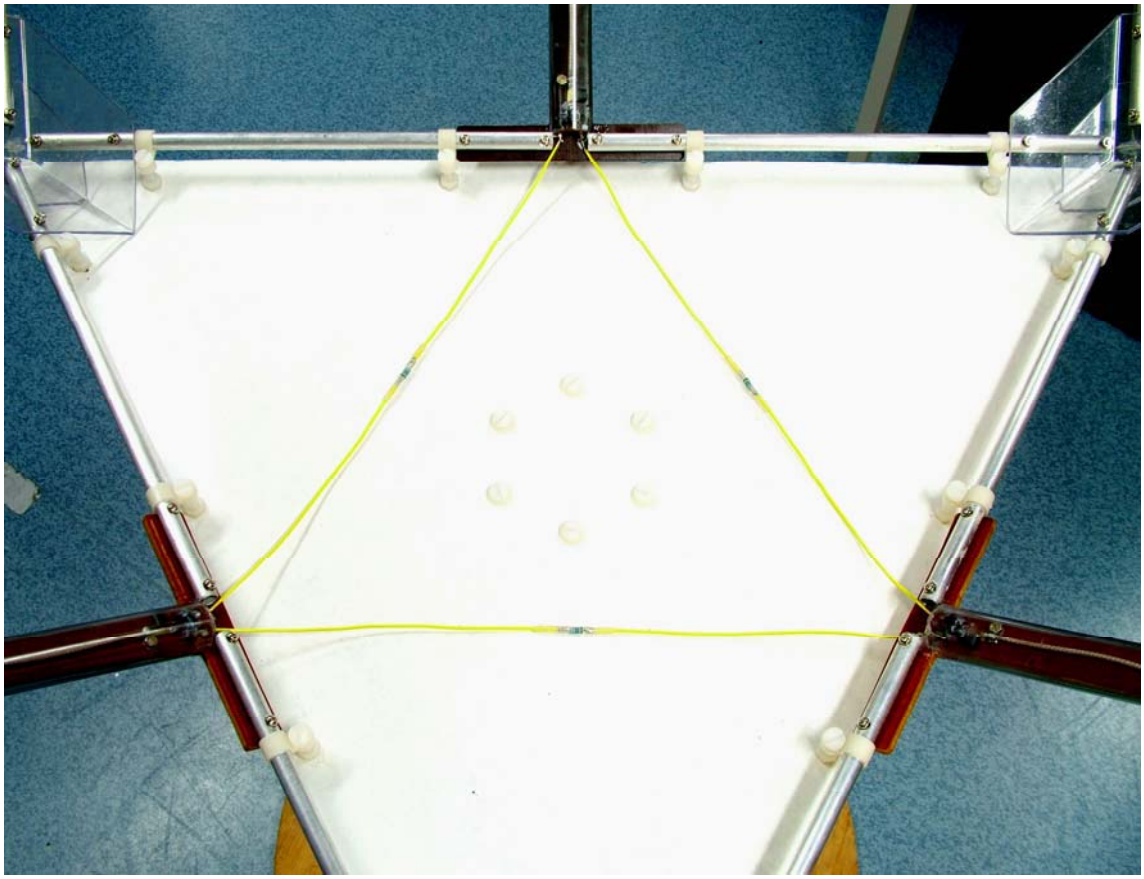

Figure 27: The base of the assembled Small Rhombicuboctahedron tri-axial twin-loop antenna showing the location of the three 750 Ω parasitic suppression resistors with their yellow connecting leads

3.8 Loop Antenna Construction Notes

Nickel-plated brass screws and nuts were used in the assembly of the loop antenna to control corrosion induced by the weather. Tin plated steel solder lugs were held onto the ends of the aluminium tubes by the brass screws and nuts. The wires at the crossover points were soldered between these lugs. This arrangement did not prove reliable with time. Moisture induced corrosion in the interface between the lug and aluminium tube made the connection noisy with the slightest movement of the antenna. Future designs will have the copper wire at the crossover points soldered to the inside surface of the aluminium tubes using "ALUSOL" aluminium solder manufactured by Multicore. Aluminium is a good conductor of heat. Initial tests on the suitability of "ALUSOL" found it was necessary to pre-heat the tubes with a hot air gun before soldering. The wires will then be shaped as seen in Figure 28 and normal solder used to ensure connection between the wires at their overlapping. Painted or spray-on lacquer will be used to protect the wire and solder joints from the elements. The aluminium tubes mounted at right angles, not shown in the figure, will have the wires soldered to the inside of the tubes drooping in a downward direction towards their wire overlapping point. The strain relief of the copper wire as seen in Figure 28 is necessary due to the flexing of the structure as it is being assembled. The completed assembly has very little movement.

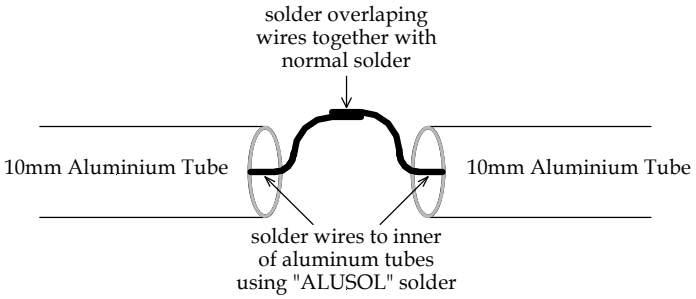

Figure 28: Proposed connection at the loop's crossover points for future designs

There is a problem in the antenna test field with some of the local bird wildlife. Sulphur Crested Cockatoos are quite at home hanging upside down on a thin wire to peck at the underside of anything that looks interesting to them. The crossover connections at the corners of the Giselle loops have only been damaged when flocks of these birds have visited the antenna test field. Their destructive habits are well known to Australian field engineers who maintain long haul microwave links. The crossover links, 300 Ω ribbon and the loop terminations need to be fully enclosed to protect them from this menace.

3.9 Points to Consider When Designing a Small Rhombicuboctahedron to Cover a Portion of the HF Band

Suppose that only the 7 to 16 MHz part of the HF band is of interest and that a quiet rural area has been chosen as the site for the antenna. Sensitivity is of prime concern and will necessitate the largest loop possible. Equation (15) can be rearranged to give the total length of conductor at the highest frequency of 16 MHz before the depth of null starts to degrade below -30 dB. This returns a total length of conductor of 18.75 m. There are 18 sections that make up this length (16 in the aluminium tubes and 2 in the 300 Ω ribbon), giving 1.04 m/section. This includes the length of tube and wires used at the loop's crossover points. It will also be the distance between the parallel loops. The large distance between the twin-loops indicates larger diameter tubes can be used say, 20 mm. The length of parallel conductor between the terminations of the twin-loops will be 8 x 1.04 m = 8.33 m. Equation (8) can now be used to calculate the expected differential inductance of 15.89 uH. Add to this the expected inductance of a 1.04 m length of 300 Ω ribbon of 1.63 uH, extrapolated from the measurement on the 0.66 m long line, gives a total expected differential inductance of 17.5 uH. The geometric mean of the inductive reactance at 7 MHz and 16 MHz is $\sqrt{769 \times 1759}$ = 1163 Ω. Divide this by 2 yields 581 Ω for each of the two terminations. Equation (7) is used to find the low frequency -3 dB point of 5.28 MHz. This is below the frequency of 7 MHz therefore low frequency compensation to extend the low frequency response will not be required. The loop matching circuit stepping up one of the amplifiers unbalanced 50 Ω input (one half of the 100 Ω balanced) to one of the loop's balanced 581 Ω terminations needs to be designed. The value of 1200 Ω (total value of termination resistors fitted per loop) is recommended for the parasitic damping resistors. The nearest preferred value on the high side should be chosen as there are detrimental effects encountered to the loop's sensitivity if the value approaches that of the terminations. Finally, the bandpass filter in the RF amplifier box needs to be re-engineered where necessary to suit the required bandwidth.

4. Conclusion

The Giselle antenna provides an effective solution to the problem of measuring the polarisation state of incident HF radio waves. Its sensitivity as a wide-band receiving antenna is comparable with that of other antennas of similar size, while its unique symmetry results in superior accuracy and uniformity of the determination of signal polarisation. It should find application in HF direction finding, communication and HF radar systems where signal polarisation is important.

5. Acknowledgements

The sole responsibility for the accuracy of any technical writing lies with its author. Information obtained from references or discussions with colleagues is still the responsibility of the author for it was the author's decision to use or reject such information. With this in mind, this author wishes to acknowledge the contributions made to this document by the following people.

Peter Wilinski – For his advice, guidance and assistance in the mechanical construction of the Giselle array.

Angus Massie – Who brought to my attention the problems with traditional tri-axial loop antennas (north/south, east/west loops and a waist loop) and the maths needed to analyse data collected from a tri-axial array with different parameters between its loops and ground. Also, for the many technical discussions out of which the solution to the problem arose leading to the design of the MKI array, and finally, for naming the Giselle antenna array.

Dallas Taylor, Dr. John Asenstorfer and **Dr. Stuart Anderson –** For vetting the document and their subsequent suggestions which helped to make it easier to read.

Intelligence Surveillance and Reconnaissance Division (ISRD) – The Giselle antenna array was conceived, funded, designed, built and tested while this author and his colleagues were part of ISRD. During the 2007 restructuring of DSTO a portion of ISRD, which this author and some colleagues were part of, was transferred to the newly created C3ID. While this report is published through C3ID, this author wishes to acknowledge the role played by ISRD in the development of the Giselle array.

6. References

1. "Admiralty Handbook of Wireless Telegraphy" (1931) chapters XVIII and XIX, H.M. Stationery Office.

2. Wadell, Brian C. (1991) "Transmission Line Design Handbook" Artech House, ISBN 0-89006-436-9.

3. Terman, Frederick Emmons (1955) "Electronic and Radio Engineering" fourth edition.

4. Pender, Harold & McIlwain, Knox (1944) "Electrical Engineers Handbook, Electric Communication and Electronics" third edition, publisher John Wiley & Sons Inc.

5. Morton, A. H. (1966) "Advanced Electrical Engineering" Pitman Publishing Limited, ISBN 0-237-40172-6.

6. Bueche, Frederick (1969) Professor of Physics University of Dayton, "Introduction to Physics for Scientists and Engineers" international student edition, McGraw-Hill Book Company, LCCCN 69-13598.

7. Ponizovskaya, E.V. et al, (2002) "Losses for Microwave Transmission in Metamaterials for Producing Left-Handed Materials: The Strip Wires" arXiv:cond-mat/0206429v1 24June2002.

8. Langford-Smith, F. (1957) "Radiotron Designer's Handbook" fifth impression, Wireless Press.

9. "Reference Data for Radio Engineers" (1975) Howard W. Sams & Co., Inc., Indianapolis, Indiana 46268. ISBN 0-672-21218-8.

10. Grover, Frederwick W. (1946) "Inductance Calculations" D. Van Nostrand Company Inc., 250 Fourth Avenue, New York.

11. Vasilescu, Gagriel (2005) "Electronic Noise and Interfering Signals" ISBN 3-540-40741-3.

12. Gibilisco, Stan (2003) "Geometry Demystified" McGraw Hill, ISBN 0-07-141650-1.

13. Reyner, J. H. (1959) "Radio and Electronics" The New Era Publishing Co. Ltd., 45 Oxford Street, London, W.C.1.

14. King, Ronold W. P. (1945) "Electromagnetic Engineering, Vol. I. Fundamentals" McGraw-Hill Book Company, Inc.

15. Martinsen, W. (2003) "Construction Techniques for LC Highpass and Lowpass Filters used in the 1MHz to 1GHz Frequency Range" technical note DSTO-TN-0531, DSTO Information Sciences Laboratory, PO Box 1500, Edinburgh, South Australia 5111, Australia.

16. Van Valkenburg, M. E. (1955) Associate Professor of Electrical Engineering, University of Illinois, "Network Analysis" Published by Prentice-Hall.

17. Misra, Devendra K. (2001) "Radio-Frequency and Microwave Communication Circuits" ISBN: 0-471-41253-8.

18. "Recommendation ITU-R PI.372-6" section 6B: Radio Noise, 1994.

19. Jenkins, Herndon H. (1991) "Small-Aperture Radio Direction-Finding" Artech House, Inc., ISBN: 0-89006-420-2.

20. Davies, Kenneth (1990) "Ionospheric Radio" ISBN: 0-86341-186-X

21. Maslin, Nicholas (1987) "HF Communications, a systems approach" Pitman Publishing, ISBN: 0-273-02675-5

22. "IRE Standards on Methods of Measuring Noise in Linear Twoports, 1959"' Proceedings of the IRE, January 1960, pg. 60-68.

23. Nanevicz, J.E., Vance, E.F. and Hamm, J.M. "Observation of Lightning in the Frequency and Time Domains", SRI International, Electromagnetic Sciences Laboratory, Menlo Park, California 94025, USA.

24. Kraus, John D. & Marhefka, Ronald J. (2003) "Antennas For All Applications" McGraw-Hill Companies Inc., ISBN: 0-07-232103-2.

Appendix A: Basic Loop Theory

The following discussion of basic loop theory will be limited to receiving loops. For simplicity only the *E* field's contribution to the loop's open circuit voltage is considered.

Voltage induced into a straight length of wire

A wire conductor laying at right angles to the direction of travel of an oscillating *E* field and whose orientation is in the same plane as the *E* field, will have a voltage induced across its ends proportional to the conductor length and the field strength, equation (A.1) [1, pg. 810]. Equation (A.1) assumes the length of conductor is very short when compared to the wavelength of the oscillating *E* field.

$$V_{o/c} = El \tag{A.1}$$

where: $V_{o/c}$ = instantaneous open circuit voltage appearing across the ends of a straight conductor (volts)

E = instantaneous magnitude of oscillating *E* field (volts/m)

l = length of conductor (m)

Voltage induced into a loop antenna

For ease of explanation, a one-turn loop antenna will be considered using four equal straight lengths of wire taking the form of a square loop constructed in the X Z plane. This is seen at the top of Figure A1. A sinusoidal oscillating *E* field is travelling in the X direction, from left to right. The vertical sides AB and DC of the loop will have voltages appearing across their ends as described by equation (A.1). Sides AB and DC are also displaced in the X plane and therefore will have a difference in phase in induced voltage from the travelling *E* field. $V_{AB,}$ in the example of Figure A1, will lead V_{DC} with the difference in phase being proportional to the distance between the two sides of the loop and inversely proportionally to the wavelength of the oscillating *E* field. These two sides of the loop are part of a series circuit and hence only the difference between their potentials will appear at the loop's output terminals. Note that there is a 90 degree phase shift between the *E* field at the centre of the loop, Figure A1 (A), and the voltage appearing at the loop's output terminals, Figure A1 (E).

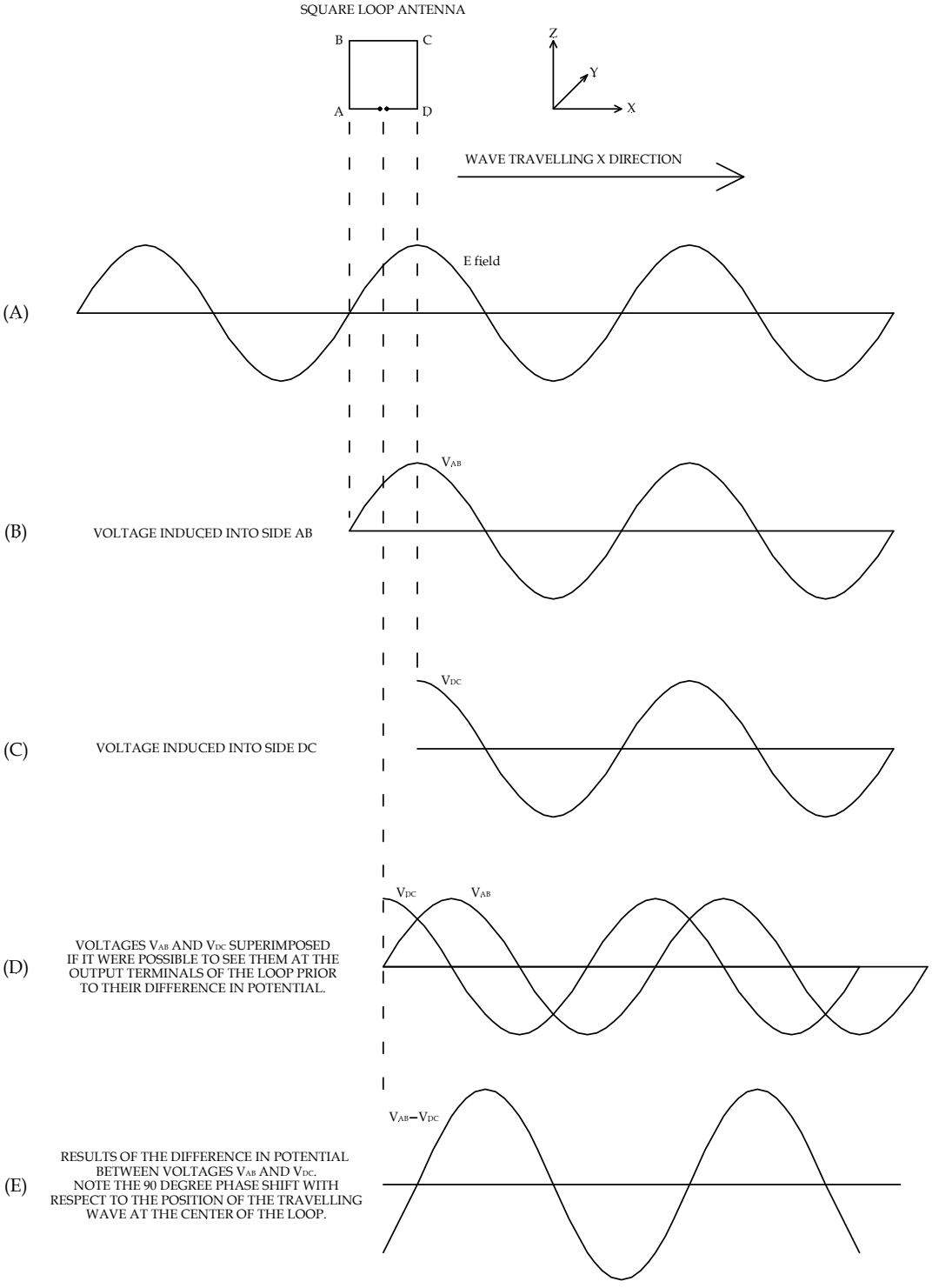
SQUARE LOOP ANTENNA
B
C
A
D
Z
Y
X
WAVE TRAVELLING X DIRECTION
E field
(A)
V_{AB}
(B)
VOLTAGE INDUCED INTO SIDE AB
V_{DC}
(C)
VOLTAGE INDUCED INTO SIDE DC
V_{DC}
V_{AB}
(D)
VOLTAGES V_{AB} AND V_{DC} SUPERIMPOSED IF IT WERE POSSIBLE TO SEE THEM AT THE OUTPUT TERMINALS OF THE LOOP PRIOR TO THEIR DIFFERENCE IN POTENTIAL.
$V_{AB}-V_{DC}$
(E)
RESULTS OF THE DIFFERENCE IN POTENTIAL BETWEEN VOLTAGES V_{AB} AND V_{DC}. NOTE THE 90 DEGREE PHASE SHIFT WITH RESPECT TO THE POSITION OF THE TRAVELLING WAVE AT THE CENTER OF THE LOOP.

Figure A1

A commonly used equation for the open circuit voltage induced into a loop antenna [3, pg. 1047] is:

$$V_{o/c} = \frac{2\pi E N A f}{300} \cos\phi \tag{A.2}$$

where: $V_{o/c}$ = instantaneous open circuit voltage appearing at the output terminals of a receiving loop antenna (volts)
E = instantaneous magnitude of oscillating E field (volts/m)
N = number of turns in loop
A = area of loop (m^2)
f = frequency of oscillating E field (MHz)
ϕ = angle between loop plane and direction of travel of the oscillating E field.
300 = velocity of RF propagation (Mm/s)

Like equation (A.1), it also assumes that the total length of conductor in the loop is very short when compared with the wavelength of the oscillating E field.

The effective height of a loop antenna is [4, ch. 7 pg. 60]:

$$h_{eff} = \frac{2\pi N A f}{300} \tag{A.3}$$

where: h_{eff} = effective height of loop antenna (m)
N = number of turns in loop
A = area of loop (m^2)
f = frequency of oscillating E field (MHz)

which is equation (A.2) with the E term removed. h_{eff} can be substituted for l in equation (A.1) to derive the induced $V_{o/c}$.

Loop antennas whose total length of conductor is somewhat less than the wavelength of the E field oscillating frequency are inherently insensitive. This is due to the voltages induced into various diametrically opposed elements of the loop being subtracted from each other and only their difference appearing at the loop's output terminals. Their sensitivity is usually made acceptable at a wanted spot frequency by resonating the lumped inductance with an external capacitance multiplying the induced voltages by the circuit Q, equation (A.4).

$$V_{o/c} = \frac{2\pi E Q N A f}{300} \cos\phi \tag{A.4}$$

This technique of increasing loop sensitivity is clearly not suitable for broadband work. Also, equation (A.2) and those derived from it become inaccurate when applied to large loops used in the upper part of the HF band. This equation assumes a uniform distribution of current throughout the length of the loop's conductor. However it is a good approximation for loops whose perimeter is less than 0.1 λ of the oscillating E field's wavelength.

Equation (A.5), which has been modified from radians to degrees and from which equation (A.2) was derived, was obtained from [1, pg. 815]. The sine term makes allowances for the width of a rectangular loop being an appreciable percentage of the E field wavelength.

$$V_{o/c} = \left| 2ENh \sin\left(180 \frac{sf}{300}\right) \cos\phi \right| \quad \text{(A.5)}$$

$$h_{eff} = \left| 2Nh \sin\left(180 \frac{sf}{300}\right) \cos\phi \right| \quad \text{(A.6)}$$

where: $V_{o/c}$ = instantaneous open circuit voltage appearing at the output terminals of a receiving loop antenna (volts)
h_{eff} = effective height of loop antenna (m)
E = instantaneous magnitude of oscillating E field (volts/m)
N = number of turns in loop
h = height of loop (m)
s = width of loop (m)
f = frequency of oscillating E field (MHz)
ϕ = angle between loop plane and direction of travel of the oscillating E field.
Note: angles are in degrees.

Equation (A.5) has been modified by this author to equation (A.7) which takes into account both:

- the non-uniform distribution of currents throughout the loop's conductor and,
- makes allowances for the time it takes for the induced voltage to traverse the length of conductor used in a rectangular loop and the effect the standing waves developed has upon the loop's output voltage.

$$V_{O/C} = \left| 2ENh \sin\left(180 \frac{sf}{300}\right) \cos\left(90 \frac{(2h+2s)Nf}{vn300}\right) \cos\phi \right| \quad \text{(A.7)}$$

To make it easier to see how the travelling waves are developed, Figure A2 (A) shows a square loop in which the termination and its opposing point in the loop are being pulled apart. In (B) an easily recognised balanced transmission line is forming until finally in (C) the termination appears connected to a shorted balanced transmission line whose length is half the loop's perimeter. It is the standing waves developed by this shorted line that dictates the loop's response with frequency. The loop's output voltage will maximise at a parallel line length of 0.25 λ of the oscillating E field and odd multiples thereof. This is where the line appears as a parallel resonant circuit across the loop's termination resistor. The loop will be the least sensitive when the line length is 0.5 λ of the oscillation E field and even multiples thereof. This is where the line appears as a short circuit across the termination shorting any voltage appearing across its terminals.

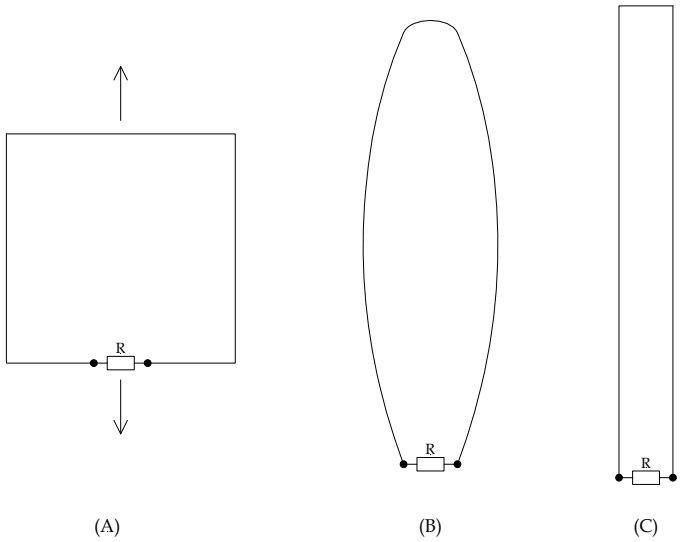

Figure A2: (A) a square loop showing where the termination and its opposing point are to be pulled apart, (B) forming the transmission line and (C) the completed easily recognised short circuit transmission line

Equation (A.7) indicates that for a given length of wire, the large area of a one-turn loop returns a better loop sensitivity than one of a smaller area of multiple turns. Equation (A.7) also shows an increase in $V_{o/c}$ with increasing frequency. There is however, an upper frequency limit for any given loop due to the time it takes for the induced voltage to traverse the total length of conductor used. This upper limit is usually where the total length of conductor is 0.5 λ of the oscillating *E* field or, if it is easier to think in terms of transmission lines as in Figure A2, where half the total length of conductor is 0.25 λ of the oscillating *E* field. Increasing the frequency of oscillations of the applied *E* field beyond this limit usually results in a decrease in induced $V_{o/c}$.

Equation (A.7) was used to generate the graphs of Figure A3 simulating a fixed length of four metres of conductor used to make a single turn and also 2, 3, and 4 turn loops. A value for v=0.925 was chosen. This brings equation (A.7)'s calculated response into agreement with both NEC-2 and a loop's measured response. Notice the single turn loop sensitivity is greater than the multi-turn loops when using the same length of conductor. Traditional loop antennas have lumped L and distributed C that form a parallel resonant circuit and is seen as a localised peak in the loop response. This peak is usually below the frequency where the decrease in gain through the total length of conductor approaching 0.5 λ takes effect. This peaking effect due to resonance was not considered in Figure A3.

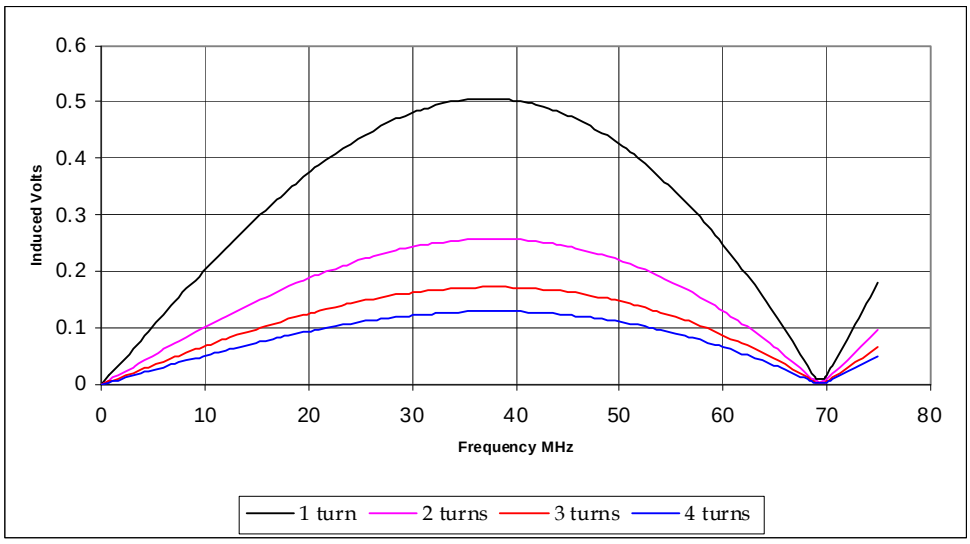

Figure A3: Open circuit voltage appearing across the terminals of a single and various multi-turn loops constructed using a fixed four metre length of conductor

Equation (A.7) is used for vertically polarised ground wave signals received by a vertical loop oriented normal to the *xy*-plane. It does not take into account elevation nor does it show the dependence on polarisation. Sky-waves however can arrive at the receiving loop at any polarisation and azimuth with an elevation angle anywhere from the zenith to a few degrees above the horizon line. Equation (A.7) has been further modified [19, pg. 13] to equation (A.8) to reflect the expected $V_{o/c}$ of a received sky-wave signal.

$$V_{O/C} = \left| 2ENh\sin\left(180\frac{sf}{300}\right)\cos\left(90\frac{(2h+2s)Nf}{vn300}\right)(\sin\phi\cos\psi - \cos\phi\cos\theta\sin\psi)\right| \qquad \text{(A.8)}$$

where: $V_{o/c}$ = relative instantaneous loop open circuit output voltage (volts)
E = instantaneous magnitude of oscillating E field (volts/m)
h = height of rectangular loop (m)
s = width of rectangular loop (m)
N = number of turns in loop
n = number of terminating resistors
f = frequency of oscillating E field (MHz)
v = velocity factor.
ϕ = angle between the loop plane and direction of travel of oscillating E field
ψ = polarisation tilt angle of the incident E field
θ = Elevation angle referenced to the zenith
Note: angles are in degrees.

The Box Loop Antenna

There is also another problem arising from a multi-turn loop antenna which degrades the depth of null. Figure A4 shows a four turn box type loop antenna. The loop has been constructed in the X, Z plane with the turns displaced in the Y plane. A vertically polarised oscillating *E* field travelling in the Y direction (the loop's null) will induce into the vertical sides of the loop a voltage proportional to the magnitude of the *E* field at that particular point. Because the vertical sides are displaced in the Y plane, the same direction as the travelling *E* field, there will be differences in the magnitude of the induced voltages between the individual turns of the loop. The differences between these voltages appear as an output voltage at the terminals of the loop and hence degrade the depth of null. The loop is most sensitive to an *E* field travelling in any direction in the X, Z plane.

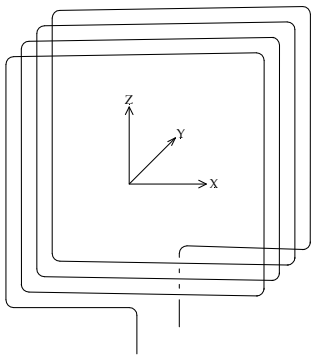

Figure A4

The Pancake or Spiral Loop Antenna

The pancake loop, Figure A5, was developed to overcome the degradation of null of the box loop. The turns are coplanar, displaced in the X, Z plane, and not the Y plane. The theory being that the summation of voltages induced into the sides of the loop from an *E* field travelling in the Y direction will be equal and series opposing preserving the loop's depth of null. However, close examination of the length of the opposite sides of the individual turns will reveal small differences in their length due to the spiral layout. The induced voltages into the opposing sides of the loop will not be equal, their difference degrading the loop's null. The degradation in null is proportional to the pitch of the spiral and the number of turns.

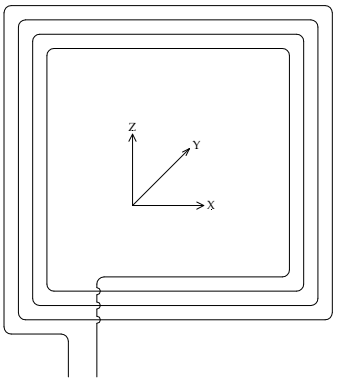

Figure A5

Both the Box and the Pancake loops suffer from the distributed capacitance between the windings forming a resonant circuit with the loop's lumped inductance. This resonance produces a peak in the loop's response proportional to the circuit's loaded Q.

The Vertical Antenna Effect

The vertical antenna effect refers to a loop antenna's unwanted ability to act as a short vertical monopole antenna. This is primarily due to imbalances in its design and construction that leads to degradation of the loop's nulls and distortion of the loop's figure-of-eight pattern. Figure A6 shows a single turn loop antenna connected to the input of a balanced amplifier. C1 represents the distributed capacitance to ground of both side AB of the loop and the horizontal section between point A and the input of the differential amplifier. Likewise C2 is the distributed capacitance of side DC and its horizontal section to the amplifier's inverting input. If great care has been placed in loop construction and field installation then C1 will be equal to C2. Under this condition a vertically oscillating *E* field travelling in the Y direction will induce equal voltages into sides AB and DC. Both the vertical sides of the loop, which are acting as vertical monopoles, will be connected to their respective images in the ground via the same value of capacitance. The current flowing through C1 and C2 will be the same and hence their voltage drops with respect to ground will be equal. There will be no difference in voltage at the inputs to the differential amplifier and hence no output. This is the ideal null in a loop antenna.

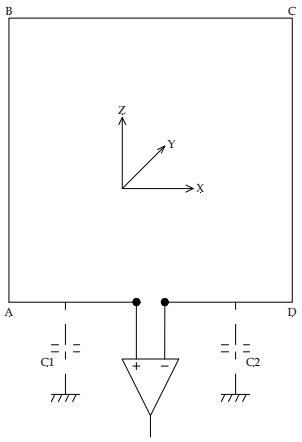

Figure A6

However, variations in loop component manufacture and loop antenna installation will produce subtle differences in the loop's distributed capacitance to ground presented to each input of the differential amplifier. C1 now, does not equal C2. The difference in impedance between the respective sides of the loop and their antenna images in the ground produces differences in voltage drops across C1 and C2 and a corresponding output from the amplifier. The expected distributed capacitance to ground is in the order of a few pF and is dependant on the loop construction and its proximity to ground. There is an expected reactance in the order of a few KΩ at the maximum frequency of 30 MHz for the HF band increasing to many tens of KΩ at the bands lower frequency end. An input impedance of the differential amplifier of about 1KΩ will swamp the reactance of C1 and C2 at the low frequency end of the band and as such should not adversely affect the loop's null. As the frequency is raised, the reactance of C1 and C2 will fall and be of concern, especially at the band's upper frequency end. Lowering the amplifiers input impedance would eventually swamp the variances in the distributed capacitance at the upper frequencies at the cost of lowering loop sensitivity. Another way of minimising the variation in distributed capacitance to ground is to swamp it by adding a larger fixed equal capacitance between the differential inputs and ground. In broadband work, the value of this capacitance is a trade-off between the reduction of loop sensitivity versus the improvement in loop symmetry at the higher frequencies and the subsequent decrease in the loop's resonance. If the loop is to operate at only one frequency then this is an ideal way to tune the loop.

A better method for broadband work is to maintain the high input impedance of the amplifier, thereby preserving the loop sensitivity, and install trimmer capacitors between each input of the differential amplifier and ground. These capacitors are initially adjusted for minimum capacitance. A portable transmitter is placed at some distance exactly on the loop axis. A transmit frequency is selected in the upper frequency range of the loop. This is where the loop's distributed capacitance to ground has the most influence on the receive pattern. Only the trimmer capacitor that produces an increase in the loop's depth of null is adjusted. The other is left at minimum capacitance. This is the last adjustment that is made to correct a loop's pattern and is usually made with the loop installed in its place of service. A word of caution; the transmission line between the loop and the receiver is capable of distorting the receive pattern. This problem needs to be addressed first otherwise adjusting the loop trimmer capacitor will induce an error to correct for an error, resulting in an error correction at a spot frequency only. The problems associated with long transmission lines between the loop antenna and the receiver are covered later in this appendix. This description of the vertical antenna effect has highlighted the importance of loop symmetry to ground.

The Shielded Loop

The problems arising from the vertical antenna effect can be overcome through the use of a faraday shield. The shielded loop usually takes the form of a co-axial line as seen in Figure A7. The outer shield, which is open circuit at the top, prevents the *E* field from influencing the inner conductor making this a true *H* field loop. The price that is paid is the large distributed capacitance lowers the loop's parallel resonant (anti-resonant) frequency limiting its usefulness as a broadband antenna. Also, the *E* field is prevented from making its contribution to the loop's output voltage making the antenna very insensitive. *H* field loops are usually made efficient at a wanted spot frequency by bringing the loop's distributed inductance into resonance by adding an appropriate capacitor thereby magnifying the induced current by the circuit Q.

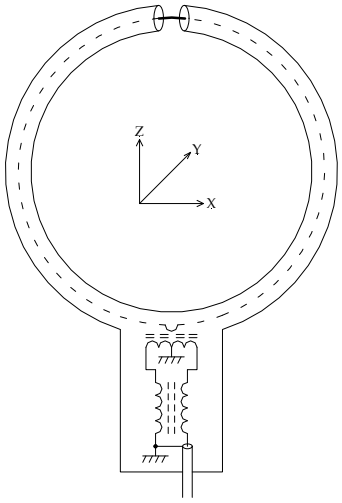

Figure A7

Differential Voltages induced into a co-axial Transmission Line from an Externally Travelling Transverse Electromagnetic Wave

A travelling transverse electromagnetic wave is made up of an *E* and *H* fields at right angles to each other. The effect that these two travelling waves have upon a length of co-ax will now be considered. The *H* field will be considered first.

Copper has a relative permeability of one and therefore will not have any effect on the propagation of the *H* field unless the copper conductor is part of a closed conducting loop. In this case the induced EMF will cause a current to flow and a counter *H* field will be produced. This is the principle of electromagnetic shielding. The important thing to realise is that the presence of copper in the propagation path does not distort *H* field space unless a current is able to flow in the conductor. The *H* field will therefore pass through both the inner and outer conductors of the co-ax unaffected.

The time varying travelling *H* field will however induce a voltage in both the inner and outer conductors of the co-ax. According to Faraday's law the induced EMF will be [5, pg. 349]:

$$E = -N\frac{d\Phi}{dt} \tag{A.9}$$

where: E = the induced EMF from a time varying magnetic field (volts)
N = the number of turns
Φ = the magnetic flux linking the circuit (Weber)
t = time in seconds

The negative sign indicates that the induced EMF will produce a current whose flux will oppose the change in the original flux (Lenz's law). The inner and outer of the co-ax are connected via the input impedance of the receiver at one end and the impedance of the antenna at the other. Because the same number of flux lines links both the inner and outer of the co-ax the same voltage will be induced into both. Notice that the cross sectional area of the conductor is not a factor in determining the induced voltage, only the flux linkage and its rate of change. There is no difference in voltage between the inner and outer of the co-ax and therefore no differential current can flow. The *H* field component will not have any effect on the differential voltages appearing between the inner and outer conductors of a length of co-ax cable.

Copper has a very high relative permittivity, [7] quotes it as a complex permittivity of $-2000 + i10^6$ and [6, pg. 460] cites metals in general as having an infinite permittivity. Either way, it is clear that the presence of copper in the path of a travelling *E* field will distort *E* field space. Figuratively, the copper will attract the lines of *E* field to it compacting them more and more tightly within the boundaries of the metal until the force of repulsion between lines of force of the same sense overcomes the force of attraction of the high permittivity. The force of a line of flux now entering the copper from the transmission side propagates through the compacted *E* field within the copper and finally pushes out a line on the other side so that that line can continue its journey in the direction of propagation.

Figure A8 (A) shows a vertical monopole antenna at right angles to the ground and connected to the input of a receiver. The receiver is also connected to ground. A travelling vertical *E* field will induce a voltage across the ends of the rod, equation (A.1), causing a current to flow through the input load of the receiver to the antenna's image that appears in the ground. Figure A8 (B) now shows a vertical length of co-ax cable used to connect an antenna mounted at some height above ground to a receiver at ground level. The outer braid of the co-ax, usually made of copper, will act just like a vertical antenna and have appearing across its ends a voltage proportional to both its vertical length and the strength of the *E* field.

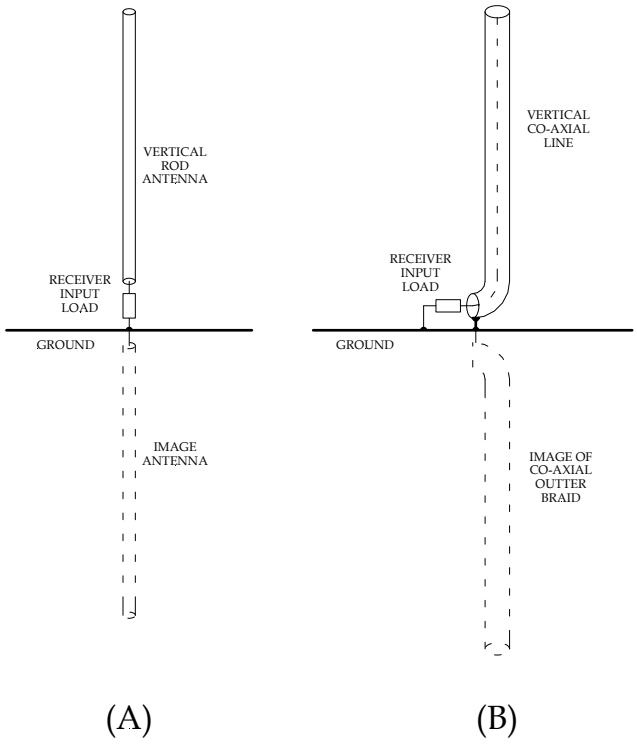

Figure A8

The presence of the dielectric between the inner and outer of the co-axial cable, whose relative permittivity is very, very much smaller than that of copper, acts as a barrier between the inner and outer conductors of the co-ax. The travelling *E* field preferring to remain within the confines of the outer braid of the co-ax which offers the path of least resistance due to its very high permittivity as it journeys in the direction of propagation. The outer braid acts as a Faraday shield and as such prevents the travelling *E* field from having any direct influence in generating a potential difference between the inner and outer of the co-ax cable.

It might be an idea at this point to review the following law and rules relating to magnetic flux. They will be found useful in understanding the effects time varying magnetic fields have on conducting media.

Faraday's law: The voltage induced in a circuit is proportional to the rate at which the magnetic flux linkages of the circuit are changing.

Left-hand rule for a current-carrying wire: If the fingers of the left hand are placed around the wire in such a way that the thumb points in the direction of electron flow, the fingers will be pointing in the direction of the magnetic field produced by the current flow in the wire.

Left-hand rule for induced currents: The thumb and fingers of an open left-hand are placed at right angles on the same plane. If the fingers point in the direction of the magnetic lines of flux and the palm is facing in the direction in which the lines of flux are travelling, as if it were pushing the lines of flux in that direction, then the extended thumb points in the direction of the induced electron current flow.

Figure A9 shows a close up view of the lower portion of the current example of the voltage induced into the outer braid of the co-ax cable. The *E* field pointing in the upward direction will cause a current to flow downwards in the co-ax's outer braid travelling towards its image appearing in the ground. This current will generate magnetic lines of flux in a counter-clockwise (CCW) direction when viewed from above. If the assumption is made that the travelling *E* field is increasing in intensity (V/m) as it would if was working its way up towards the peak of a sine wave, then the current flowing in the outer braid of the co-ax would also increase. The magnetic lines of flux generated by this increasing current would expand moving away from the current generating it. The ***Left-hand rule for induced currents*** will show that the current this induces into the inner of the co-ax is in the opposite direction to the current in the outer braid that caused it. A potential difference now exists between the inner and outer conductors of the co-ax. There are two things that affect the magnitude of this difference:

1. the strength of the external *E* field and,
2. the distance between the inner and outer of the co-ax cable.

While the first is self-evident the second is not as obvious and will need some explaining. Equation (A.10) is known as the Biot-Savart law and equation (A.11) shows its relationship to Faraday's Law, equation (A.9).

$$\frac{dH}{ds} = i\frac{\sin\theta}{r^2} \tag{A.10}$$

$$\Phi = \mu HA \tag{A.11}$$

where: H = magnetic field intensity (ampere-turn/m)
Φ = magnetic flux linking the circuit (Weber)
i = current flowing in element ds of wire.
ds = vector element of length along the wire.
r = distance between ds and the point where H is being determined.
θ = angle between r and element ds.
μ = permeability of magnetic path
A = cross sectional area of magnetic path (m^2)

It will be seen that the magnetic field (*H*) surrounding a conductor is proportional to the current and inversely proportionally to the square of the distance. Small diameter co-ax cable like RG-188 have a smaller distance between the inner and outer conductors than say RG-213 therefore, the co-efficient of magnetic coupling will be greater in the RG-188 than it would be in the larger diameter of the RG-213 due of the inverse square law with distance. By a similar reasoning co-ax cable with a higher characteristic impedance will have a lower magnetic coupling between the braid and the inner conductor due to the thinner inner conductor than a lower impedance cable with the same outer dimensions and a thicker inner conductor.

This process of the *E* field causing a current to flow in the outer braid which in turn induces an opposite current to flow in the inner conductor creating a differential voltage drop between the inner conductor and outer braid is very inefficient and difficult to notice in a normal antenna installation using high gain antennas. Recall that the output voltage is the difference between two voltages induced into the opposite sides of the loop by the *E* field. The

differential voltage that appears between the inner and outer conductors of co-ax cable by an external *E* field now becomes a significant percentage of the loop's output voltage, especially in the loop's nulls, and has the potential to distort the classic figure-of-eight pattern of the loop. It is possible to use a co-ax cable with two insulated outer braids. The outer most braid could be used as a Faraday shield by connecting the two braids together at the receiver end, which would be earthed, and the far end of the outer braid would be left open circuit at the antenna. The inner braid and centre conductor could then be used as normal co-ax coupling the antenna signal to the receiver. While there is merit in this solution it should be realised that there would still be a small differential voltage created between the co-axial inner braid and centre conductor. This difference would be due to the inverse square law with distance of the magnetic flux generated by the current in the Faraday shield. There would be more lines of flux cutting the inner braid being closer to the source of magnetic field than there would be in the centre conductor that is further away. Another solution to this problem could be the use of a shielded twisted pair. Such cables are in common use in LAN networks between modems of computers, however they are lossy, especially when used over distances of 30 m or more. This loss is also frequency dependant.

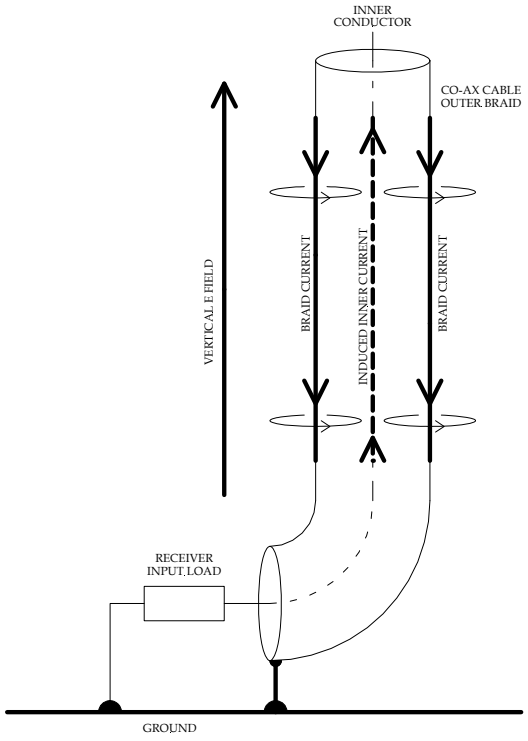

Figure A9

The most effective way to null the unwanted effects of the generation of a differential voltage in a co-axial cable from an external time varying *E* field is to have two co-axial lines running in parallel between the loop antenna and the receiver, see Figure A10. The loop antenna's output signal is presented as a differential voltage between the two co-axial inner conductors. The differential impedance presented by the two inner conductors of the parallel co-axial transmission lines is twice the characteristic impedance of a single line. The differential

voltages induced between the centre conductor and outer braid in each co-ax line from an externally propagating *E* field will be of the same magnitude and phase in both co-axial lines provided the distance between the two co-axes is very small with respect to the wavelength of the oscillating *E* field. For the HF band this is generally not of concern as the shortest wavelength of the *E* field at 30 MHz is 10 metres. A balanced to unbalanced transformer (balun) is used directly at the receiver's input connector to transform the differential signals between the inner conductors of the balanced transmission line to the receiver's unbalanced input. It is clear that only differential signals can be coupled to the input of the receiver and that the common mode voltages induced by the external *E* field are isolated by the action of the balun.

Very long runs of the twin co-ax between the loop antenna and the receiver can have differences in the induced voltages between the two inner conductors that are of concern. Equation (A.1) shows the relationship between the *E* field and the conductor length, in this case the co-ax's outer braids. Longer runs mean larger induced voltages appearing across the ends of the co-axial braids. Larger induced voltages also mean larger differences between their magnitudes caused by the slight displacement in space of the two outer braids. Such a long run may benefit from the twin co-ax cable undergoing a full twist every 10 metres or so alternately displacing the co-axes in space in order to equalise the effects of the *E* field.

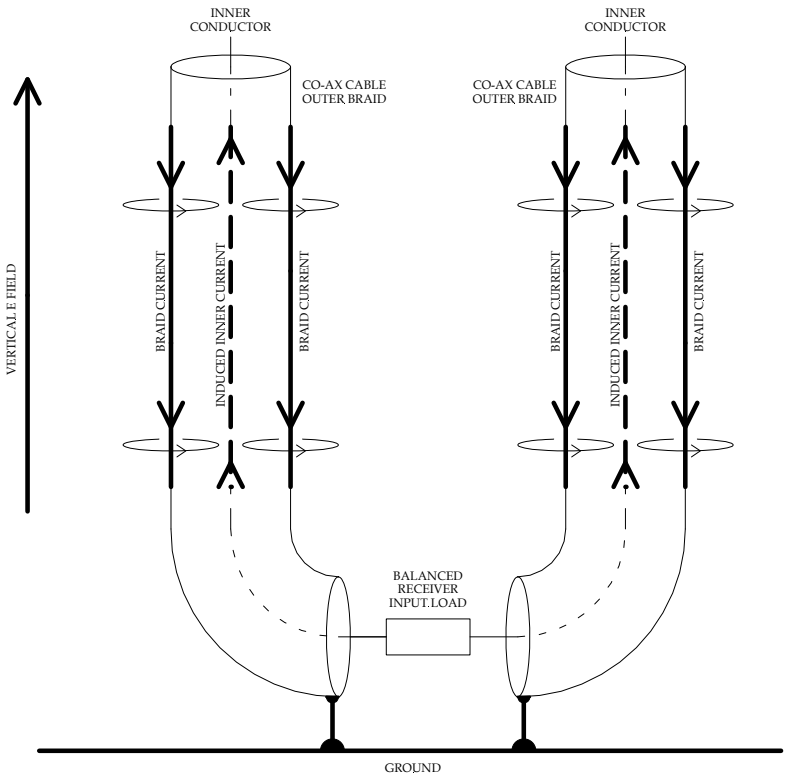

Figure A10

Appendix B: Derivation of the Antenna Noise Figure Equation

Effective Area

The power density, in watts/m², in an electromagnetic wave in free space is:

$$P_D = \frac{E^2}{120\,\pi} \tag{B.1}$$

where: E = electric field strength in (V/m)

The power, in watts, potentially available to an antenna to be delivered to its load is therefore:

$$P_L = P_D A_e \tag{B.2}$$

where: A_e = antenna effective area (m²)

The maximum power that can be extracted from P_D by a receiving antenna will be somewhat less due to losses. The effective area of any antenna is the effective area of an isotropic radiator multiplied by the directivity of the antenna under consideration:

$$A_e = \frac{D\lambda^2}{4\,\pi} \tag{B.3}$$

where: λ = free space wavelength of travelling E field
D = directivity of antenna
= 1 for an isotropic
= 1.5 for a small loop
= 1.64 for a half wave dipole
= 3 for a short vertical monopole

Equation (B.3) assumes the antenna to be lossless and capable of extracting all the available power and delivering it to the input of a receiver. In Figure B1(A) the circuit elements in the dashed box represent the schematic equivalent of free space where the E field is shown as a voltage generator and the resistor the impedance of free space. The high impedance RF voltmeter connected across the circuit will reflect the voltage of the voltage generator i.e. the E field. This is how the HE010 E field probe antenna works. The power available in the wave in free space is defined by equation (B.1). Maximum power transfer theorem states that maximum power is transferred from the energy source to the load when they are conjugate impedances. In the simplified diagram there are no reactive components to worry about so a 377 Ω resistor is placed directly across the circuit. This is shown in Figure B1(B) where the termination represents the combined radiation resistance of the antenna and the receiver input impedance. The 120π Ω free space impedance and the 377 Ω termination form a voltage divider network. The high impedance voltmeter will now indicate half the magnitude of the value of the E field. Also, there is as much power lost in the 120π Ω free space impedance as there is dissipated in the 377 Ω termination. The power dissipated in the termination is ¼ of the available power as defined by equation (B.1). The effective area as defined in equation (B.3) needs to be modified to reflect the maximum power that a matched receive antenna can extract from a wave in free space. Equation (B.3) now becomes:

$$A_e = \frac{D\lambda^2}{4\pi} \bullet \frac{1}{4} \tag{B.4}$$

The effective area (A_e in m²) of any receive antenna is therefore [8, pg. 896, eq. (22)]:

$$A_e = \frac{D\lambda^2}{16\pi} \tag{B.5}$$

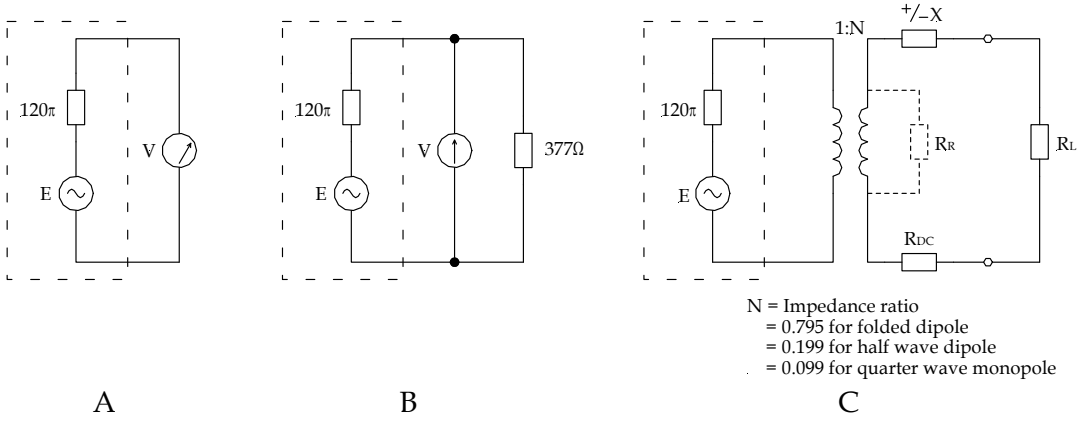

Figure B1: Circuit equivalent of the interface between an electromagnetic wave in free space and an antenna

The 377 Ω termination as seen in Figure B1(B) is made up of a series combination of resistances and reactances. This is portrayed in Figure B1(C). Here, the antenna is being viewed as an ideal impedance transformer, transforming the impedance of free space into the antenna radiation resistance R_R. R_R is the impedance seen between the terminals of the secondary of the transformer, shown dotted in the diagram. N, the transformation ratio, is antenna dependant and also frequency dependant for non-resonant antennas. R_{DC} is the DC resistance of the antenna wire, $^{+}/_{-}$ X is the off resonance reactance caused by the standing waves on the antenna wire and R_L is the input resistance presented by the receiver usually via a matching network.

Rearranging equation (B.2) gives the effective area (A_e in m²) of any antenna as :

$$A_e = \frac{P_L}{P_D} \tag{B.6}$$

Equation (B.1) has defined P_D in terms of the open circuit voltage or, the unterminated E field. If equation (B.6) is to be used to find the effective area of an antenna then P_L needs to be defined in the same terms as P_D, that is, the open circuit voltage appearing at the antenna terminals.

$$P_L = \frac{E_L^2}{R_L} \quad = \frac{E_{OC}^2}{4R_L} \tag{B.7}$$

where: E_L = matched terminated voltage developed across load R_L
E_{OC} = antenna open circuit voltage

Equation (B.6) now becomes:

$$A_e = \frac{P_L}{P_D} = \frac{\frac{E_{OC}^2}{4R_L}}{\frac{E^2}{120\pi}} = \frac{30\pi E_{OC}^2}{R_L E^2} \tag{B.8}$$

Assuming the polarisation of the *E* field is in the same direction as the maximum reception of the antenna and the output impedance of the antenna and the load are conjugate, then the effective height (h_e) of an antenna is:

$$h_e = \frac{2E_L}{E} = \frac{E_{OC}}{E} \tag{B.9}$$

where: E_{OC} = antenna open circuit voltage (V)
E_L = is the matched signal voltage across the antenna load (V)
E = electric field strength in (V/m)

Squaring both sides of equation (B.9) and substituting h_e^2 into equation (B.8) for the ratio of the two voltages gives:

$$A_e = \frac{30\pi h_e^2}{R_L} \tag{B.10}$$

Gain

The numerical power gain (*G*) of an antenna with respect to a reference antenna is:

$$G = \frac{measured\ effective\ area\ of\ antenna}{effective\ area\ of\ reference\ antenna} \tag{B.11}$$

Substituting equation (B.6) for the numerator and equation (B.5) for the denominator,

$$G = \frac{\frac{P_L}{P_D}}{\frac{D\lambda^2}{16\pi}} = \frac{16\pi P_L}{D\lambda^2 P_D} \tag{B.12}$$

and substituting equations (B.7) and (B.1) for P_L and P_D respectively in equation (B.12) gives:

$$G = \frac{E_{OC}^2 16\pi 120\pi}{4R_L E^2 D\lambda^2} = \frac{480 E_{OC}^2 \pi^2}{R_L E^2 D\lambda^2} \tag{B.13}$$

Squaring both sides of equation (B.9) gives:

$$h_e^2 = \frac{E_{OC}^2}{E^2} \tag{B.14}$$

Substituting h_e^2 into (B.13) for the ratio of the two voltages, the numerical power gain of an antenna is given as:

$$G = \frac{480 h_e^2 \pi^2}{R_L D\lambda^2} \tag{B.15}$$

The gain of any antenna relative to an isotropic is found by letting D = 1 in equation (B.15). Expressing the gain in dB:

$$G_{(dBi)} = 10\log_{10} G \tag{B.16}$$

for a 50 Ω system where D=1 this becomes:

$$G_{(dBi)} = 10\log_{10}\left(94.75\left(\frac{h_e}{\lambda}\right)^2\right) \tag{B.17}$$

or

$$G_{(dBi)} = 19.766 + 20\log_{10}\left(\frac{h_e}{\lambda}\right) \tag{B.18}$$

Antenna Noise Factor

The noise factor (f) of any device is defined in its basic form as [22]:

$$f = \frac{n_o}{G n_i} \tag{B.19}$$

where: n_o = output noise power
n_i = input noise power = thermal noise = kT_oB
G = numerical power gain

For an antenna, the numerical power gain is defined in equation (B.15). Using this in (B.19) gives:

$$f = \frac{R_L D \lambda^2}{480 \pi^2 h_e^2} \bullet \frac{n_o}{k T_o B} \tag{B.20}$$

where: n_o = output noise power measurement, same bandwidth as B and usually carried out with the antenna installed in a screened room,
k = Boltzmann's constant = 1.380622E-23 (JK^{-1})
T_o = standard temperature of 290K
B = bandwidth (Hz)
D = antenna directivity
h_e = effective height of antenna

Antenna Noise Figure

The antenna noise figure (F_{dB}) expressed in dB is:

$$F_{dB} = 10\log_{10}\left(\frac{R_L D \lambda^2}{480 \pi^2 h_e^2} \bullet \frac{n_o}{k T_o B}\right) \tag{B.21}$$

Receive Antennas with Internalised Electronic Gain

If the receive antenna has internalised electronic gain, as in an RF amplifier, then either the measured output noise power (n_o) from the output of the amplifier needs to be divided by the numerical power gain of the amplifier or, the reference noise power at the standard temperature (kT_oB) needs to be multiplied by the numerical power gain of the amplifier. Equation (B.22) is to be used when a receive antenna has an internal RF amplifier as part of the design and the measured output noise power (n_o) is taken at the output of the RF amplifier.

$$F_{dB} = 10\log_{10}\left(\frac{R_L D\lambda^2}{480\pi^2 h_e^2} \bullet \frac{n_o}{G k T_o B}\right) \tag{B.22}$$

where: G = numerical power gain of electronic amplifier

Appendix C: Straight Wire, Differential and Common Mode Inductances

This basic discussion of the inductance of a wire is limited to a uniform current flowing in the wire (the same value of current flowing throughout the length of wire in the inductor) and does not cover the effects of non-uniform current distribution. It has been written to help the reader grasp the complex nature of small air wound inductors. Large short air wound inductors with non-uniform current flow as used in loop antennas are even more complex in nature and are covered in the main text and *Appendix A*.

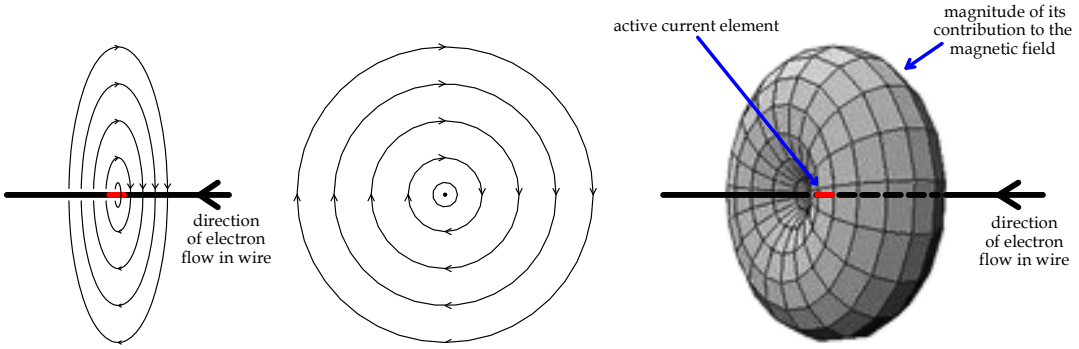

Figure C1

Figure C1 (a) shows a wire in free space with an electron current flowing through it from right to left. The current flowing in the wire sets up concentric circles of magnetic lines of flux centred on the axis of an element of the wire (seen in red) with the direction of the lines of flux shown by the arrows. Notice that the lines of flux are at right angles to the wire that is guiding the flow of electrons. Figure C1 (b) is the same length of wire viewed end on with the current flowing out of the page. These simple diagrams, which are most commonly used in introductory texts, do not tell the complete story. Equation (C.1) is the Biot-Savart Law and describes the magnetic field (H) generated by a current flowing through an element of the wire. It clearly shows that the strength of the magnetic field is dependant upon the $\sin\phi$. Figure C1 (c) is the three dimensional surface contour (horn torus) of the outer ring as seen in (a).

$$\frac{dH}{ds} = i\frac{\sin\phi}{r^2} \tag{C.1}$$

where: i = current flowing in element ds of wire
ds = vector element of length of wire
r = distance between ds and the point where H is being determined
ϕ = angle between r and element ds

From this it can be seen that the self-inductance of a straight length of wire is inductance in its simplest form. That is, lines of flux are not linking elements of the wire with any other parts of itself. The full length of the wire lies on the ϕ of zero degrees where no field exists. The inductance of a length of straight wire is [10]:

$$L = 0.002l\left[\log_e \frac{2l}{r} - \frac{3}{4}\right] \qquad \text{at low frequencies} \qquad \text{(C.2)}$$

$$L = 0.002l\left[\log_e \frac{2l}{r} - 1\right] \qquad \text{at high frequencies} \qquad \text{(C.3)}$$

where: L = inductance (μH)
l = length of wire (cm)
r = radius of round wire (cm)

If the straight length of wire is bent in any direction, then elements of the wire will be linked by magnetic lines of flux to other elements. The self-inductance of the total length of wire will be reduced by an amount proportional to the flux linkages between the elements. This phenomenon of reduction in self-inductance of a length of wire through mutual coupling to itself is the basis of differential inductance. The straight length of wire will now be bent to form a one-turn loop as seen in Figure C2.

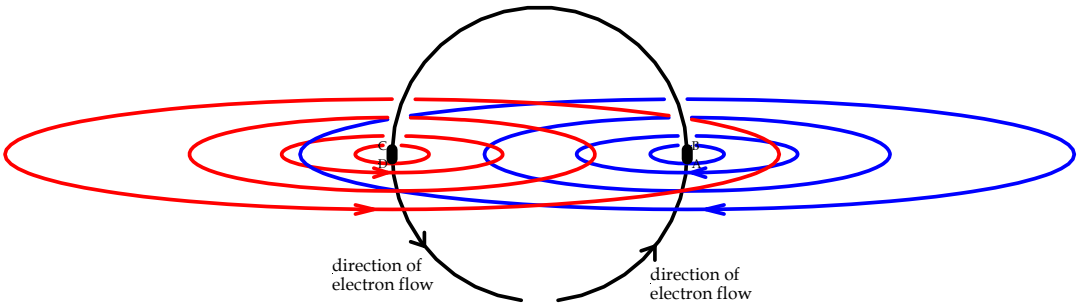

Figure C2

Two diametrically opposed elements of the loop are shown in bold. An electron current shown by the arrows will produce lines of magnetic flux centred on the elements with their indicated direction; *left-hand rule for a current-carrying wire,* see *Appendix A*. Different colours have been chosen for the magnetic fields surrounding the elements to prevent confusion between fields. If the assumption is made that the current in the wire is increasing, then the current induced into an element from the rate of change in flux from the one diametrically opposed will be in the same direction as the main current flowing through that element; *left-hand rule for induced currents,* again see *Appendix A*. This has the effect of aiding the current flow and not opposing it as expected by Lenz's law. The effect of opposing Lenz's law, or reducing the elements self-inductance, is governed by the Biot-Savart law; i.e. the inverse square law with distance. The smaller the diameter of the one turn loop, the stronger the fields will be from the diametrically opposed elements (for a given current) and the greater the effect the diametrically opposed elements have on reducing the loops self inductance. This is the

reason why an equivalent straight length of wire to the circumference of the one turn loop will always return a larger self-inductance than that of the one turn loop.

The self-inductance of a single turn circular loop can be calculated using the following equation obtained from [9, ch. 6 pg. 9]:

$$L = \frac{r}{254}\left(3.193 Log_e \frac{16r}{d} - 6.386\right) \tag{C.4}$$

where: L = inductance (uH)
r = mean radius of single turn loop (cm)
d = diameter of wire (cm)

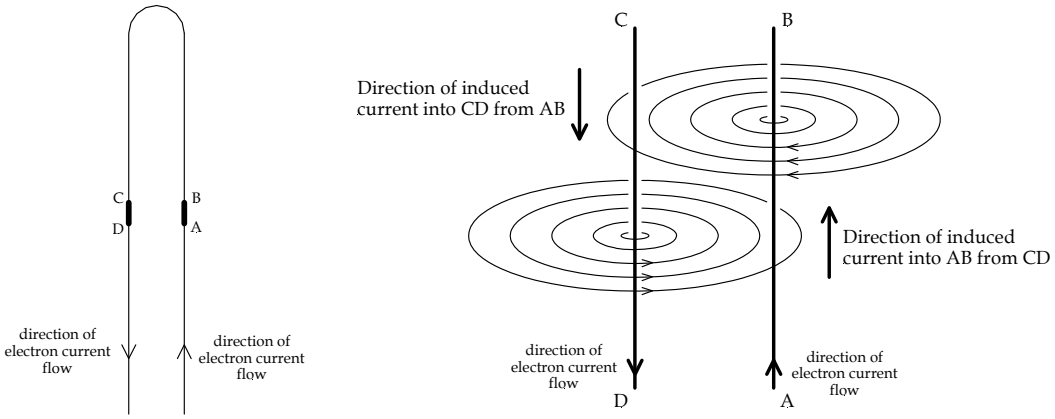

Figure C3

The sides of the one turn loop will now be squashed together to form an inverted U shaped parallel wire conductor, Figure C3 (a). Opposing elements AB and CD are highlighted and are enlarged in Figure C3 (b). The direction of the magnetic fields and induced currents for an expanding magnetic field are indicated in Figure C3 (b).

As in the case of the one turn loop, applying the left-hand rules will show the induced currents are in the same direction as the main current flow and hence have the effect of reducing the self inductance of the elements. The difference being that the elements are much closer together and the reduction in their self-inductance is more pronounced. This is the case of ordinary parallel wire transmission line whose conductors have a length (l) that is large compared to their separation (D). The self-inductance of the circuit, more commonly known as *differential mode inductance*, is [11, pg. 363]:

$$L_{diff} = 0.004 l\left(\ln\frac{D}{r} + \frac{1}{4} - \frac{D}{l}\right) \tag{C.5}$$

where: L_{diff} = differential-mode inductance of parallel conductors (μH)
l = length of parallel conductors (cm)
D = distance between centres of parallel conductors (cm)
r = radius of parallel conductors (cm)

The key point to note in equation (C.5) is that differential mode inductance is proportional to both the length and the distance *D* between the parallel conductors.

The straight length of wire that was used in the above examples will now be used to form the two-turn loop seen in Figure C4. The arrows indicate the direction of electron current flow. The effects of differential inductance as can be seen in Figure C4 (b) has already been covered above. The difference being that there two adjacent elements interacting with two diagonally adjacent elements (two turn coil) reducing the self-inductance of each element even more. It should be remembered that the inverse square law means that the reduction in inductance is going to be small unless the distance between the diagonally opposite elements is very small, as would be the case of a very small diameter coil, usually in the nH range.

Figure C5 shows the parallel elements CD and GH of adjacent turns. With the time varying electron current indicated, the *left-hand rule for induced currents* shows that the mutually induced currents oppose the flow of the main current in each element. This has the effect of increasing the self-inductance of both elements. The Biot-Savart law also governs the increase in self-inductance. The closer the two elements are together the greater the effect maximising just before the elements make electrical contact or, if the elements are insulated, when the insulation touches.

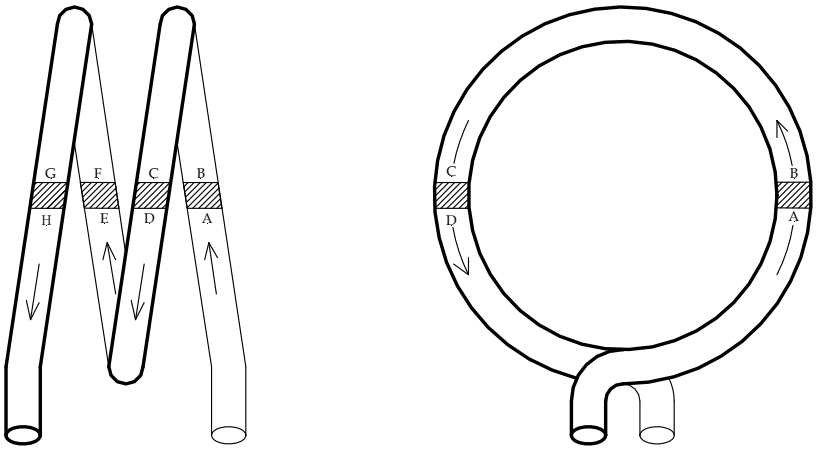

arrows indicate direction of electron current flow

(a)

arrows indicate direction of electron current flow

(b)

Figure C4

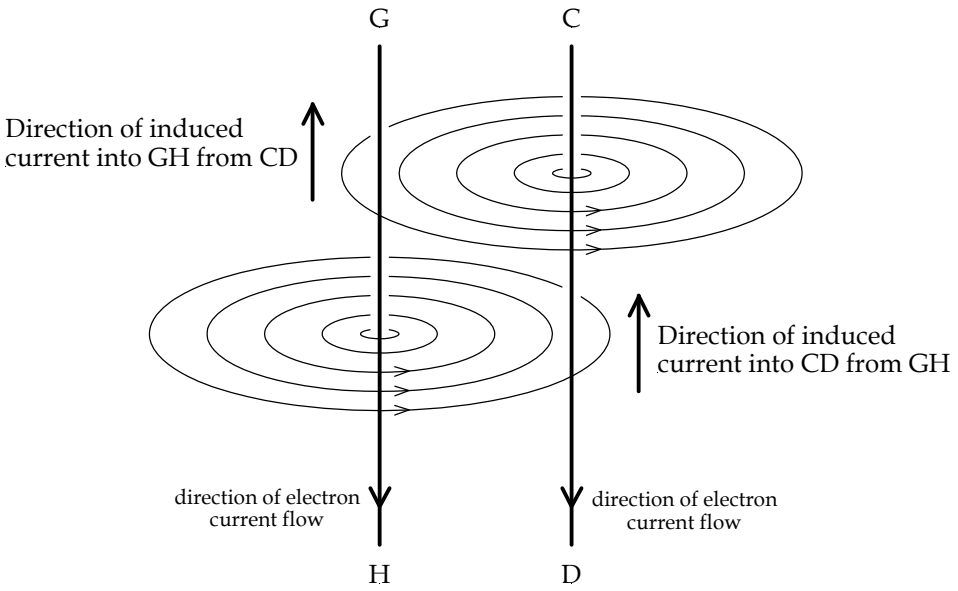

Common mode currents in parallel wires

Figure C5

Because the main current flowing through both parallel elements is in the same common direction the effect that these two elements of wire have upon the inductance of each other is known as the *common mode inductance*. Two parallel straight wires, distance D between their axis, have a common mode inductance of [11, pg. 362] :

$$L = 0.002\,l\left(\ln\frac{2l}{\sqrt{r\,D}} - \frac{7}{8}\right) \tag{C.6}$$

where: L = common-mode inductance of parallel conductors (μH)
l = length of parallel conductors (cm)
D = distance between centres of parallel conductors (cm)
r = radius of parallel conductors (cm)

From the foregoing it can be seen that the factors that have to be considered when calculating the self-inductance of a single layered coil are quite complex and not easily calculated. There are many equations contained in texts that try to predict the low frequency inductance of single layer coils. The one by Wheeler seems to be the most popular.

Equation (C.7) is Wheeler's formula for calculating the approximate low frequency inductance for short air wound coils in which the values of l are between one tenth of r and two thirds of r. Note the inductance varies as the square of the turns, i.e. if the number of turns is doubled, for a given l and r, the inductance is quadrupled.

$$L = \frac{0.394 r^2 n^2}{\left(9 - \frac{r}{5l}\right) r + 10 l} \tag{C.7}$$

where: L = low frequency inductance (uH)
r = coil radius (cm)
l = coil length (cm)
n = number of turns

When l is greater than two thirds of r, equation (C.7) simplifies to:

$$L = \frac{0.394 r^2 n^2}{9r + 10 l} \tag{C.8}$$

Wheeler's formula does not take into account the variation in a coil's inductance with the thickness of the wire. The formula given below, due to Reyner [13], gives the inductance of normal air wound coils to within a few percent. If the wire used to construct the coil is of appreciable thickness an additional correction factor is introduced by the second part of the expression.

$$L = \frac{0.2 n^2 D^2}{3.5 D + 8 l} \times \frac{D - 2.25 t}{D} \tag{C.9}$$

where: L = low frequency inductance (uH)
D = outside diameter of coil (inches)
l = coil length (inches)
n = number of turns
t = winding thickness (inches)

Both Wheeler's and Reyner's equations work well with coils in the few cm diameter range but become less accurate as the coil's diameter is made either very small or very large. Also, there are other factors that alter the low frequency inductance value of coils when they are used at radio frequencies. Some of these are the effects of the coil's distributed capacitance and a non-uniform current distribution in the length of conductor used to make the coil. The effect the distributed capacitance of a coil has on its low frequency inductance as its operating frequency is raised is covered in [15]. The non-uniform current distribution is of special concern to builders of receiving loop antennas and is discussed the main text and *Appendix A*.

In short, no simple formula can accurately predict the inductance of normally wound solenoid coils. Such formula needs to be modified to suit the diameter of the coils and the amount of internal coupling within the coil, i.e. the distance between elements of the coil to all other elements and the direction of current flow within those elements. This is reflected in the proliferation of various inductance formulae in R.F. texts to cover coils of various sizes. Any formula used to predict the low frequency inductance of a coil should be treated as a guide and there is no substitute for the direct measurement of a coil's inductance at its intended frequency of use.

Appendix D: The Differential Inductance of the Twin-Loop Receive Antenna

The following is offered to describe the differential currents in the Giselle twin-loop receive antenna from a travelling time varying *E* field and the dominant role the differential inductance plays.

Figure D1 (A) shows the instantaneous voltages induced into the vertical sides of the twin-loop from a travelling time varying vertically orientated *E* field. The length of the arrows indicate their relative magnitudes; V1 = V2, V3 = V4 and V1 > V3. The conductors in the twin-loop antenna form a closed loop. Any voltage induced into any part of this loop will cause a current to flow in the opposite direction to the direction of the induced voltage. Figure D1 (B) shows the direction of currents created by the induced voltages.

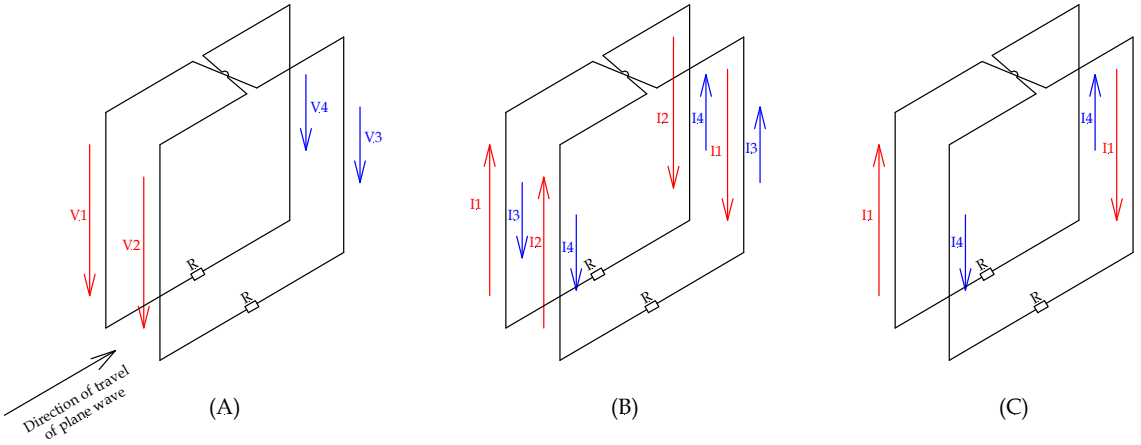

Figure D1: Instantaneous induced voltages (A) and resulting currents (B) into the twin-loop Giselle antenna from a time varying travelling E field. In (C) only one of the two differential currents flowing is shown.

The flow of currents is complex as the induced voltages make their presence known across the two termination resistors R. In (C) two currents I1 and I4 have been isolated. These currents are differential and give rise to a differential inductance between the two parallel conductors of the twin-loop. I2 and I3 are also differential currents in the parallel conductors and they too give rise to a differential inductance between them. The value of differential inductance in the Giselle two-turn loop is usually much smaller and appears in shunt with the straight two-turn inductance of a short air wound coil and therefore usually predominates.

Appendix E: Faraday Shielded Test Loop

The Faraday shielded test loop described in this appendix is used to check the functionality of the tri-axial receiving loops. The test loop is connected to a signal generator via an arbitrary length of 50 Ω coax. The test loop is held by hand at approximately the intersection of the three axes of the receiving loops. The test loop is rotated until the plane of the test loop lines up with the plane of one of the three receiving loops. This is the orientation where maximum coupling occurs between the two loops. The expected difference in dB between the signal power delivered to the test loop from the signal generator to the power at the output of the RF amplifier is given in equation (E.1). It is based on the Biot-Savart law, equation (C.1) in *Appendix C*.

$$dB = 20Log_{10}\frac{1}{\left(\frac{D_1}{D_2}\right)^2} - 9 + G_{dB} \tag{E.1}$$

where: dB = expected attenuation between the signal power delivered to the input terminals of the test loop to the power at the output of the RF amplifier of the receiving loop when the two axis of the loops are co-located and their planes aligned. (dB)
D_1 = equivalent mean circular diameter of receiving loop (m)
D_2 = mean diameter of circular test loop (m)
G_{dB} = gain of R.F. amplifier in twin-loop = 22 in the current design (dB)

For an octagonal loop, D_1 is:

$$D_1 = \sqrt{6.1472\,S^2} \tag{E.2}$$

where: D_1 = diameter of circle of equivalent area to that of an octagonal loop (m)
S = length of one of the sides of the eight sides of the octagon (m)

and for a square loop:

$$D_1 = 1.1284\,S \tag{E.3}$$

where: D_1 = diameter of circle of equivalent area to that of a square loop (m)
S = length of the side of the square (m).

The input impedance of the test loop is a relatively constant 50 Ω from 1 MHz to 60 MHz, see Figure E1. There is a small increase in input resistance of a few ohms as the frequency is raised due to radiation losses. This relatively constant input impedance means that the generated *H* field can be readily calculated from the loop area and the R.F. power presented to the test loop's input terminals.

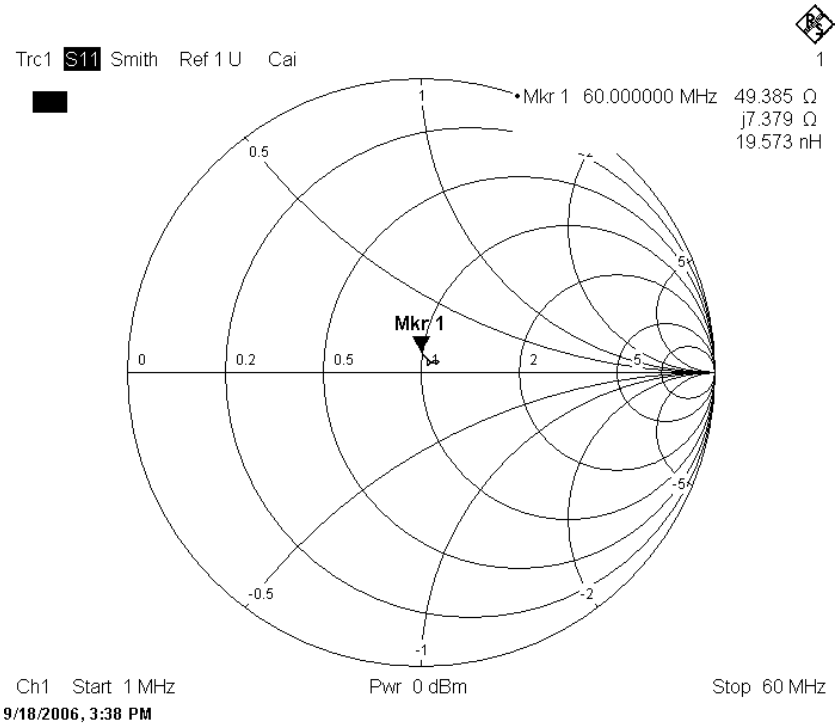

Figure E1: Input S11 of the test loop from 1 MHz to 60 MHz. Marker is at 60 MHz.

Figure E2 describes the electrical and mechanical construction of the test loop. T2 is a balun transforming the un-balanced 50 Ω from the co-ax cable into 50 Ω balanced. T1 is a step-up transformer stepping the 50 Ω balanced to 200 Ω balanced to differentially drive the centre conductor of the shielded loop. The circular loop itself is made from two equal lengths of RG-402 semi-rigid 50 Ω co-ax. The outer sheaths of the co-ax are earthed at the driving end only thus forming a Faraday shield around the inner. The two inner conductors are connected together via a 200 Ω resistive termination.

Changing the apparent characteristic impedance of the co-axial line

The characteristic impedance of a transmission line can be calculated from its distributed L and C per unit length, equation (E.4).

$$Z_o = \sqrt{\frac{L}{C}} \tag{E.4}$$

where Z_o = characteristic impedance (ohms)
L = distributed inductance per unit length (H)
C = distributed capacitance per unit length (F)

The distributed inductances of the two equal lengths of the centre conductor of the coax in the test loop are added together as would normally be expected for a series circuit. The break in the outer sheaths of the co-ax at the 200 Ω termination end has the effect of connecting the distributed capacitances of the two equal lengths of co-ax in series halving the capacitance seen by the centre conductor to each of the outer sheaths. With the distributed inductance being doubled and the distributed capacitance halved, it follows that the co-ax's characteristic

impedance appears to have doubled. There is an upper frequency limit to this effect due to the build up of standing waves of currents flowing on the outer conducting sheath as the frequency is raised. This limit is when the length of co-ax between the source and termination exceeds 0.05 that of the free space wavelength, equation (E.5).

$$f_{MHz} = \frac{300}{20l} \tag{E.5}$$

where f_{MHz} = upper frequency limit due to standing waves (MHz)
l = length of co-ax line between the signal source and the terminations (m)

In the current design the length of co-ax between the source and termination is 0.251 m. Using this value in equation (E.5) returns an upper frequency limit for the test loop of 59.7 MHz. Up to this frequency the two lengths of 50 Ω co-ax have the apparent characteristic impedance of 100 Ω each. Above this frequency the co-axial cable appears reactive as the effects of standing waves predominates and the generated *H* field from the test loop becomes complex to determine.

The 3.3 pF compensation capacitor in shunt with the 200 Ω termination was chosen to minimise the unwanted reactance that is present at the 50 Ω input to the test Tx loop antenna. Its value is proportional to the area of the loop. A test loop of say four times the area to the one described here would require a compensation capacitor value of 4 x 3.3 = 13.2 pF.

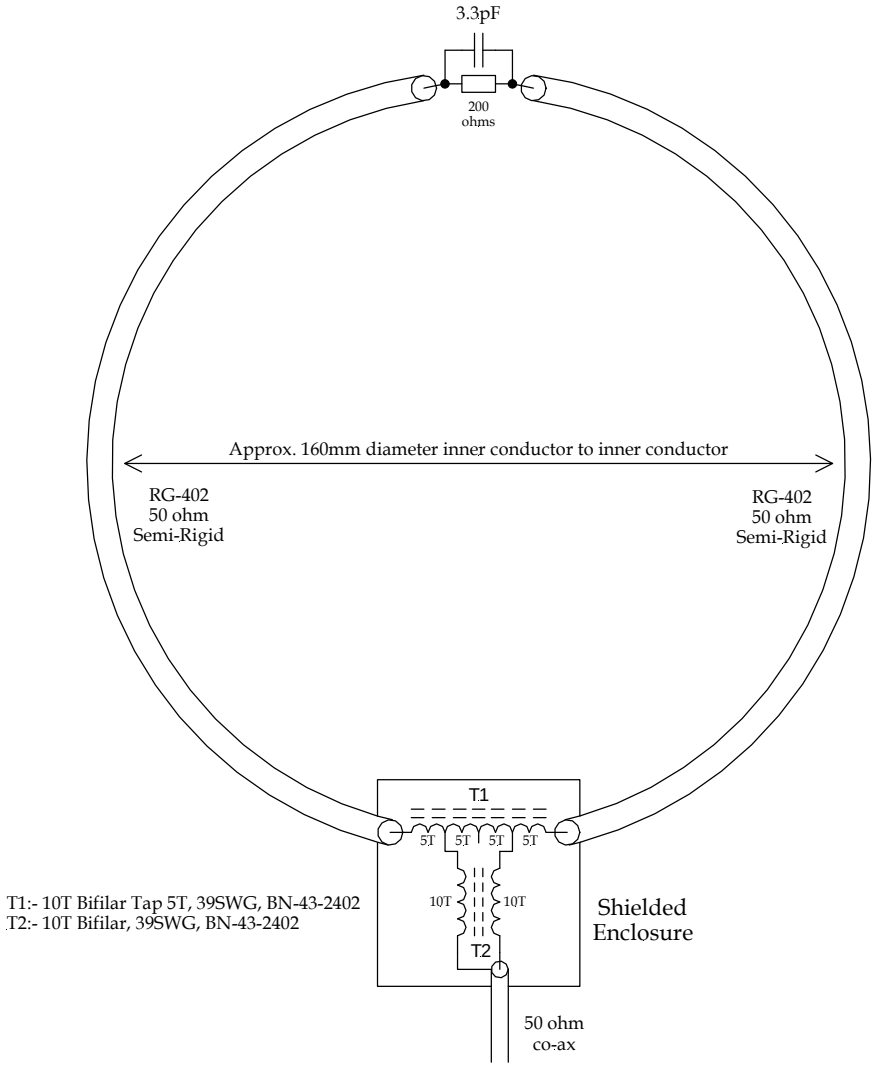

Figure E2: The Faraday Shielded Tx loop used to test the Giselle twin-loop array

Appendix F: Using a Shielded Loop to Generate and Measure an E field

Using the Tx Loop to generate a known E far field

The Tx loop can also be used to generate a known *E* far field using the following equation from [24, pg. 213].

$$E = \frac{120\,\pi^2 IA\,f^2}{d\,300^2}\sin\theta \tag{F.1}$$

The *H* far field can be found by dividing the above equation for the *E* field by the free space impedance (120π) giving:

$$H = \frac{\pi\, IA\,f^2}{d\,300^2}\sin\theta \tag{F.2}$$

where: E = *E* far field in Volts/metre
H = *H* far field in Amps/metre
I = current flowing in loop (A)
A = area of loop (m^2)
f = frequency (MHz)
d = distance between the centre of the loop and the point where the field needs to be calculated (m)
θ = angle between the axis of the loop and the point where the field is to be calculated.

Using an Rx Loop to measure a generated E far field

In the Tx loop the RF source was an exciter connected to the antenna's matching circuit and the load for this source was the 200 Ω termination diametrically opposed on the loop. In the Rx loop the RF source is the time varying *E* field and the load is the 200 Ω presented by the loop matching circuit as it steps up the 50 Ω input impedance of the receiver. The 200 Ω termination resistor needs to be removed and the two inners of the co-ax connected together, see Figure F2. The loop needs to be made as large as possible for best sensitivity before the effects of standing waves on the outer shield causes significant deviation from equation (F.3).

$$E = \frac{V300}{G_f\,2\pi\,f\,A}\sqrt{\frac{R_L}{R_R}} \tag{F.3}$$

where: E = *E* field strength (V/m)
V = measured terminated voltage at the input to the receiver (V)
f = frequency (MHz)
A = area of loop (m^2)
R_L = impedance presented to the inner conductors of the co-axial loop, 200 Ω for the design in Figure F2 (Ω)
R_R = input impedance of the measuring receiver, 50 Ω
G_f = ground factor, 2 for perfect ground, 1 for free space.

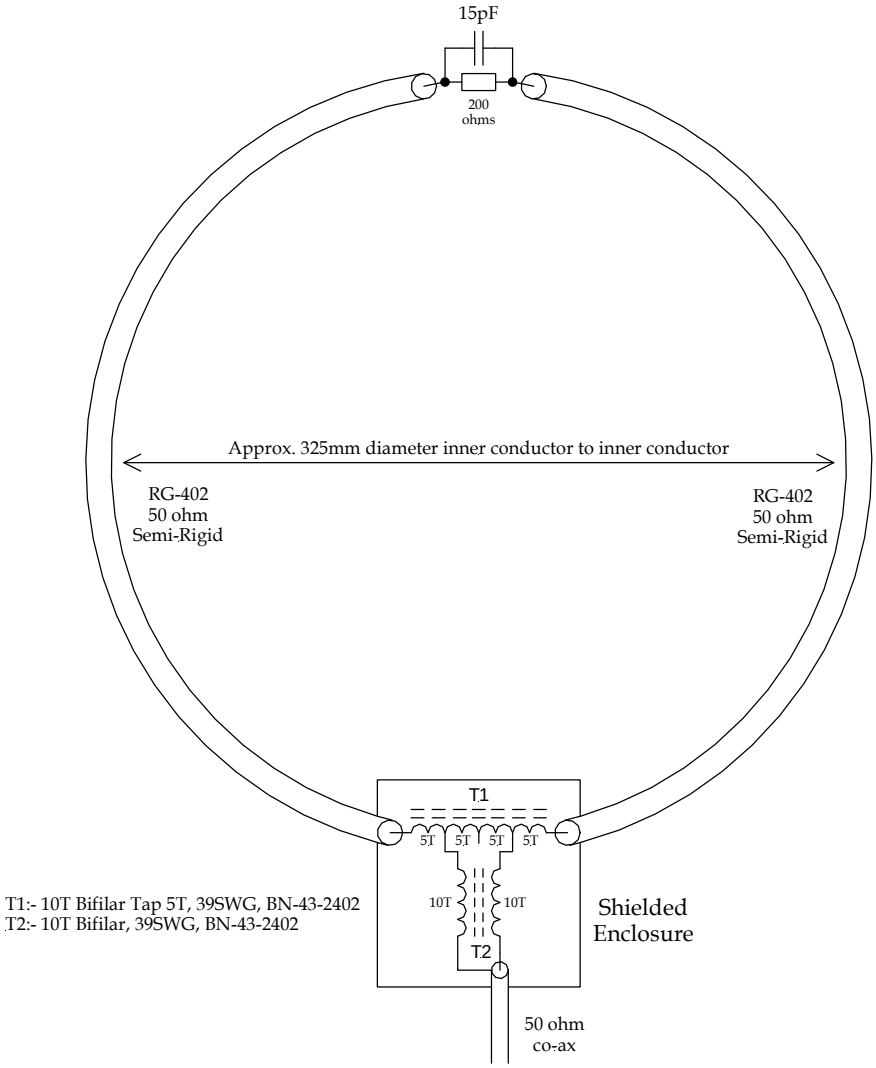

Figure F1: The Faraday Shielded Tx Loop which can be used to generate a known E field intensity as described by equation (F.1)

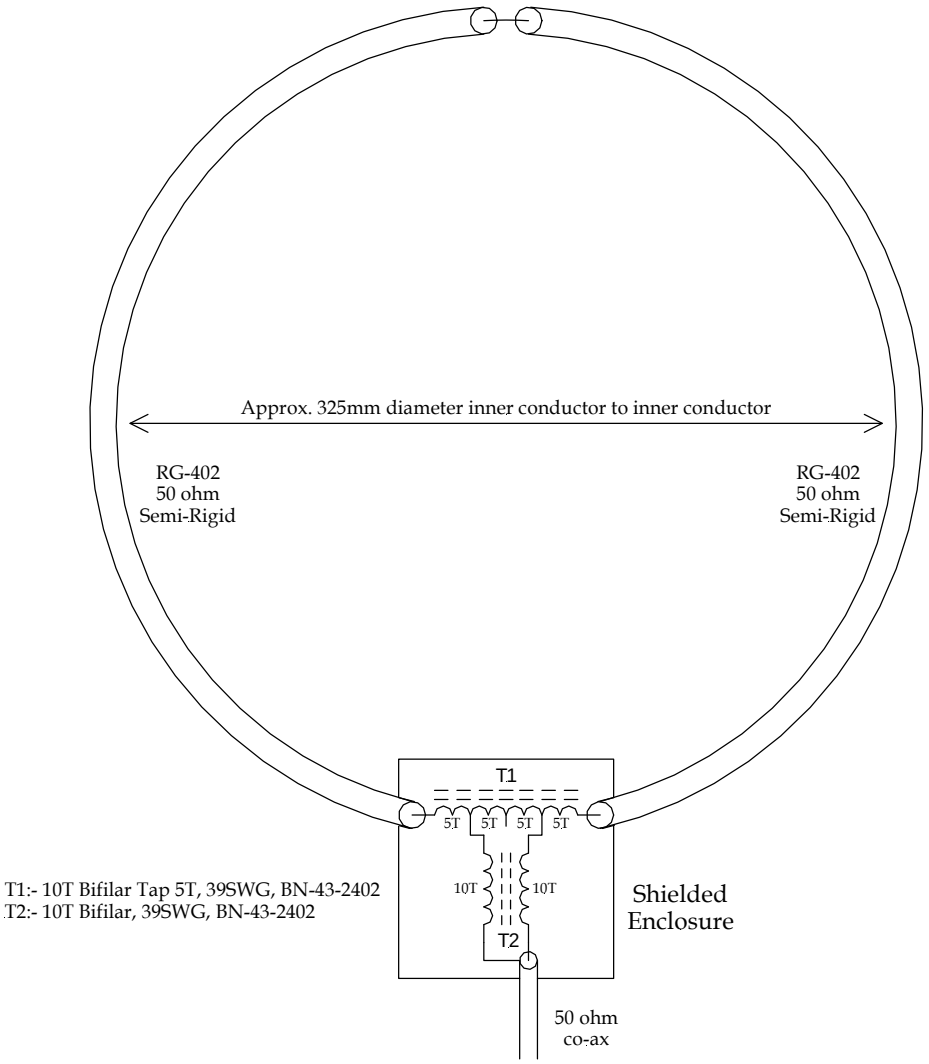

Figure F2: The Faraday Shielded Rx Loop which can be used to measure the intensity of an E field using equation (F.3)

Appendix G: NEC-4 Simulation

The following four pages contain the NEC-4 listing for the twin-loop tri-axial Giselle array. There are many limitations that have been placed on the simulated geometrical model due to shortcomings of NEC-4. The main limitation is NEC-4 does not like large abrupt changes in wire diameter. In the real world the loop's crossovers were made using 40 mm lengths of 1mm diameter wire that were soldered to the insides of the 10 mm diameter aluminium tubes. There are two abrupt changes at each crossover, 10 mm to 1 mm then 1mm back to 10 mm. As expected, the accumulation of errors induced by the 32 abrupt changes in wire diameter in the NEC-4 simulation of the twin-loop produced intolerable errors. A fixed wire diameter of 2 mm was used in the whole simulated geometrical structure as a compromise between this and other NEC-4 geometric layout guidelines.

The simulation was carried out in free space (absence of a ground plane) to discount the effects on the array by ground reflections. All simulated receive pattern plots have a 1 V/m plane wave traversing the structure.

The following three parameters in the standard polar coordinate system were used to describe the direction of travel of the plane wave in order to measure the peak in response and the depth of null of one of the three twin-loops in the array. For the current in the 377 Ω loads in tag numbers 119 and 120 in loop 2, the maximum (I_{max}) was found by setting the Poynting vector and polarisation of the traversing 1V/m wave to:

theta	35 degrees
phi	180 degrees
eta	90 degrees

and to measure the current at the null (I_{min}):

theta	55 degrees
phi	0 degrees
eta	0 degrees

where: theta: elevation angle with respect to the positive Z axis,
phi: azimuth angle with respect to the positive X axis and rotating in the XY plane towards the Y axis and,
eta: wave polarisation angle with respect to the direction of the Z axis.

The difference in *dB* between these two currents, or the depth of null, was calculated using:

$$dB = 20\log_{10}\frac{I_{\min}}{I_{\max}} \tag{F.1}$$

Loops 1 and 3 are expected to produce very simular plots due to the geometric symmetry between loops.

NEC-4 Listing of the Giselle Antenna

```
CM 0.66 m/side OCT 2 TURN GISELLE LOOP ARRAY
CE
GW 1 5 -0.01 0.33 -0.796 -0.31 0.33 -0.796 0.001
GW 2 5 0.31 0.33 -0.796 0.01 0.33 -0.796 0.001
GW 3,10, 0.344,0.33,-0.782, 0.782,0.33,-0.344, 0.001
GW 4,10, 0.796,0.33,-0.31, 0.796,0.33,0.31, 0.001
GW 5,10, 0.782,0.33,0.344, 0.344,0.33,0.782, 0.001
GW 6,5, 0.31,0.33,0.796, 0.005,0.33,0.796, 0.001
GW 7,5, -0.005,0.33,0.796, -0.31,0.33,0.796, 0.001
GW 8,10, -0.344,0.33,0.782, -0.782,0.33,0.344, 0.001
GW 9,10, -0.796,0.33,0.31, -0.796,0.33,-0.31, 0.001
GW 10,10, -0.782,0.33,-0.344, -0.344,0.33,-0.782, 0.001
GW 11 5 -0.01 -0.33 -0.796 -0.31 -0.33 -0.796 0.001
GW 12 5 0.31 -0.33 -0.796 0.01 -0.33 -0.796 0.001
GW 13,10, 0.344,-0.33,-0.782, 0.782,-0.33,-0.344, 0.001
GW 14,10, 0.796,-0.33,-0.31, 0.796,-0.33,0.31, 0.001
GW 15,10, 0.782,-0.33,0.344, 0.344,-0.33,0.782, 0.001
GW 16,5, 0.31,-0.33,0.796, 0.005,-0.33,0.796, 0.001
GW 17,5, -0.005,-0.33,0.796, -0.31,-0.33,0.796, 0.001
GW 18,10, -0.344,-0.33,0.782, -0.782,-0.33,0.344, 0.001
GW 19,10, -0.796,-0.33,0.31, -0.796,-0.33,-0.31, 0.001
GW 20,10, -0.782,-0.33,-0.344, -0.344,-0.33,-0.782, 0.001
GW 21 1 -0.005 0.33 0.796 0.005 0.33 0.796 0.001 !Top Transmission Line
GW 22 1 -0.005 -0.33 0.796 0.005 -0.33 0.796 0.001 !Top Transmission Line
GW 27,1, 0.31,0.33,-0.796, 0.33,0.33,-0.796, 0.001
GW 28,1, 0.33,0.33,-0.796, 0.344,0.33,-0.782, 0.001
GW 29,1, -0.31,0.33,-0.796, -0.33,0.33,-0.796, 0.001
GW 30,1, -0.33,0.33,-0.796, -0.344,0.33,-0.782, 0.001
GW 31,1, 0.782,0.33,-0.344, 0.782,0.33,-0.324, 0.001
GW 32,1, 0.782,0.33,-0.324, 0.796,0.33,-0.31, 0.001
GW 33,1, -0.782,0.33,-0.344, -0.782,0.33,-0.324, 0.001
GW 34,1, -0.782,0.33,-0.324, -0.796,0.33,-0.31, 0.001
GW 35,1, 0.796,0.33,0.31, 0.782,0.33,0.324, 0.001
GW 36,1, 0.782,0.33,0.324, 0.782,0.33,0.344, 0.001
GW 37,1, -0.796,0.33,0.31, -0.782,0.33,0.324, 0.001
GW 38,1, -0.782,0.33,0.324, -0.782,0.33,0.344, 0.001
GW 39,1, 0.344,0.33,0.782, 0.33,0.33,0.796, 0.001
GW 40,1, 0.33,0.33,0.796, 0.31,0.33,0.796, 0.001
GW 41 1 -0.344 0.33 0.782 -0.324 0.33 0.782 0.001
GW 42 1 -0.324 0.33 0.782 -0.31 0.33 0.796 0.001
GW 43 1 0.31 -0.33 -0.796 0.324 -0.33 -0.782 0.001
GW 44 1 0.324 -0.33 -0.782 0.344 -0.33 -0.782 0.001
GW 45,1, -0.31,-0.33,-0.796, -0.33,-0.33,-0.796, 0.001
GW 46,1, -0.33,-0.33,-0.796, -0.344,-0.33,-0.782, 0.001
GW 47,1, 0.782,-0.33,-0.344, 0.782,-0.33,-0.324, 0.001
GW 48,1, 0.782,-0.33,-0.324, 0.796,-0.33,-0.31, 0.001
GW 49,1, -0.782,-0.33,-0.344, -0.782,-0.33,-0.324, 0.001
GW 50,1, -0.782,-0.33,-0.324, -0.796,-0.33,-0.31, 0.001
GW 51,1, 0.796,-0.33,0.31, 0.782,-0.33,0.324, 0.001
GW 52,1, 0.782,-0.33,0.324, 0.782,-0.33,0.344, 0.001
GW 53 1 -0.796 -0.33 0.31 -0.796 -0.33 0.33 0.001
GW 54 1 -0.796 -0.33 0.33 -0.782 -0.33 0.344 0.001
GW 55,1, 0.344,-0.33,0.782, 0.33,-0.33,0.796, 0.001
GW 56,1, 0.33,-0.33,0.796, 0.31,-0.33,0.796, 0.001
GW 57,1, -0.344,-0.33,0.782, -0.33,-0.33,0.796, 0.001
```

```
GW 58,1, -0.33,-0.33,0.796, -0.31,-0.33,0.796, 0.001
GW 59 1 0.01 -0.33 -0.796 -0.01 -0.33 -0.796 0.001 !Loop Load
GW 60 1 0.01 0.33 -0.796 -0.01 0.33 -0.796 0.001 !Loop Load
CM END OF 1ST TWIN LOOP
CE
GW 61 5 -0.01 0.33 -0.796 -0.31 0.33 -0.796 0.001
GW 62 5 0.31 0.33 -0.796 0.01 0.33 -0.796 0.001
GW 63,10, 0.344,0.33,-0.782, 0.782,0.33,-0.344, 0.001
GW 64,10, 0.796,0.33,-0.31, 0.796,0.33,0.31, 0.001
GW 65,10, 0.782,0.33,0.344, 0.344,0.33,0.782, 0.001
GW 66,5, 0.31,0.33,0.796, 0.005,0.33,0.796, 0.001
GW 67,5, -0.005,0.33,0.796, -0.31,0.33,0.796, 0.001
GW 68,10, -0.344,0.33,0.782, -0.782,0.33,0.344, 0.001
GW 69,10, -0.796,0.33,0.31, -0.796,0.33,-0.31, 0.001
GW 70,10, -0.782,0.33,-0.344, -0.344,0.33,-0.782, 0.001
GW 71 5 -0.01 -0.33 -0.796 -0.31 -0.33 -0.796 0.001
GW 72 5 0.31 -0.33 -0.796 0.01 -0.33 -0.796 0.001
GW 73,10, 0.344,-0.33,-0.782, 0.782,-0.33,-0.344, 0.001
GW 74,10, 0.796,-0.33,-0.31, 0.796,-0.33,0.31, 0.001
GW 75,10, 0.782,-0.33,0.344, 0.344,-0.33,0.782, 0.001
GW 76,5, 0.31,-0.33,0.796, 0.005,-0.33,0.796, 0.001
GW 77,5, -0.005,-0.33,0.796, -0.31,-0.33,0.796, 0.001
GW 78,10, -0.344,-0.33,0.782, -0.782,-0.33,0.344, 0.001
GW 79,10, -0.796,-0.33,0.31, -0.796,-0.33,-0.31, 0.001
GW 80,10, -0.782,-0.33,-0.344, -0.344,-0.33,-0.782, 0.001
GW 81 1 -0.005 0.33 0.796 0.005 0.33 0.796 0.001 !Top Transmission Line
GW 82 1 -0.005 -0.33 0.796 0.005 -0.33 0.796 0.001 !Top Transmission Line
GW 87,1, 0.31,0.33,-0.796, 0.33,0.33,-0.796, 0.001
GW 88,1, 0.33,0.33,-0.796, 0.344,0.33,-0.782, 0.001
GW 89 1 -0.31 0.33 -0.796 -0.324 0.33 -0.782 0.001
GW 90 1 -0.324 0.33 -0.782 -0.344 0.33 -0.782 0.001
GW 91,1, 0.782,0.33,-0.344, 0.782,0.33,-0.324, 0.001
GW 92,1, 0.782,0.33,-0.324, 0.796,0.33,-0.31, 0.001
GW 93,1, -0.782,0.33,-0.344, -0.782,0.33,-0.324, 0.001
GW 94,1, -0.782,0.33,-0.324, -0.796,0.33,-0.31, 0.001
GW 95 1 0.796 0.33 0.31 0.796 0.33 0.33 0.001
GW 96 1 0.796 0.33 0.33 0.782 0.33 0.344 0.001
GW 97,1, -0.796,0.33,0.31, -0.782,0.33,0.324, 0.001
GW 98,1, -0.782,0.33,0.324, -0.782,0.33,0.344, 0.001
GW 99,1, 0.344,0.33,0.782, 0.33,0.33,0.796, 0.001
GW 100,1, 0.33,0.33,0.796, 0.31,0.33,0.796, 0.001
GW 101,1, -0.344,0.33,0.782, -0.33,0.33,0.796, 0.001
GW 102,1, -0.33,0.33,0.796, -0.31,0.33,0.796, 0.001
GW 103,1, 0.31,-0.33,-0.796, 0.33,-0.33,-0.796, 0.001
GW 104,1, 0.33,-0.33,-0.796, 0.344,-0.33,-0.782, 0.001
GW 105,1, -0.31,-0.33,-0.796, -0.33,-0.33,-0.796, 0.001
GW 106,1, -0.33,-0.33,-0.796, -0.344,-0.33,-0.782, 0.001
GW 107 1 0.796 -0.33 -0.33 0.796 -0.33 -0.31 0.001
GW 108 1 0.796 -0.33 -0.33 0.782 -0.33 -0.344 0.001
GW 109 1 -0.782 -0.33 -0.344 -0.796 -0.33 -0.33 0.001
GW 110 1 -0.796 -0.33 -0.33 -0.796 -0.33 -0.31 0.001
GW 111,1, 0.796,-0.33,0.31, 0.782,-0.33,0.324, 0.001
GW 112,1, 0.782,-0.33,0.324, 0.782,-0.33,0.344, 0.001
GW 113,1, -0.796,-0.33,0.31, -0.782,-0.33,0.324, 0.001
GW 114,1, -0.782,-0.33,0.324, -0.782,-0.33,0.344, 0.001
GW 115,1, 0.344,-0.33,0.782, 0.33,-0.33,0.796, 0.001
GW 116,1, 0.33,-0.33,0.796, 0.31,-0.33,0.796, 0.001
```

```
GW 117,1, -0.344,-0.33,0.782, -0.33,-0.33,0.796, 0.001
GW 118,1, -0.33,-0.33,0.796, -0.31,-0.33,0.796, 0.001
GW 119 1 0.01 -0.33 -0.796 -0.01 -0.33 -0.796 0.001 !Loop Load
GW 120 1 0.01 0.33 -0.796 -0.01 0.33 -0.796 0.001 !Loop Load
CM END OF 2ND TWIN LOOP
CE
GW 121 5 -0.01 0.33 -0.796 -0.31 0.33 -0.796 0.001
GW 122 5 0.31 0.33 -0.796 0.01 0.33 -0.796 0.001
GW 123,10, 0.344,0.33,-0.782, 0.782,0.33,-0.344, 0.001
GW 124,10, 0.796,0.33,-0.31, 0.796,0.33,0.31, 0.001
GW 125,10, 0.782,0.33,0.344, 0.344,0.33,0.782, 0.001
GW 126,5, 0.31,0.33,0.796, 0.005,0.33,0.796, 0.001
GW 127,5, -0.005,0.33,0.796, -0.31,0.33,0.796, 0.001
GW 128,10, -0.344,0.33,0.782, -0.782,0.33,0.344, 0.001
GW 129,10, -0.796,0.33,0.31, -0.796,0.33,-0.31, 0.001
GW 130,10, -0.782,0.33,-0.344, -0.344,0.33,-0.782, 0.001
GW 131 5 -0.01 -0.33 -0.796 -0.31 -0.33 -0.796 0.001
GW 132 5 0.31 -0.33 -0.796 0.01 -0.33 -0.796 0.001
GW 133,10, 0.344,-0.33,-0.782, 0.782,-0.33,-0.344, 0.001
GW 134,10, 0.796,-0.33,-0.31, 0.796,-0.33,0.31, 0.001
GW 135,10, 0.782,-0.33,0.344, 0.344,-0.33,0.782, 0.001
GW 136,5, 0.31,-0.33,0.796, 0.005,-0.33,0.796, 0.001
GW 137,5, -0.005,-0.33,0.796, -0.31,-0.33,0.796, 0.001
GW 138,10, -0.344,-0.33,0.782, -0.782,-0.33,0.344, 0.001
GW 139,10, -0.796,-0.33,0.31, -0.796,-0.33,-0.31, 0.001
GW 140,10, -0.782,-0.33,-0.344, -0.344,-0.33,-0.782, 0.001
GW 141 1 -0.005 0.33 0.796 0.005 0.33 0.796 0.001 !Top Transmission Line
GW 142 1 -0.005 -0.33 0.796 0.005 -0.33 0.796 0.001 !Top Transmission Line
GW 147,1, 0.31,0.33,-0.796, 0.33,0.33,-0.796, 0.001
GW 148,1, 0.33,0.33,-0.796, 0.344,0.33,-0.782, 0.001
GW 149 1 -0.31 0.33 -0.796 -0.324 0.33 -0.782 0.001
GW 150 1 -0.324 0.33 -0.782 -0.344 0.33 -0.782 0.001
GW 151,1, 0.782,0.33,-0.344, 0.782,0.33,-0.324, 0.001
GW 152,1, 0.782,0.33,-0.324, 0.796,0.33,-0.31, 0.001
GW 153,1, -0.782,0.33,-0.344, -0.782,0.33,-0.324, 0.001
GW 154,1, -0.782,0.33,-0.324, -0.796,0.33,-0.31, 0.001
GW 155 1 0.796 0.33 0.31 0.796 0.33 0.344 0.001
GW 156 1 0.796 0.33 0.344 0.782 0.33 0.344 0.001
GW 157,1, -0.796,0.33,0.31, -0.782,0.33,0.324, 0.001
GW 158,1, -0.782,0.33,0.324, -0.782,0.33,0.344, 0.001
GW 159,1, 0.344,0.33,0.782, 0.33,0.33,0.796, 0.001
GW 160,1, 0.33,0.33,0.796, 0.31,0.33,0.796, 0.001
GW 161,1, -0.344,0.33,0.782, -0.33,0.33,0.796, 0.001
GW 162,1, -0.33,0.33,0.796, -0.31,0.33,0.796, 0.001
GW 163,1, 0.31,-0.33,-0.796, 0.33,-0.33,-0.796, 0.001
GW 164,1, 0.33,-0.33,-0.796, 0.344,-0.33,-0.782, 0.001
GW 165,1, -0.31,-0.33,-0.796, -0.33,-0.33,-0.796, 0.001
GW 166,1, -0.33,-0.33,-0.796, -0.344,-0.33,-0.782, 0.001
GW 167,1, 0.782,-0.33,-0.344, 0.782,-0.33,-0.324, 0.001
GW 168,1, 0.782,-0.33,-0.324, 0.796,-0.33,-0.31, 0.001
GW 169 1 -0.782 -0.33 -0.344 -0.796 -0.33 -0.33 0.001
GW 170 1 -0.796 -0.33 -0.33 -0.796 -0.33 -0.31 0.001
GW 171,1, 0.796,-0.33,0.31, 0.782,-0.33,0.324, 0.001
GW 172,1, 0.782,-0.33,0.324, 0.782,-0.33,0.344, 0.001
GW 173,1, -0.796,-0.33,0.31, -0.782,-0.33,0.324, 0.001
GW 174,1, -0.782,-0.33,0.324, -0.782,-0.33,0.344, 0.001
GW 175 1 0.344 -0.33 0.782 0.324 -0.33 0.782 0.001
```

```
GW 176 1 0.324 -0.33 0.782 0.31 -0.33 0.796 0.001
GW 177 1 -0.344 -0.33 0.782 -0.324 -0.33 0.782 0.001
GW 178 1 -0.324 -0.33 0.782 -0.31 -0.33 0.796 0.001
GW 179 1 0.01 -0.33 -0.796 -0.01 -0.33 -0.796 0.001 !Loop Load
GW 180 1 0.01 0.33 -0.796 -0.01 0.33 -0.796 0.001 !Loop Load
CM END OF 3RD TWIN LOOP
CE
GM 0 0 0 45 0 0 0 0 1 1 60 1
GM 0 0 0 45 90 0 0 0 61 1 120 1
GM 0 0 -90 0 -45 0 0 0 121 1 180 1
GM 0 0 45 -35 0 0 0 0
GW 190 3 0.18624667 0.01 -0.84132525 -0.09028055 0.16965476 -0.84004922 0.001 !Parasitic Stopper
GW 191 3 0.18624667 -0.01 -0.84132525 -0.09028055 -0.16965476 -0.84004922 0.001 !Parasitic Stopper
GW 192 3 -0.10760087 -0.15965476 -0.83996929 -0.10760087 0.15965476 -0.83996929 0.001 !Parasitic Stopper
GS 0 0 1.000000
GE 0 0 0
GN -1
LD 0 180 1 1 377 0 0 !Loop 1 Load Resistor 1
LD 0 120 1 1 377 0 0 !Loop 2 Load Resistor 1
LD 0 59 1 1 377 0 0 !Loop 3 Load Resistor 1
LD 0 179 1 1 377 0 0 !Loop 1 Load Resistor 2
LD 0 119 1 1 377 0 0 !Loop 2 Load Resistor 2
LD 0 60 1 1 377 0 0 !Loop 3 Load Resistor 2
LD 0 190 2 2 754 0 0 !Parasitic Resistor
LD 0 191 2 2 754 0 0 !Parasitic Resistor
LD 0 192 2 2 754 0 0 !Parasitic Resistor
TL 21 1 22 1 -300.00 0 ! TV Twinlead
TL 81 1 82 1 -300.00 0 ! TV Twinlead
TL 141 1 142 1 -300.00 0 ! TV Twinlead
EX 1 1 37 0 35 0 90 1 10 0 1
FR 0 1 0 0 15 1
PT 1 119 1 1
XQ 0
EN
```

Figures F3 to F8 are the results of running the NEC-4 simulation on the Giselle array starting from 5 MHz with 5 MHz increments up to 30 MHz. Plot (A) shows the shape of the null, plot (B) the position of the null and the magnitude of null current in the loop load resistor and plot (C) the maximum induced current when the direction of travel and polarisation of the plane wave coincides with the plane of the twin-loop. Non-symmetrical plots are expected due to the plane of three twin-loop's being tilted 35 degrees relative to the Z axis. Note the depth of the nulls are in excess of -30 dB for the frequencies simulated and confirms the mutual orthogonality and electrical isolation of the three twin-loops. While there is a difference between the real world rod diameter of 10 mm and the simulated 2 mm diameter, the simulated results gives a degree of support to the validity of testing the Giselle array by rotating a small broadband test loop at the geometric centre of the array.

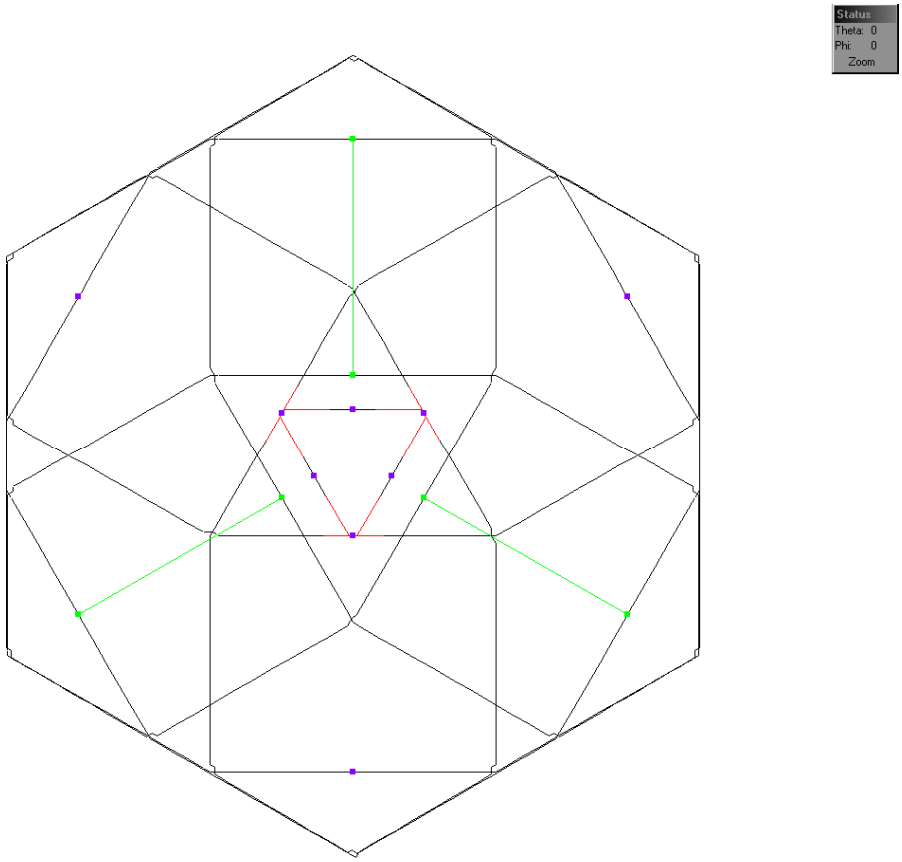

Figure G1: The Giselle antenna array as described in NEC-4 looking down the Z axis from above the array. The X axis points to the bottom of the page the Y axis to the right. The small red triangle in the centre is the location of the parasitic suppression resistors mounted at the base of the array. The three green lines are the 300 ohm TV ribbon transmission lines with a reverse connection at one end simulating a half twist. These are at the top of the array. The magenta dots are the location of the loop termination and parasitic suppression resistors.

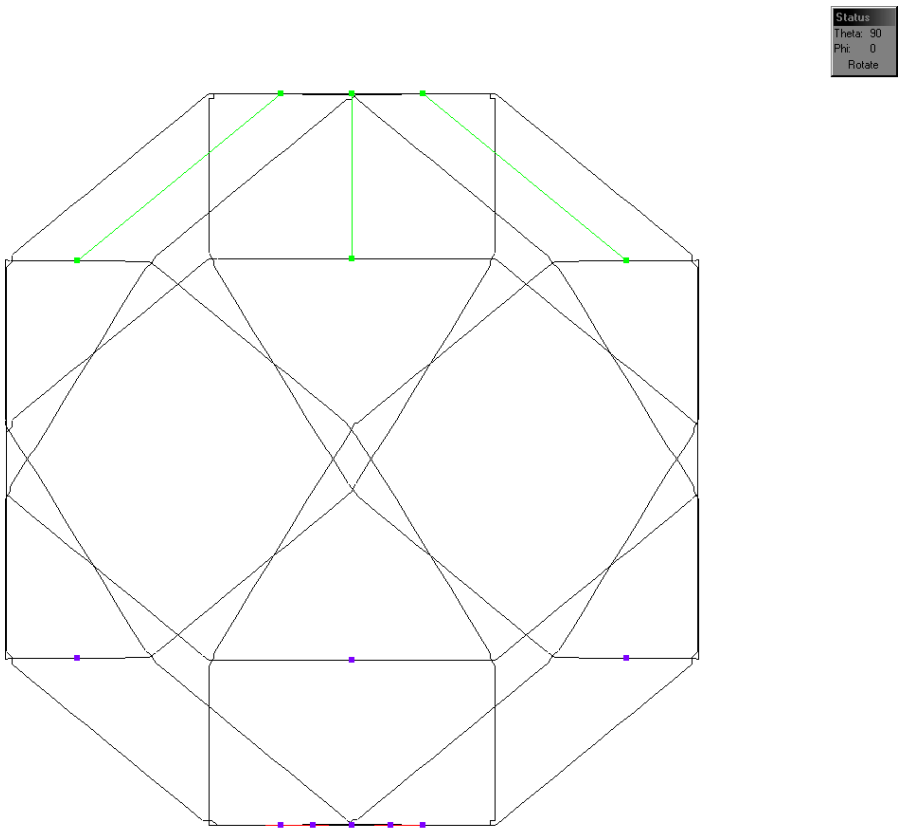

Figure G2: The array has been rotated on the Y axis 90 degrees giving this view looking along the X axis. The Z axis points to the top of the page

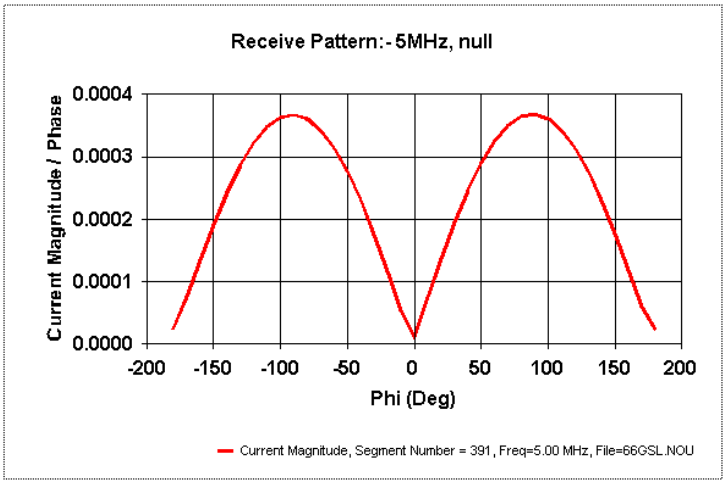

(A)

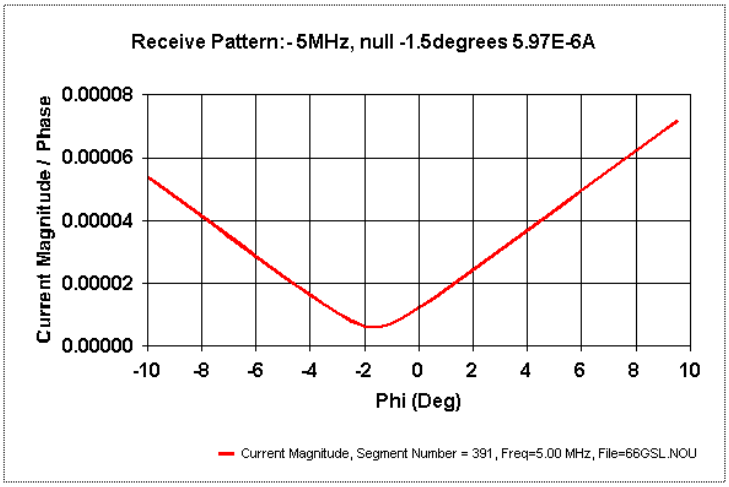

(B)

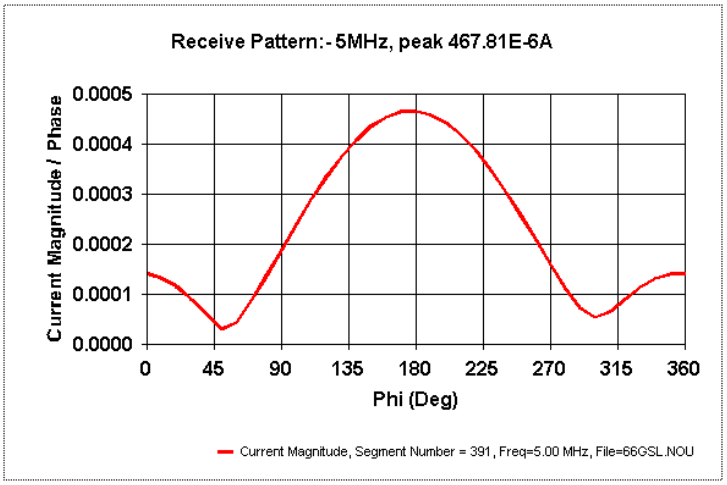

(C)

Figure G3: 5 MHz plots, peak to null ratio -37.8 dB

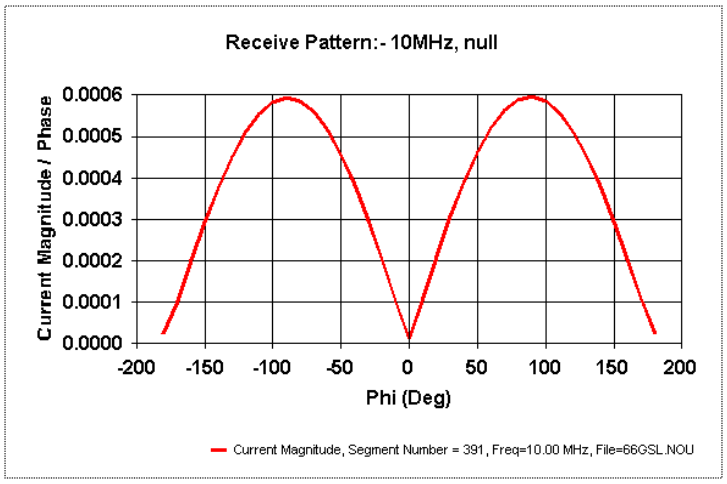

(A)

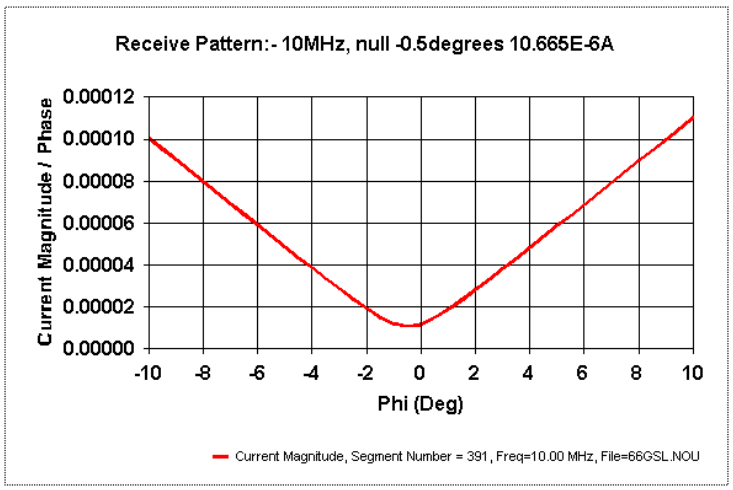

(B)

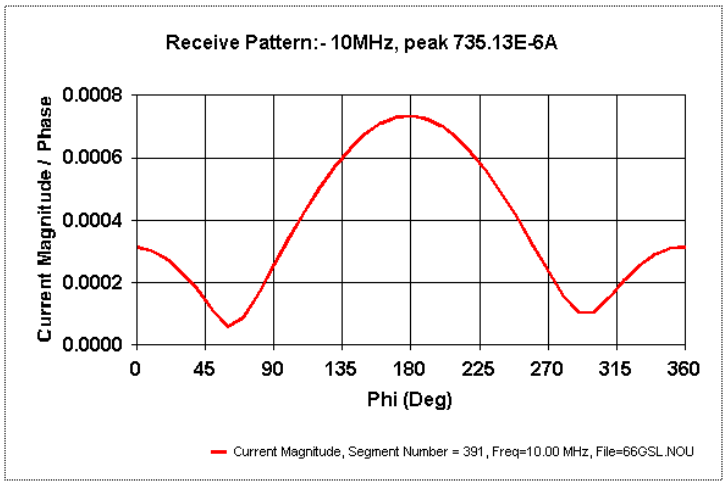

(C)

Figure G4: 10 MHz plots, peak to null ratio -36.7 dB

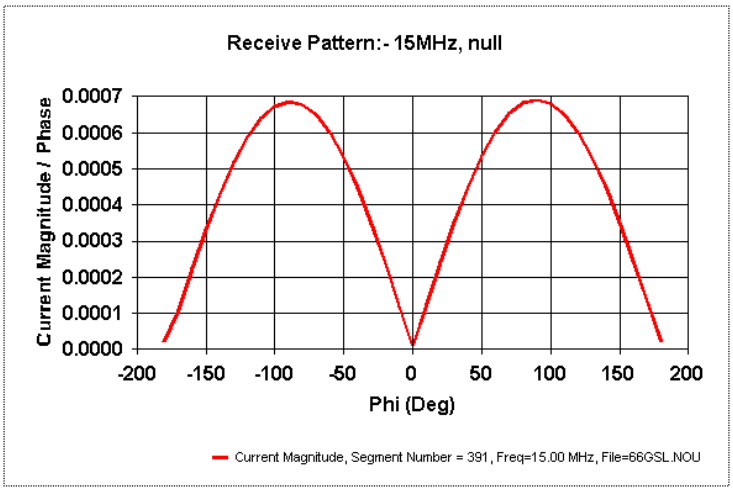

(A)

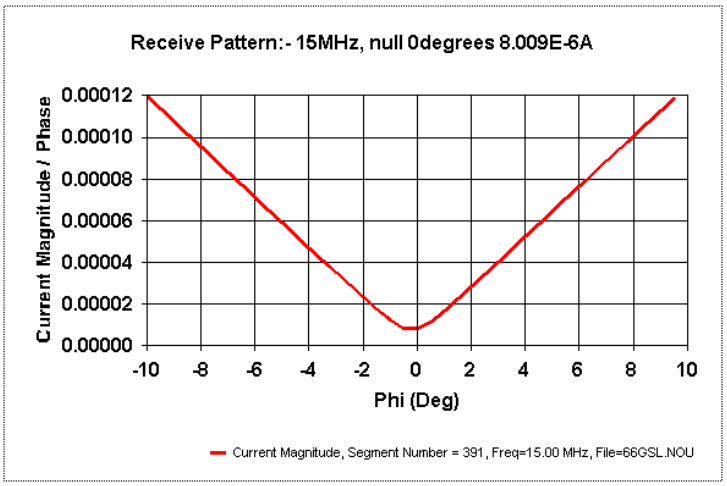

(B)

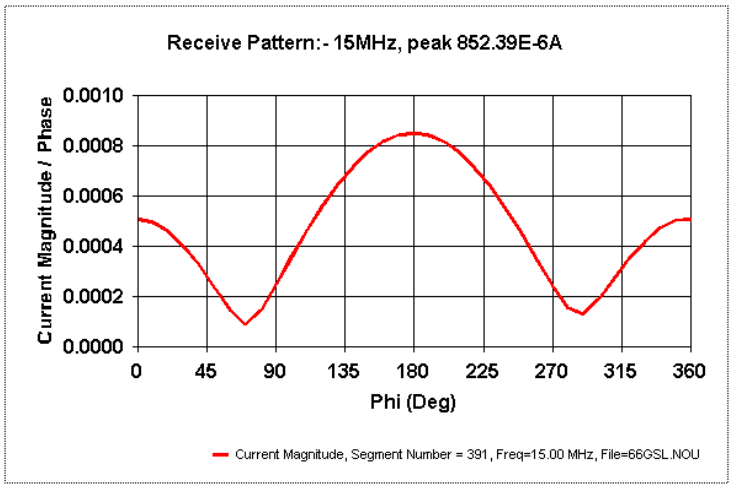

(C)

Figure G5: 15 MHz plots, peak to null ratio -40.5 dB

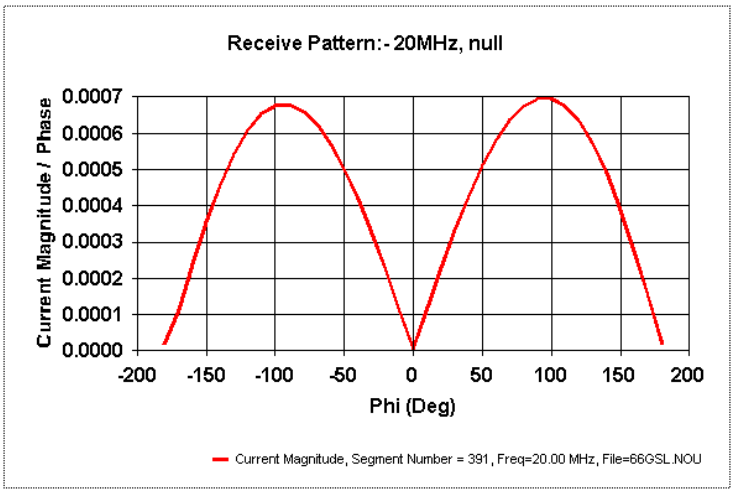

(A)

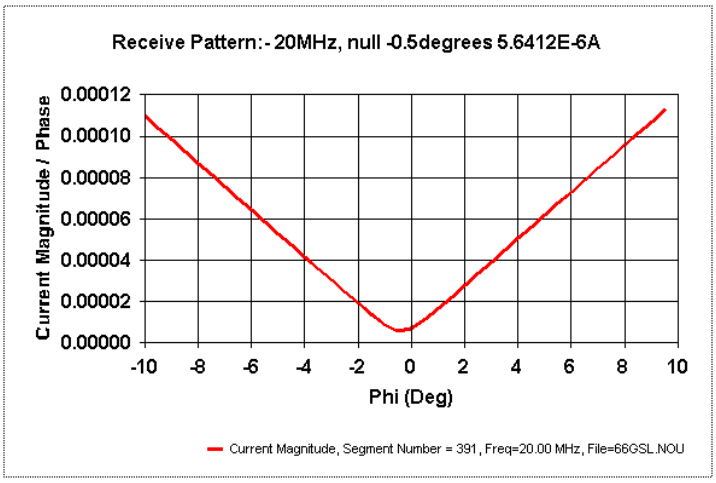

(B)

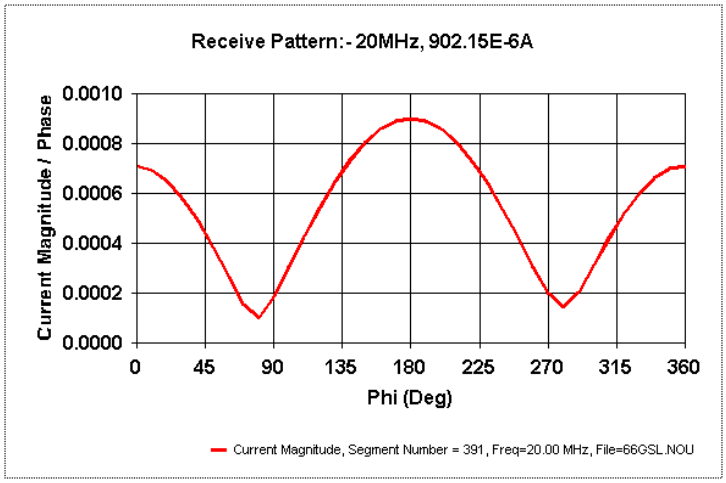

(C)

Figure G6: 20 MHz plots, peak to null ratio -44.0 dB

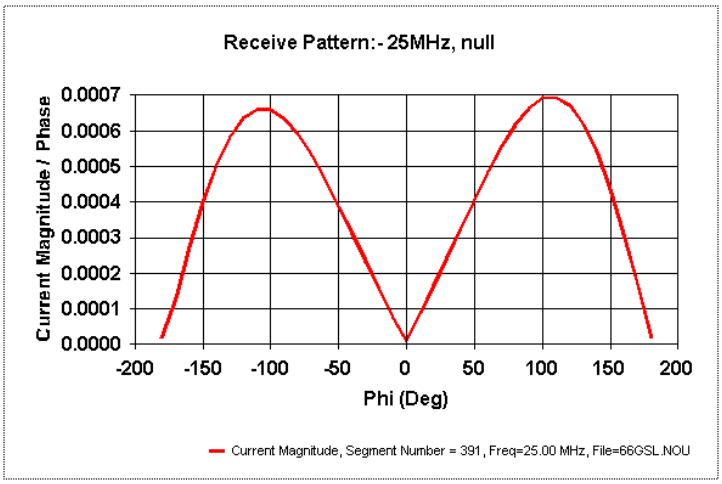

(A)

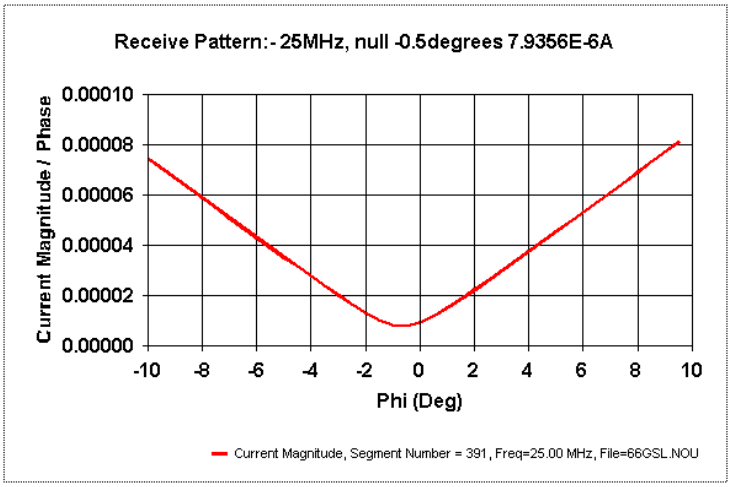

(B)

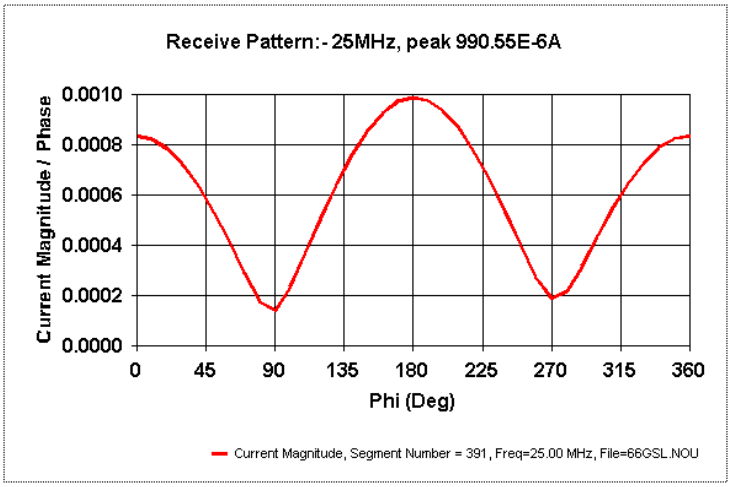

(C)

Figure G7: 25 MHz plots, peak to null ratio -41.9 dB

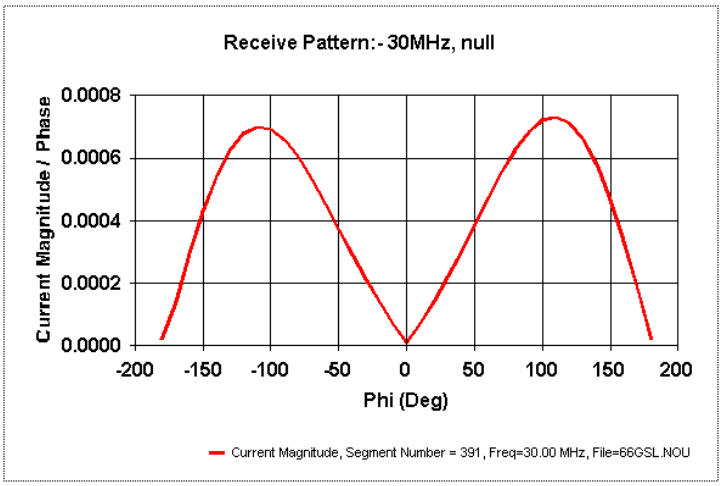

(A)

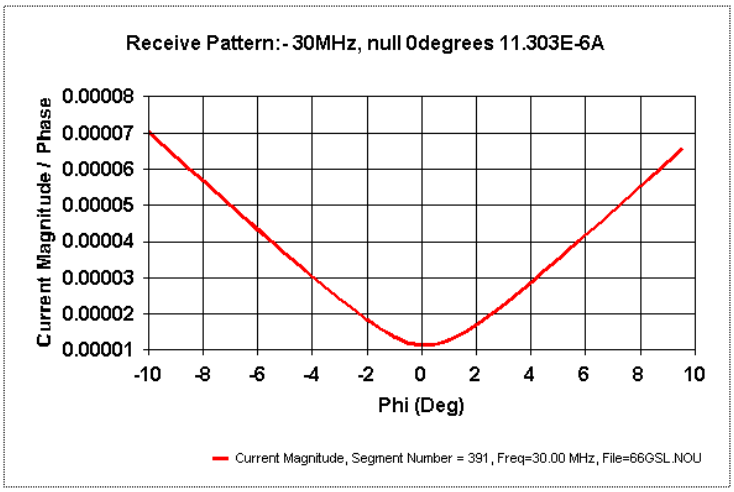

(B)

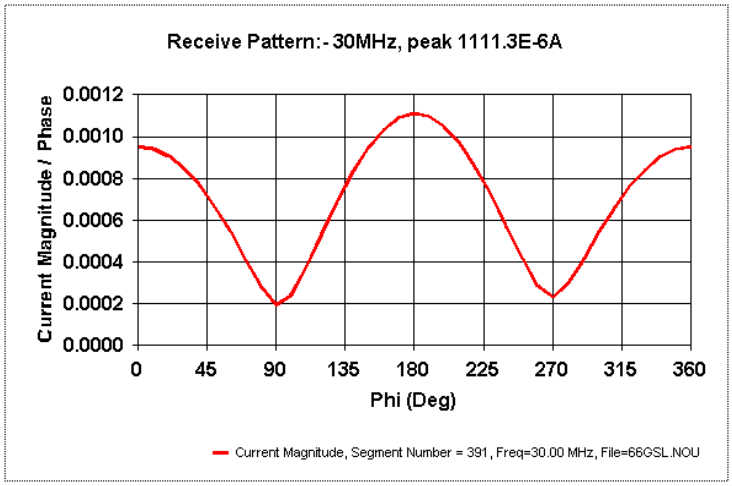

(C)

Figure G8: 30 MHz Plots, peak to null ratio -39.8 dB

Appendix H: Selected Plots of a Sky-wave AM Broadcast Signal at 12060 KHz from the MKII Array

The following figures are of a 12060 KHz sky-wave AM broadcast signal taken by attaching the three outputs of the MKII Giselle antenna array to three inputs of a MATE card (**M**ultiple **A**ntenna **T**o **E**thernet A/D converter). The horizontal axis is the number of samples; the vertical is the un-calibrated linear signal amplitude. The sample rate was 9765 samples/sec giving a total display time of 1 second. These plots were selected to highlight the rotation in polarisation of a HF sky-wave signal. They show the need for polarisation diversity of HF sky-wave signals if signal copy is paramount. It should be noted that polarisation diversity cannot be used to mitigate single site flat fading caused by two signals of comparable magnitude with ~180 degrees phase displacement being received from the same transmitter via different skywave paths. The beginning of Figure H5 appears to have started at the tail end of one of these flat fades.

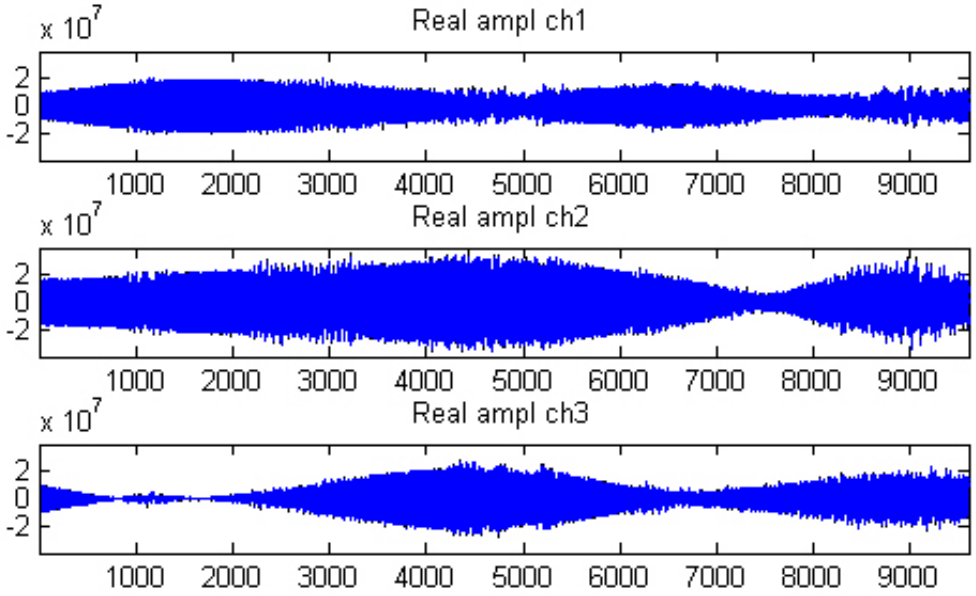

Figure H1

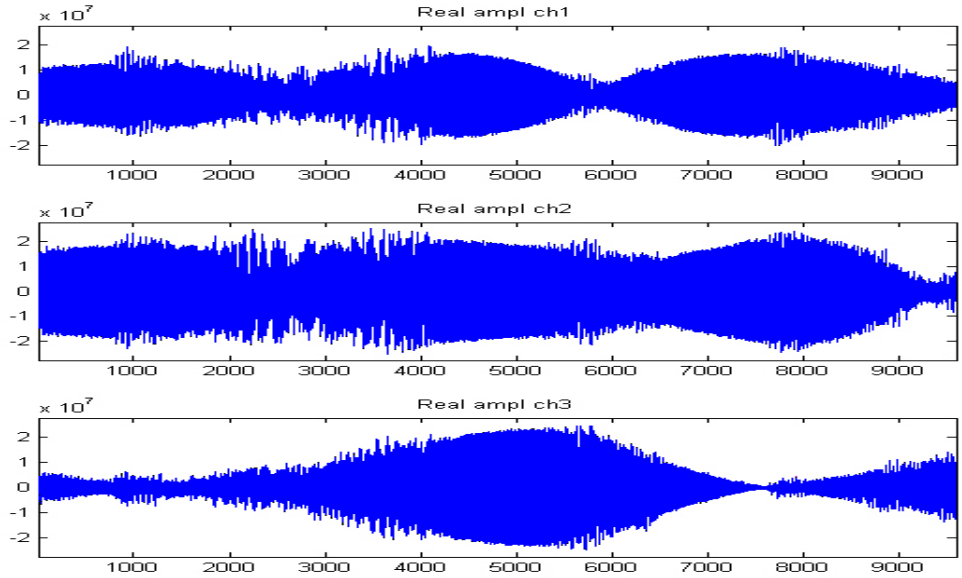

Figure H2

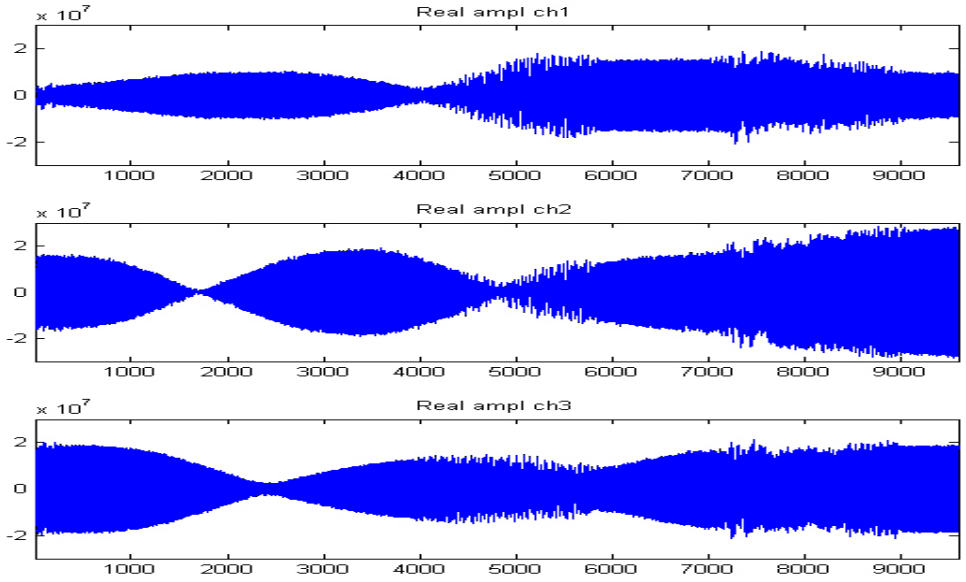

Figure H3

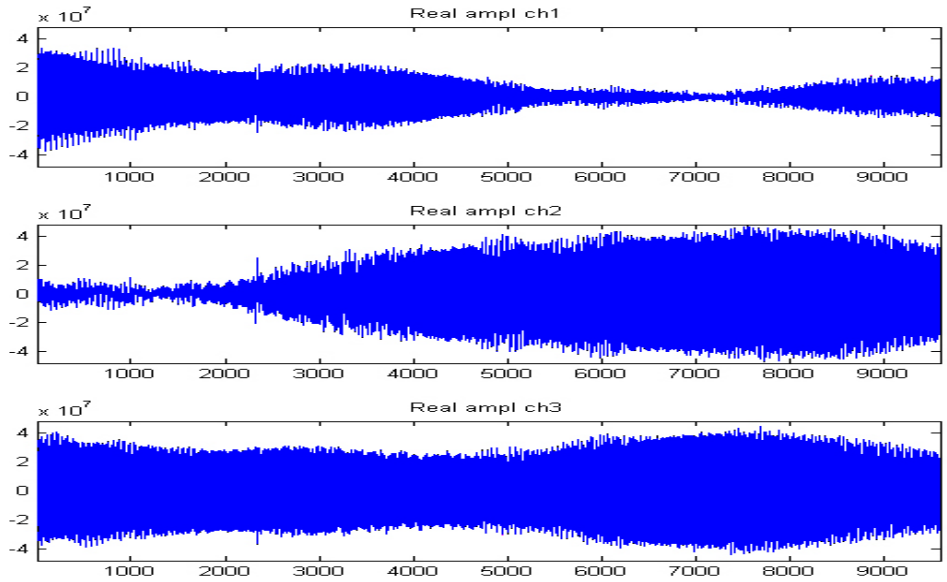

Figure H4

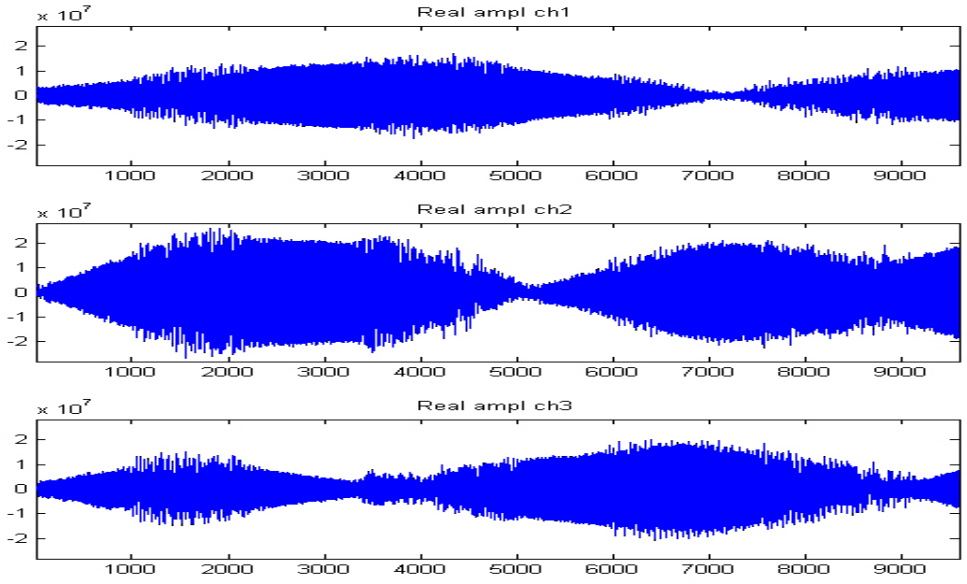

Figure H5

Appendix I: Giselle Schematics

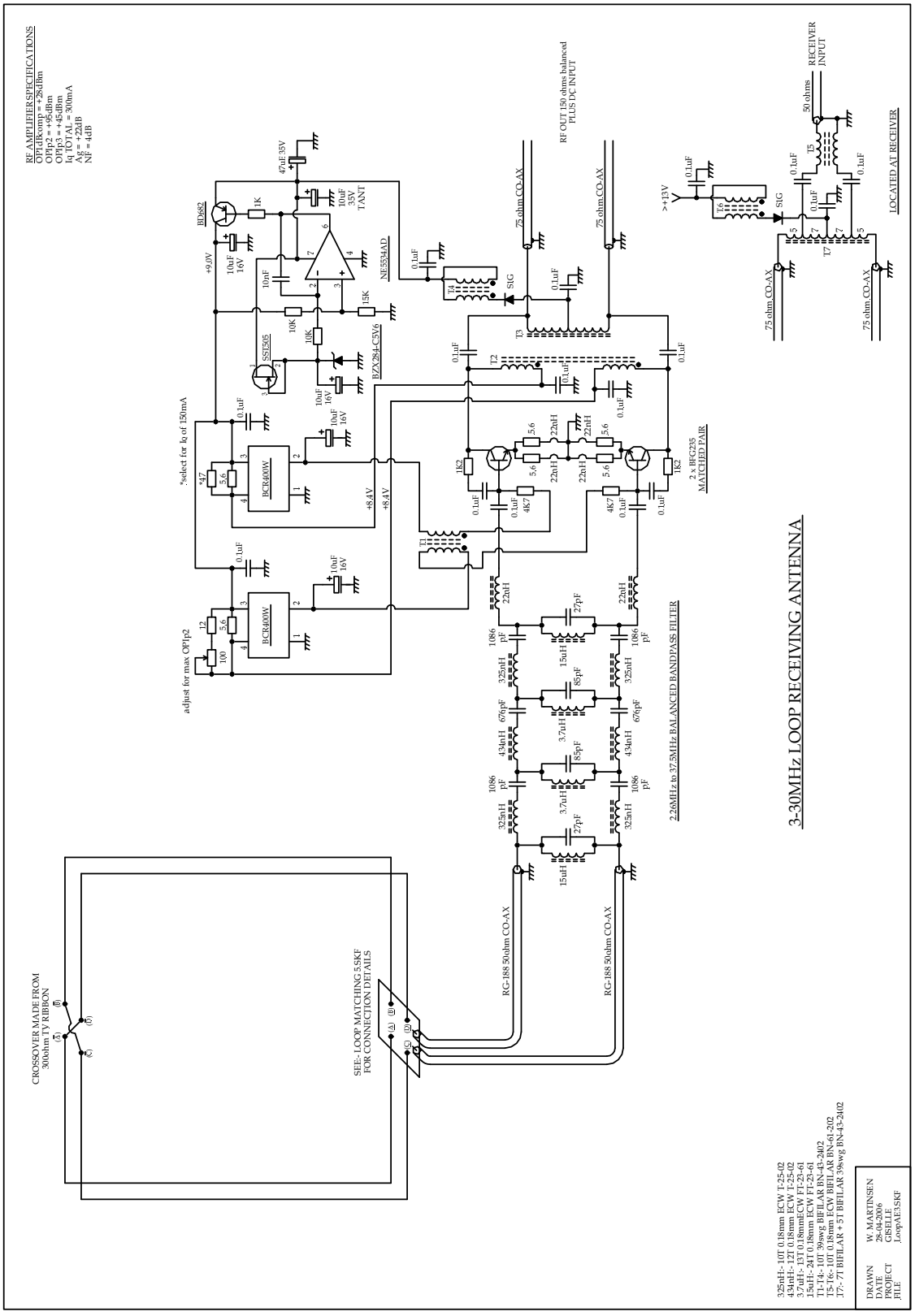
RF AMPLIFIER SPECIFICATIONS
OP1dBcomp = +29dBm
OIP3 = +45dBm
OIP2 = +65dBm
Iq TOTAL = 300mA
Avg = +22dB
NF = 4dB
3-30MHz LOOP RECEIVING ANTENNA
2.26MHz to 37.5MHz BALANCED BANDPASS FILTER
CROSSOVER MADE FROM 300ohm TV RIBBON
SEE:- LOOP MATCHING 5.5KF FOR CONNECTION DETAILS
RG-188 50ohm CO-AX
RG-188 50ohm CO-AX
RF OUT 150 ohms balanced PLUS DC INPUT
75 ohm CO-AX
75 ohm CO-AX
75 ohm CO-AX
50 ohms
RECEIVER INPUT
LOCATED AT RECEIVER
+9.0V
+13V
SIG
SIG
NE5534AD
BZX284-C5V6
2SC5085
2 x BFG235 MATCHED PAIR
adjust for max OP1p2
*select for Iq of 150mA
+8.4V
+8.4V
325nH:- 10T 0.18mm ECW T-25-02
434nH:- 12T 0.18mm ECW T-25-02
3.7uH:- 31T 0.18mm ECW FT-23-61
15uH:- 24T 0.18mm ECW FT-23-61
T1-T4:- 10T 39swg BIFILAR BN-43-2402
T5-T6:- 10T 0.18mm ECW BIFILAR BN-61-202
T7:- 7T BIFILAR + 5T BIFILAR 39swg BN-43-2402
DRAWN W. MARTINSEN
DATE 28-Jul-2006
PROJECT GISELLE
FILE LoopAE35KF

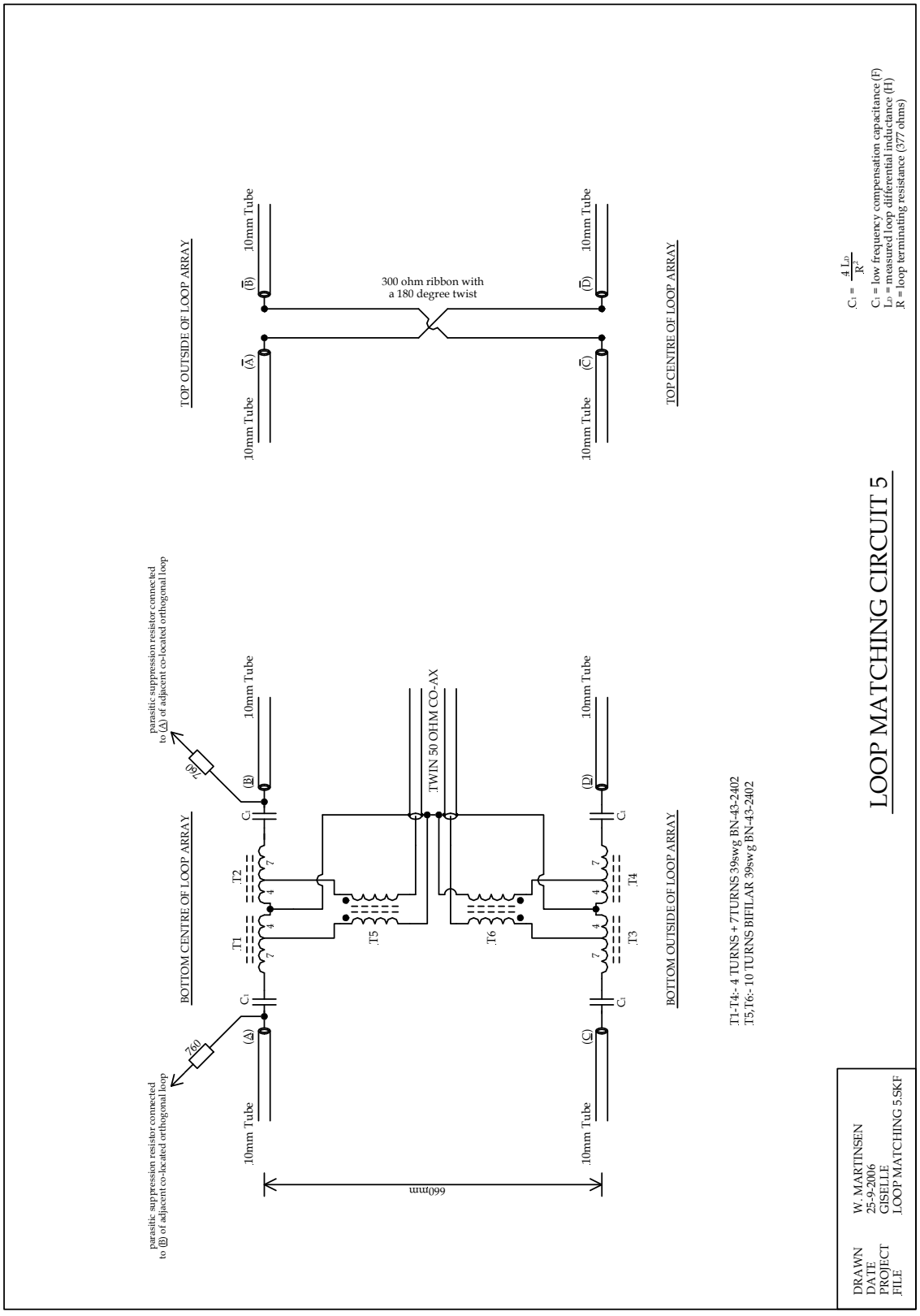
LOOP MATCHING CIRCUIT 5
TOP OUTSIDE OF LOOP ARRAY
TOP CENTRE OF LOOP ARRAY
BOTTOM CENTRE OF LOOP ARRAY
BOTTOM OUTSIDE OF LOOP ARRAY
300 ohm ribbon with a 180 degree twist
TWIN 50 OHM CO-AX
10mm Tube
660mm
T1 T2 T3 T4 T5 T6
T1-T4:- 4 TURNS + 7TURNS 39swg BN-43-2402
T5,T6:- 10 TURNS BIFILAR 39swg BN-43-2402
parasitic suppression resistor connected to (A) of adjacent co-located orthogonal loop
parasitic suppression resistor connected to (B) of adjacent co-located orthogonal loop
760
DRAWN W. MARTINSEN
DATE 25-9-2006
PROJECT GISELLE
FILE LOOP MATCHING 5.SKF
$C_1 = \frac{4 L_D}{R^2}$
C_1 = low frequency compensation capacitance (F)
L_D = measured loop differential inductance (H)
R = loop terminating resistance (377 ohms)

DEFENCE SCIENCE AND TECHNOLOGY ORGANISATION
DOCUMENT CONTROL DATA

1. PRIVACY MARKING/CAVEAT (OF DOCUMENT)

2. TITLE

Giselle: A Mutually Orthogonal Triple Twin-loop Ground-symmetrical Broadband Receiving Antenna for the HF Band

3. SECURITY CLASSIFICATION (FOR UNCLASSIFIED REPORTS THAT ARE LIMITED RELEASE USE (L) NEXT TO DOCUMENT CLASSIFICATION)

Document	(U)
Title	(U)
Abstract	(U)

4. AUTHOR(S)

W. Martinsen

5. CORPORATE AUTHOR

DSTO Defence Science and Technology Organisation
PO Box 1500
Edinburgh South Australia 5111 Australia

6a. DSTO NUMBER	6b. AR NUMBER	6c. TYPE OF REPORT	7. DOCUMENT DATE
DSTO-TR-2321	AR-014-584	Technical Report	July 2009

8. FILE NUMBER	9. TASK NUMBER	10. TASK SPONSOR	11. NO. OF PAGES	12. NO. OF REFERENCES
E 8709/8/17 pt 1	INT 05/201	ASCP	93	24

13. DOWNGRADING/DELIMITING INSTRUCTIONS

To be reviewed three years after date of publicationDSTO-TR-2321

14. RELEASE AUTHORITY

Chief,
Command, Control, Communications and Intelligence Division

15. SECONDARY RELEASE STATEMENT OF THIS DOCUMENT

Approved for public release

OVERSEAS ENQUIRIES OUTSIDE STATED LIMITATIONS SHOULD BE REFERRED THROUGH DOCUMENT EXCHANGE, PO BOX 1500, EDINBURGH, SA 5111

16. DELIBERATE ANNOUNCEMENT

No Limitations

17. CITATION IN OTHER DOCUMENTS Yes

18. DSTO RESEARCH LIBRARY THESAURUS http://web-vic.dsto.defence.gov.au/workareas/library/resources/dsto_thesaurus.shtml

Antennas; Noise; High frequency; Polarisation; Mathematics

19. ABSTRACT

This report describes development of a tri-axial mutually orthogonal broadband twin-loop receiving antenna for the HF band. The three twin-loops have been arranged so that they exhibit the same distributed parameters between themselves and ground. The upper frequency limit of the antenna is discussed and a method for extending the low frequency cut-off is presented. The antenna noise factor is calculated from measured data.